Supporting Information

Host-Guest Induced Electron Transfer Triggers Radical-Cation Catalysis

Rebecca L. Spicer,[†] Athanasios D. Stergiou,[§] Tom A. Young,[‡] Fernanda Duarte,[‡,*] Mark D. Symes[§,*] and Paul J. Lusby[†,*]

[†] EaStCHEM School of Chemistry, University of Edinburgh, Joseph Black Building, David Brewster Road, Edinburgh, Scotland EH9 3FJ, UK.

* Paul.Lusby@ed.ac.uk

[§] WestCHEM, School of Chemistry, University of Glasgow, University Avenue, Glasgow, Scotland G12 8QQ, UK.

* Mark.Symes@glasgow.ac.uk

[‡] Chemical Research Laboratory, 12 Mansfield Road, Oxford, England OX1 3TA, UK.

* Fernanda.DuarteGonzalez@chem.ox.ac.uk

Contents

1 Materials and Methods 5

2 Synthesis 5

3 Cage-Quinone Catalyzed [4+2] Cycloaddition Reactions 6

3.1 General Procedure 6

3.2 Product Identification 6

3.3 ^{1}H NMR spectra of [4+2] catalyzed reactions 7

3.3.1 *trans*-Anethole and cyclopentadiene 7

3.3.2 *trans*-Anethole and cyclohexadiene 8

3.3.3 *trans*-Anethole and isoprene 9

3.3.4 *trans*-β-methyl-*N*-vinylcarbazole and cyclopentadiene 10

3.3.5 *trans*-β-Methyl-*N*-vinylcarbazole and cyclohexadiene 11

3.4 Control Reactions 11

3.4.1 ^{1}H NMR spectra of [4+2] control reactions 12

3.5 Preparative Scale Reaction 17

3.5.1 *trans*-Anethole and cyclopentadiene 17

4 Cage-Quinone Catalyzed [2+2] Homo-Cycloaddition Reactions 18

4.1 General Procedure 18

4.2 Product Identification 18

4.3 ^{1}H NMR spectra of homo-[2+2] catalyzed reactions 19

4.3.1 *trans*-Anethole 19

4.3.2 *trans*-β-Methyl-*N*-vinylcarbazole 20

4.4 Control Reaction 21

4.4.1 ^{1}H NMR spectra of [2+2] control reaction 21

4.5 Preparative Scale Reaction 22

4.5.1 *trans*-β-Methyl-*N*-vinylcarbazole 22

5 Cage-Quinone Catalyzed [2+2] Hetero-Cycloaddition Reactions 23

5.1 β-Methylstyrene Reactions 23

5.1.1 General Procedure 23

5.2 Product Identification 23

5.2.1 ^{1}H NMR spectra of hetero-[2+2] catalyzed reaction 24

5.3 *trans*-Anethole and Styrenes 25

5.3.1 General Procedure 25

5.4 Product Identification 25

5.4.1 ^{1}H NMR spectra of hetero-[2+2] catalyzed reactions 26
6 Reaction Optimisation for Cage-Quinone Catalyzed [4+2] Cycloaddition of *trans*-anethole and cyclopentadiene 29
7 Quinone Scope for Cage-Quinone Catalyzed [4+2] Cycloaddition of *trans*-anethole and cyclopentadiene 30
7.1 General Procedure 30
7.2 ^{1}H NMR spectra of [4+2] catalyzed reactions 31
7.3 Control Reactions 31
8 **C-1**/**Q-4** Catalyzed [4+2] Cycloaddition of Cyclohexadiene 32
8.1 General Procedure 32
8.2 Product Identification 32
8.2.1 **Q-1**-cyclohexadiene cycloadduct 33
8.2.2 **Q-4**-cyclohexadiene cycloadduct 33
8.3 ^{1}H NMR spectra of [4+2] cyclohexadiene reactions 34
8.3.1 Catalysis Reaction 34
8.3.2 Control Reactions 35
9 Cage-Quinone Catalyzed Cycloaddition of *tert*-butyl benzoquinone and dimethylanthracene 36
9.1 General Procedure 36
9.2 Product Identification 36
9.2.1 **Q-1**-dimethylanthracene cycloadduct synthesis 36
9.3 ^{1}H NMR spectra of [4+2] catalyzed reactions 38
9.4 Control Reactions 39
9.4.1 ^{1}H NMR spectra of [4+2] control reactions 39
10 Determination of Binding Constants 40
10.1 Fast Exchange Titration Procedure 40
10.2 **Q-1** and **C-1** titration 41
10.3 **Q-1** and **C-2** titration 42
10.4 **Q-6** and **C-1** titration 43
10.5 **Q-8** and **C-1** titration 44
11 Electrochemical Studies 45
11.1 General Procedure 45
11.2 Cyclic Voltammograms 45
11.2.1 **Q-1** 45
11.2.2 **Q-2** 45

11.2.3 **Q-6** 46
11.2.4 **Q-8** 46
11.2.5 **Q-10** 46
11.2.6 Bromoferrocene 47
11.2.7 1,1'-Dibromoferrocene 47
11.2.8 9,10-Dimethylanthracene 47
11.2.9 Tris(*p*-bromophenyl)amine 48
11.2.10 *trans*-Anethole 48
11.2.11 *trans*-β-Methyl-*N*-vinylcarbazole 48
11.2.12 1,3-Cyclohexadiene 49
11.3 $E_{1/2}$ values 49
12 UV/Vis Electron Transfer Experiments 50
12.1 Qualitative Comparison of Cage Electron Transfer Properties 50
12.1.1 General Procedure 50
12.1.2 UV/Vis spectra 50
12.2 UV/Vis Electron Transfer Titration Experiments 53
12.2.1 General Procedure 53
12.2.2 Qualitative UV/Vis Spectra for **C-1**/**Q-1** 53
12.2.3 UV/Vis Spectra for Quantifying *K* 55
12.2.4 Fitting for *K* and Calculating *E* 56
13 Computational Studies 58
13.1 Computational Methods 58
13.2 Spin Density Plots 58
14 References 59

1 Materials and Methods

Unless stated otherwise, all reagents and solvents were purchased from Alfa Aesar, VWR, Fluorochem or Sigma Aldrich and used without further purification. Where the use of anhydrous solvent is stated, drying was carried out using a solvent purification system manufactured by Glass Contour. Column chromatography was carried out using Geduran Si60 (40-63 µm) as the stationary phase and TLC was performed on precoated Kieselgel 60 plates (0.20 mm thick, $60F_{254}$. Merck, Germany) and observed under UV light at 254 nm or 365 nm. All reactions were carried out under air, unless stated otherwise.

Abbreviations used in the Supporting Information include:

n/a	Not applicable
wrt	With respect to
RT	Room temperature
NMR	Nuclear Magnetic Resonance
COSY	Correlation Spectroscopy
NOESY	Nuclear Overhauser Effect Spectroscopy
HSQC	Heteronuclear Single Quantum Coherence
HMBC	Heteronuclear Multiple Bond Correlation
MS	Mass spectrometry
HRMS	High resolution mass spectrometry
ET	Electron transfer
CV	Cyclic voltammetry

All ^{1}H, ^{13}C and ^{19}F NMR spectra were recorded on either a 500 MHz Bruker AV III equipped with a DCH cryo-probe (Ava500), a 500 MHz Bruker AV IIIHD equipped with a Prodigy cryo-probe (Pro500) or a 400 MHz Bruker AV III equipped with BBFO+ probe (Ava400) at a constant temperature of 300 K. Chemical shifts are reported in parts per million. Coupling constants (J) are reported in hertz (Hz). Standard abbreviations indicating multiplicity were used as follows: m = multiplet, q = quartet, t = triplet, d = doublet, s = singlet, bs = broad singlet. All analysis was performed with MestReNova, Version 12.0.3. All assignments were confirmed using a combination of COSY, NOESY, HMBC and HSQC NMR.

All UV/Vis spectroscopy was carried out on a Shimadzu UV-1900 Spectrophotometer running UV Probe, Version 2.70 (Shimadzu). All data was analyzed and plotted using Origin 2015 software. All measurements were made at room temperature (16–21 °C) in CH_2Cl_2 using a fused silica cuvette with a 10 mm path length, unless stated otherwise.

2 Synthesis

Cages **C-1**[1] and **C-2**,[2] *N*-(*trans*-1-propenyl)carbazole (*trans*-β-methyl-*N*-vinylcarbazole),[3] 2,5-dibromo-1,4-benzoquinone,[4] 2,3,6,7-tetrafluoro-9,10-anthraquinone[5] and tetrabutylammonium tetrakis[3,5-bis(trifluoromethyl)phenyl]borate (NBu_4BArF)[6] were synthesized according to known literature procedures. Cyclopentadiene was freshly prepared by cracking dicyclopentadiene followed by distillation. Styrene, *p*-methylstyrene, *p*-chlorostyrene, 1,3-cyclohexadiene and isoprene were purified by vacuum distillation.

3 Cage-Quinone Catalyzed [4+2] Cycloaddition Reactions

3.1 General Procedure

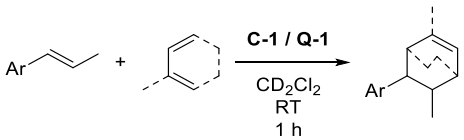

Stock solutions in CD_2Cl_2 were prepared for: 2-fluoromesitylene (internal standard, 1.20 mmol/mL), dienophile (2.40 mmol/mL), diene (4.80 mmol/mL), **Q-1** (0.12×10^{-3} mmol/mL) and cage (6.0×10^{-3} mmol/mL).

To CD_2Cl_2 (400 µL), in an NMR tube, was added internal standard (0.4 mg, 3.0×10^{-3} mmol, 0.5 eq., 25 µL), dienophile (6.0×10^{-3} mmol, 1.0 eq., 25 µL), diene (1.2×10^{-2} mmol, 2.0 eq., 25 µL) and **C-1** (1.4 mg, 3.0×10^{-4} mmol, 0.05 eq., 100 µL). The reaction was initiated by addition of **Q-1** (3.0×10^{-4} mmol, 0.05 eq., 25 µL). The reaction was monitored by recording ^{1}H NMR spectra before and 1 hour after the addition of **Q-1**. Product yields were calculated by comparing integrals of the starting material and product[s] to that of the internal standard.

3.2 Product Identification

The products of each NMR scale reaction were identified (and thereby yields calculated) by comparing the spectra to previously reported ^{1}H NMR spectroscopic data. The sources for this data are listed below:

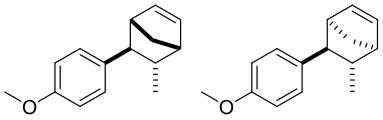

endo *exo*

J. Chem. Soc., Perkin Trans. 2 **2000**, 931–934

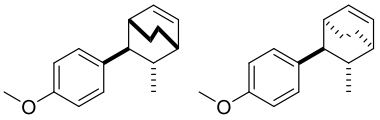

endo *exo*

Angew. Chem. Int. Ed. **2015**, 54, 6506–6510

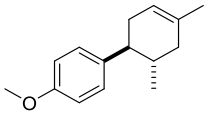

Angew. Chem. Int. Ed. **2015**, 54, 6506–6510

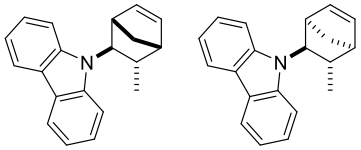

endo *exo*

Tetrahedron Lett. **2000**, 41, 5997−6000

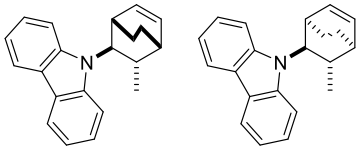

endo *exo*

Tetrahedron Lett. **2000**, 41, 5997−6000

3.3 ^{1}H NMR spectra of [4+2] catalyzed reactions

3.3.1 *trans*-Anethole and cyclopentadiene

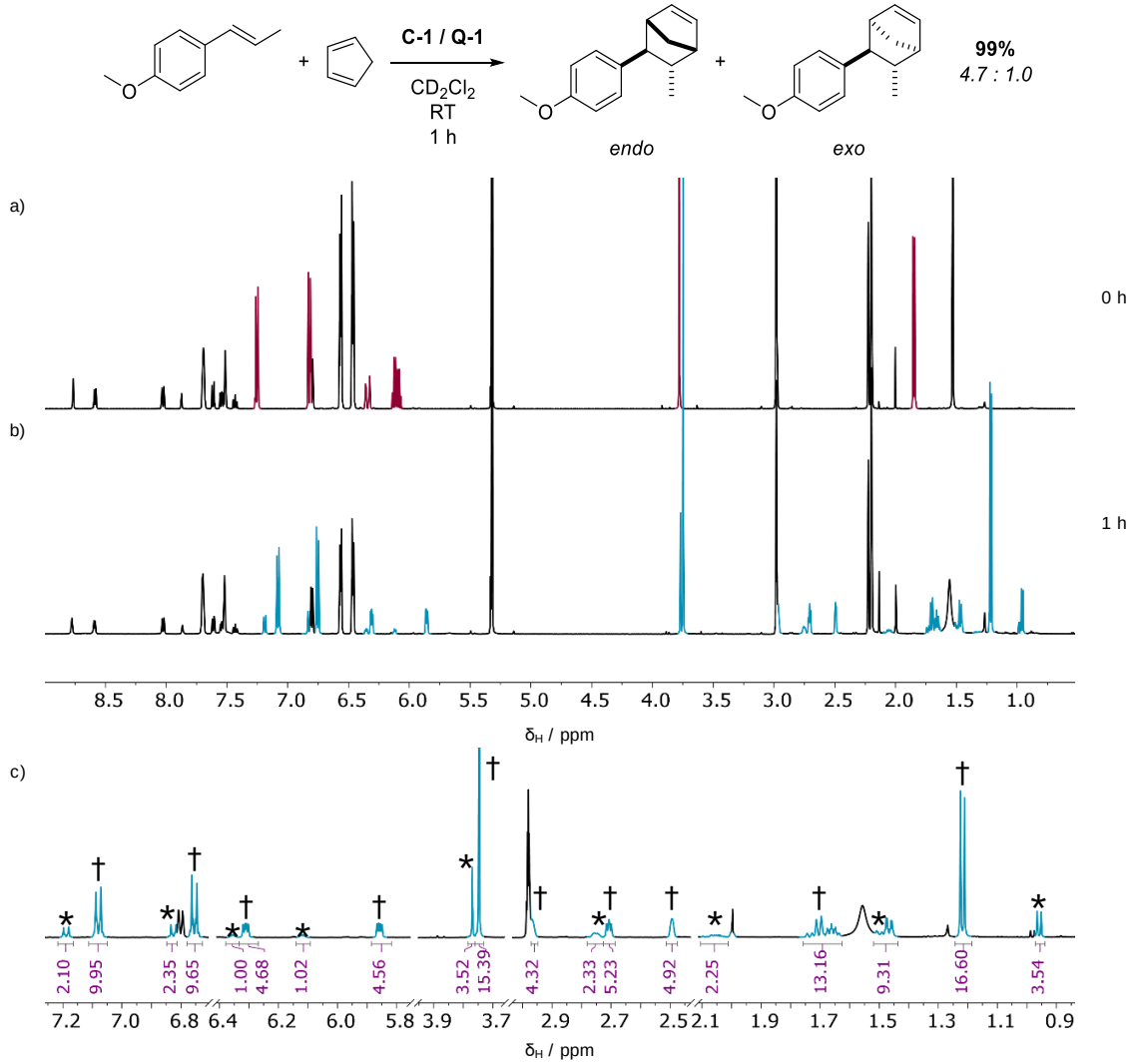

Figure S1: ^{1}H NMR spectra (500 MHz, CD_2Cl_2, 300 K) for the reaction of *trans*-anethole (10 mM) and cyclopentadiene (20 mM) in the presence of **C-1** (0.5 mM) and **Q-1** (0.5 mM). (a) *trans*-anethole, cyclopentadiene and **C-1** at T = 0 h; (b) *trans*-anethole, cyclopentadiene, **C-1** and **Q-1** at T = 1 h; (c) Partial ^{1}H NMR spectrum of (b) highlighting cycloadduct peaks. *trans*-Anethole is highlighted in red, cycloadducts are highlighted in blue (*endo* product is denoted by †, *exo* product is denoted by *).

3.3.2 *trans*-Anethole and cyclohexadiene

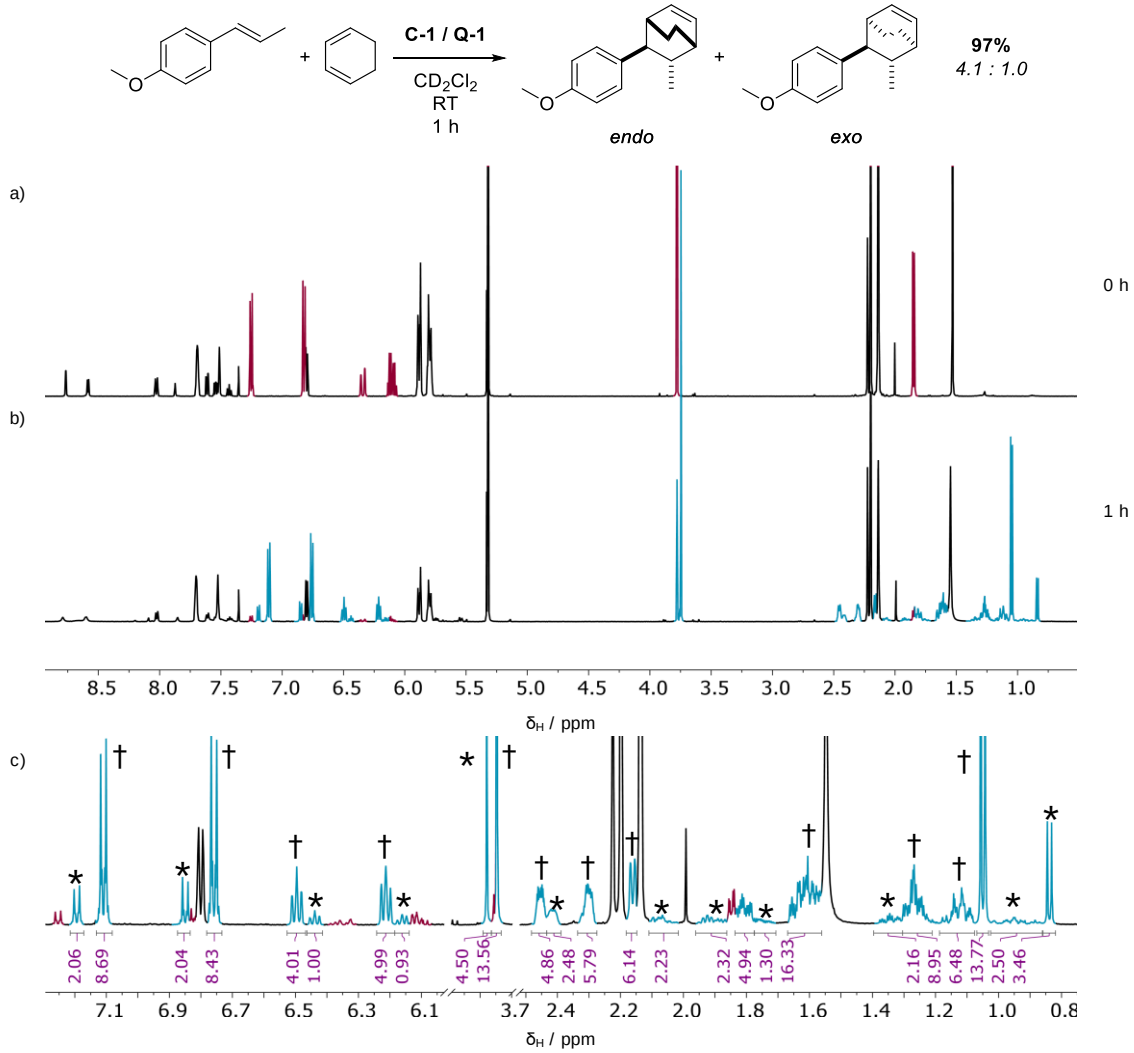

Figure S2: ^{1}H NMR spectra (500 MHz, CD_2Cl_2, 300 K) for the reaction of *trans*-anethole (10 mM) and cyclohexadiene (20 mM) in the presence of **C-1** (0.5 mM) and **Q-1** (0.5 mM). (a) *trans*-anethole, cyclohexadiene and **C-1** at T = 0 h; (b) *trans*-anethole, cyclohexadiene, **C-1** and **Q-1** at T = 1 h; (c) Partial ^{1}H NMR spectrum of (b) highlighting cycloadduct peaks. *trans*-Anethole is highlighted in red, cycloadducts are highlighted in blue (*endo* product is denoted by †, *exo* product is denoted by *).

3.3.3 *trans*-Anethole and isoprene

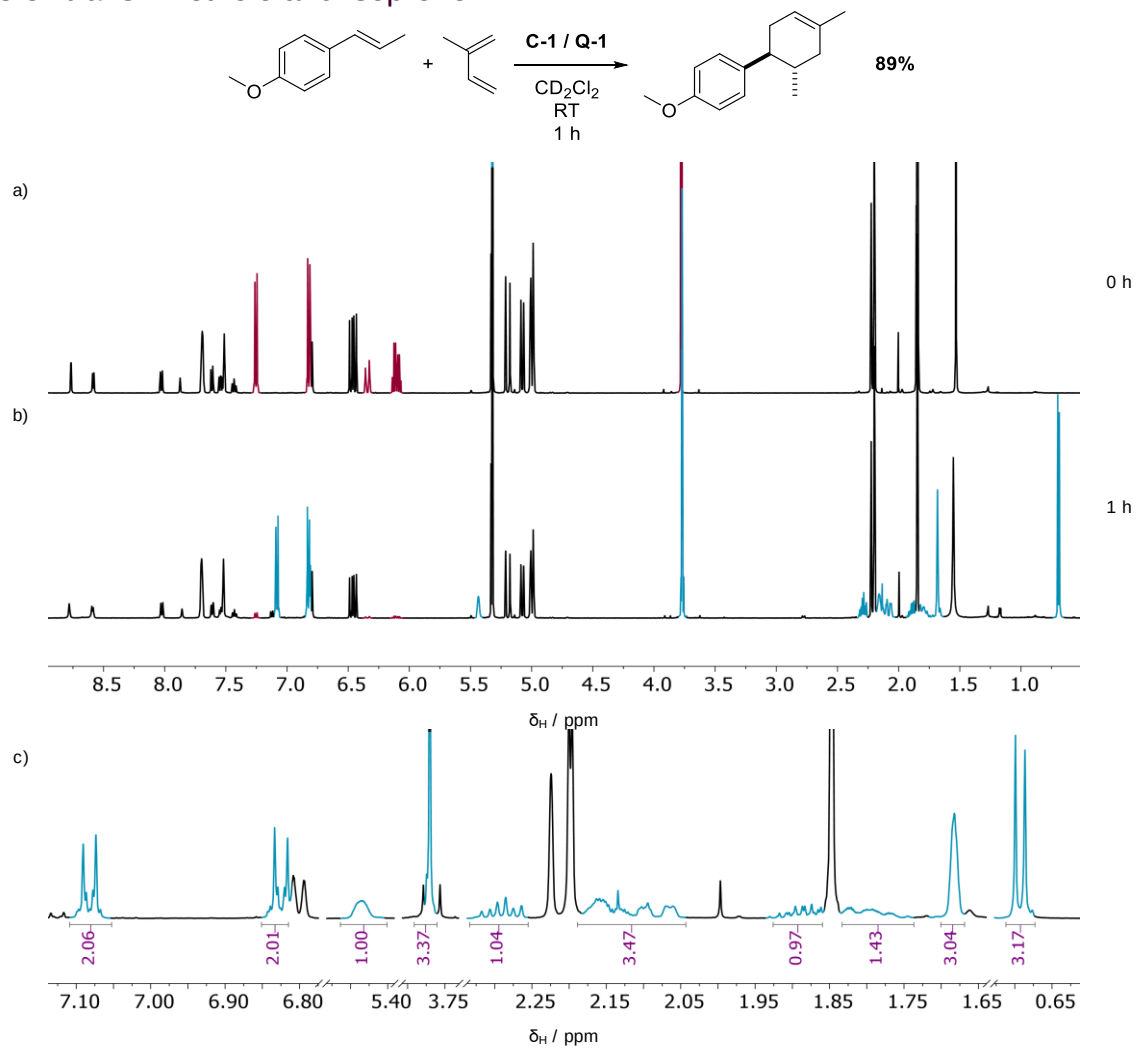

Figure S3: ^{1}H NMR spectra (500 MHz, CD_2Cl_2, 300 K) for the reaction of *trans*-anethole (10 mM) and isoprene (20 mM) in the presence of **C-1** (0.5 mM) and **Q-1** (0.5 mM). (a) *trans*-anethole, isoprene and **C-1** at T = 0 h; (b) *trans*-anethole, isoprene, **C-1** and **Q-1** at T = 1 h; (c) Partial ^{1}H NMR spectrum of (b) highlighting cycloadduct peaks. *trans*-Anethole is highlighted in red, cycloadduct is highlighted in blue.

3.3.4 *trans*-β-methyl-*N*-vinylcarbazole and cyclopentadiene

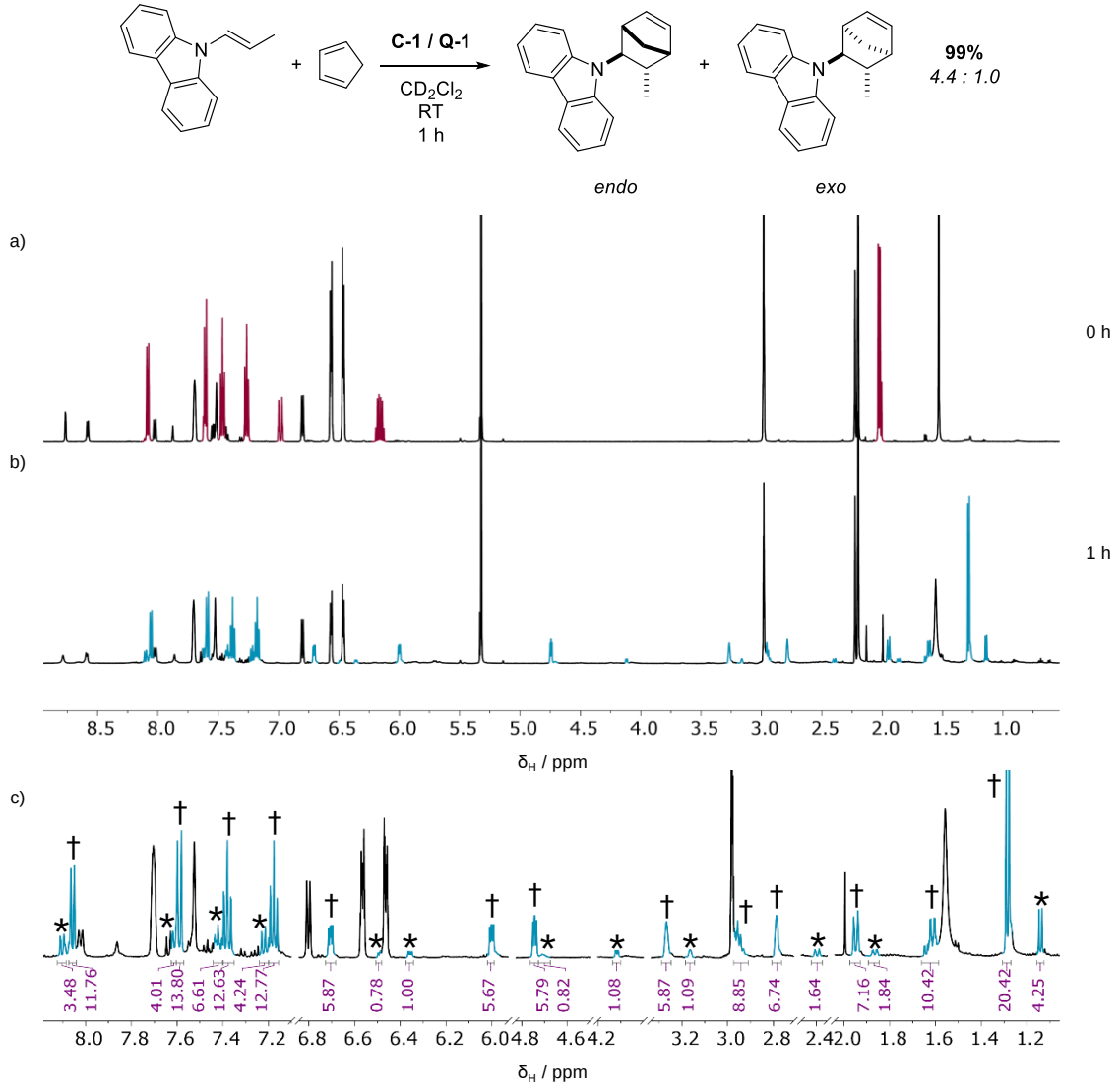

Figure S4: ^{1}H NMR spectra (500 MHz, CD_2Cl_2, 300 K) for the reaction of *trans*-β-methyl-*N*-vinylcarbazole (10 mM) and cyclopentadiene (20 mM) in the presence of **C-1** (0.5 mM) and **Q-1** (0.5 mM). (a) *trans*-β-methyl-*N*-vinylcarbazole, cyclopentadiene and **C-1** at T = 0 h; (b) *trans*-β-methyl-*N*-vinylcarbazole, cyclopentadiene, **C-1** and **Q-1** at T = 1 h; (c) Partial ^{1}H NMR spectrum of (b) highlighting cycloadduct peaks. *trans*-β-methyl-*N*-vinylcarbazole is highlighted in red, cycloadducts are highlighted in blue (*endo* product is denoted by †, *exo* product is denoted by *).

3.3.5 *trans*-β-Methyl-*N*-vinylcarbazole and cyclohexadiene

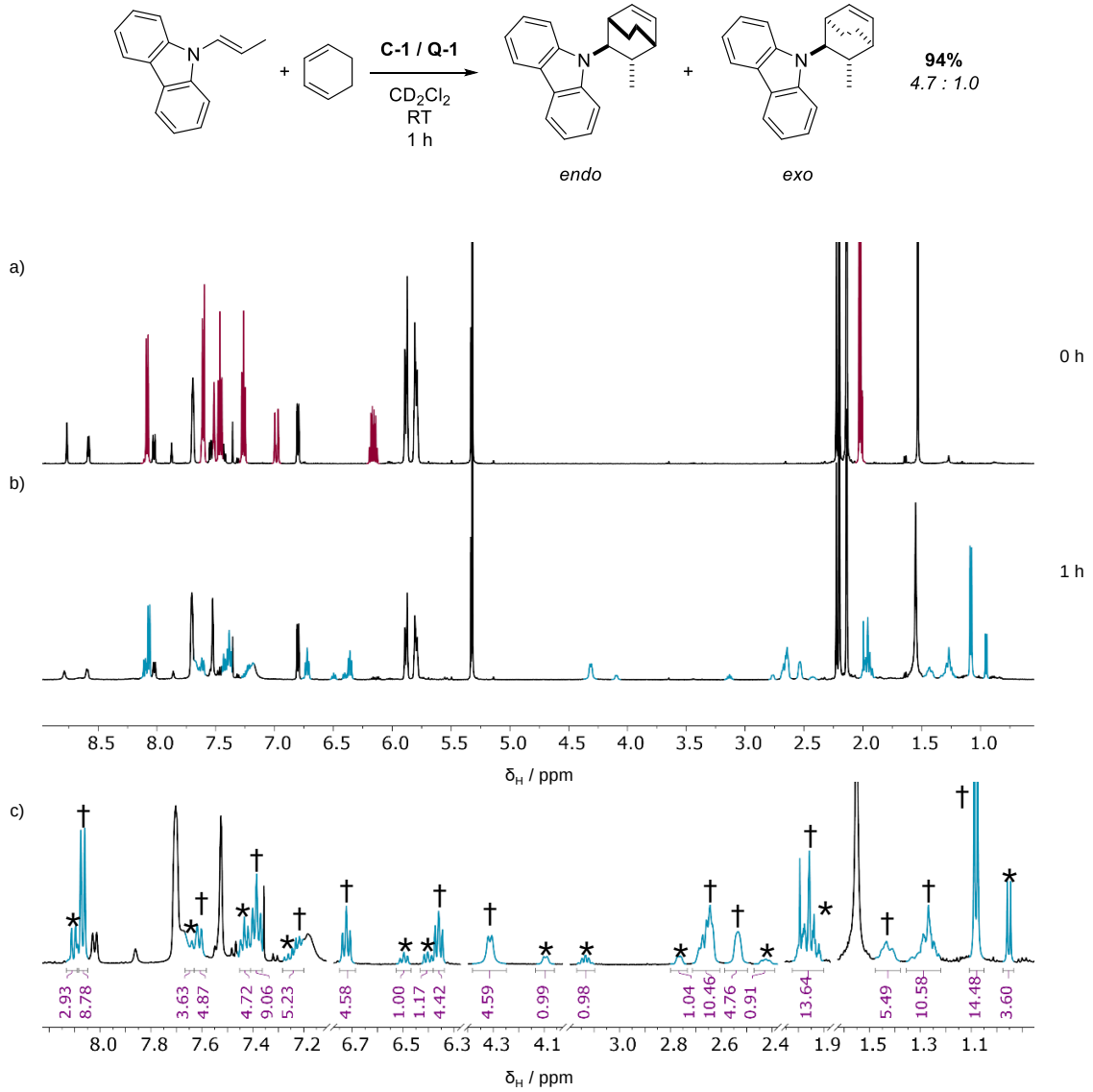

Figure S5: ^{1}H NMR spectra (500 MHz, CD_2Cl_2, 300 K) for the reaction of *trans*-β-methyl-*N*-vinylcarbazole (10 mM) and cyclohexadiene (20 mM) in the presence of **C-1** (0.5 mM) and **Q-1** (0.5 mM). (a) *trans*-β-methyl-*N*-vinylcarbazole, cyclohexadiene and **C-1** at T = 0 h; (b) *trans*-β-methylvinyl-*N*-carbazole, cyclohexadiene, **C-1** and **Q-1** at T = 1 h; (c) Partial ^{1}H NMR spectrum of (b) highlighting cycloadduct peaks. *trans*-β-methyl-*N*-vinylcarbazole is highlighted in red, cycloadducts are highlighted in blue (*endo* product is denoted by †, *exo* product is denoted by *).

3.4 Control Reactions

To ensure all components were essential for reactivity, a variety of different control reactions were carried out using *trans*-anethole and cyclopentadiene as substrates. These followed the above procedure and included the following changes:

- Omitting **C-1**.
- Omitting **Q-1**.
- Omitting **C-1** and **Q-1**.
- Displacing **Q-1** with strongly binding competitive inhibitor, anthraquinone, **Q-10**, (40 eq. wrt **Q-1**).
- Substituting **C-1** with **C-2**.
- Substituting **C-1** and **Q-1** with D_3OBArF.

Where species were omitted, stock solution volumes were replaced with CD_2Cl_2. For the competitive inhibitor reaction, **Q-10** (2.5 mg, 1.2 × 10^{-2} mmol, 2.0 eq.) was also added to the NMR tube prior to

collecting the initial ^{1}H NMR spectrum (*i.e.* prior to addition of **Q-1**). For the D_3OBArF reaction, D_3OBArF was generated *in situ* from DCl (3×10^{-4} mmol, 12 M, 0.05 eq.) and NaBArF (0.3 mg, 3×10^{-4} mmol, 0.05 eq). D_3OBArF was added after the initial ^{1}H NMR spectrum was recorded.

3.4.1 ^{1}H NMR spectra of [4+2] control reactions

3.4.1.1 Omission of components

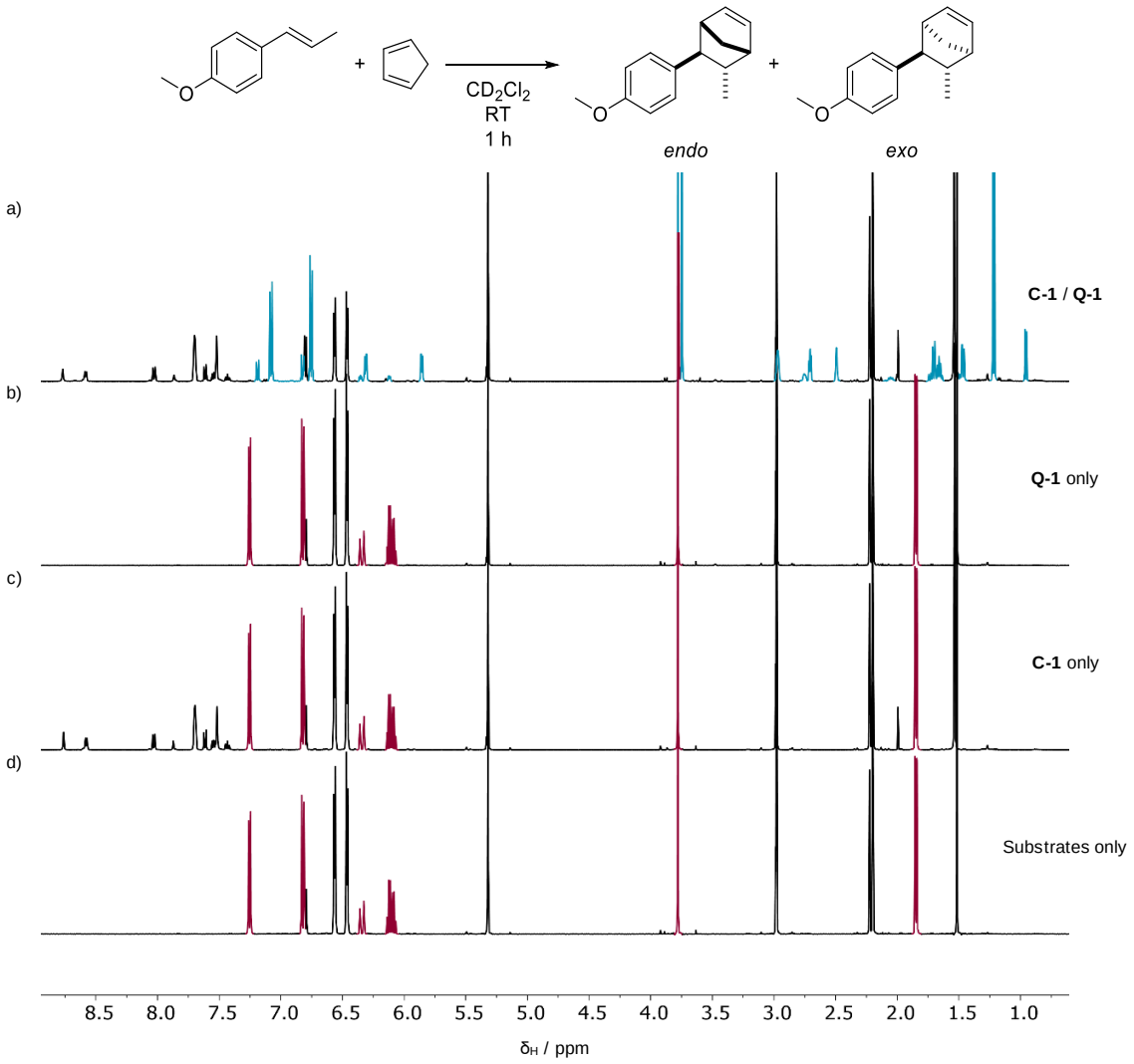

Figure S6: ^{1}H NMR spectra (500 MHz, CD_2Cl_2, 300 K) for the reaction of *trans*-anethole (10 mM) and cyclopentadiene (20 mM) at T = 1 h in the presence of (a) **C-1** (0.5 mM) and **Q-1** (0.5 mM); (b) **Q-1** (0.5 mM); (c) **C-1** (0.5 mM); (d) no additional reagents. *trans*-Anethole is highlighted in red, cycloadducts are highlighted in blue.

3.4.1.2 Competitive inhibitor (**Q-10**): *trans*-anethole, cyclopentadiene, **C-1** and **Q-1**

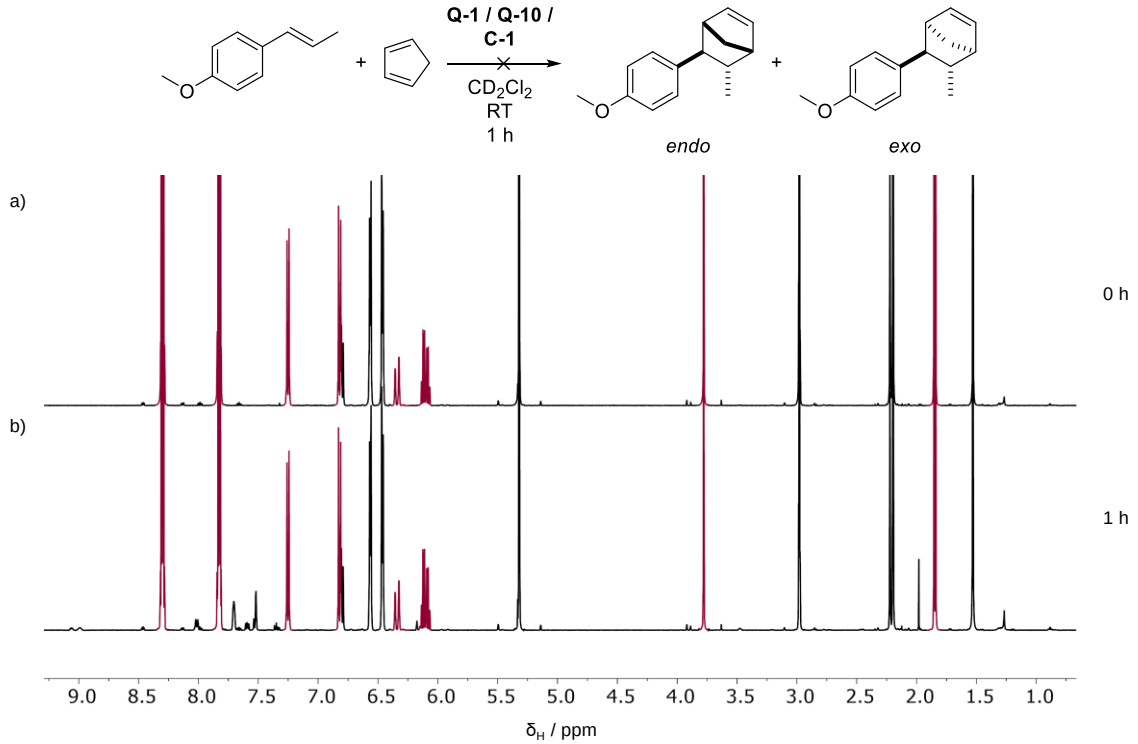

Figure S7: ^{1}H NMR spectra (500 MHz, CD_2Cl_2, 300 K) for the reaction of *trans*-anethole (10 mM) and cyclopentadiene (20 mM) in the presence of **C-1** (0.5 mM), **Q-1** (0.5 mM) and competitive inhibitor **Q-10** (20 mM). (a) *trans*-anethole, cyclopentadiene, **Q-1** and **Q-10** at T = 0 h; (b) *trans*-anethole, cyclopentadiene, **C-1**, **Q-1** and **Q-10** at T = 1 h. *trans*-Anethole is highlighted in red.

3.4.1.3 Cage screening (**C-1** vs **C-2**)

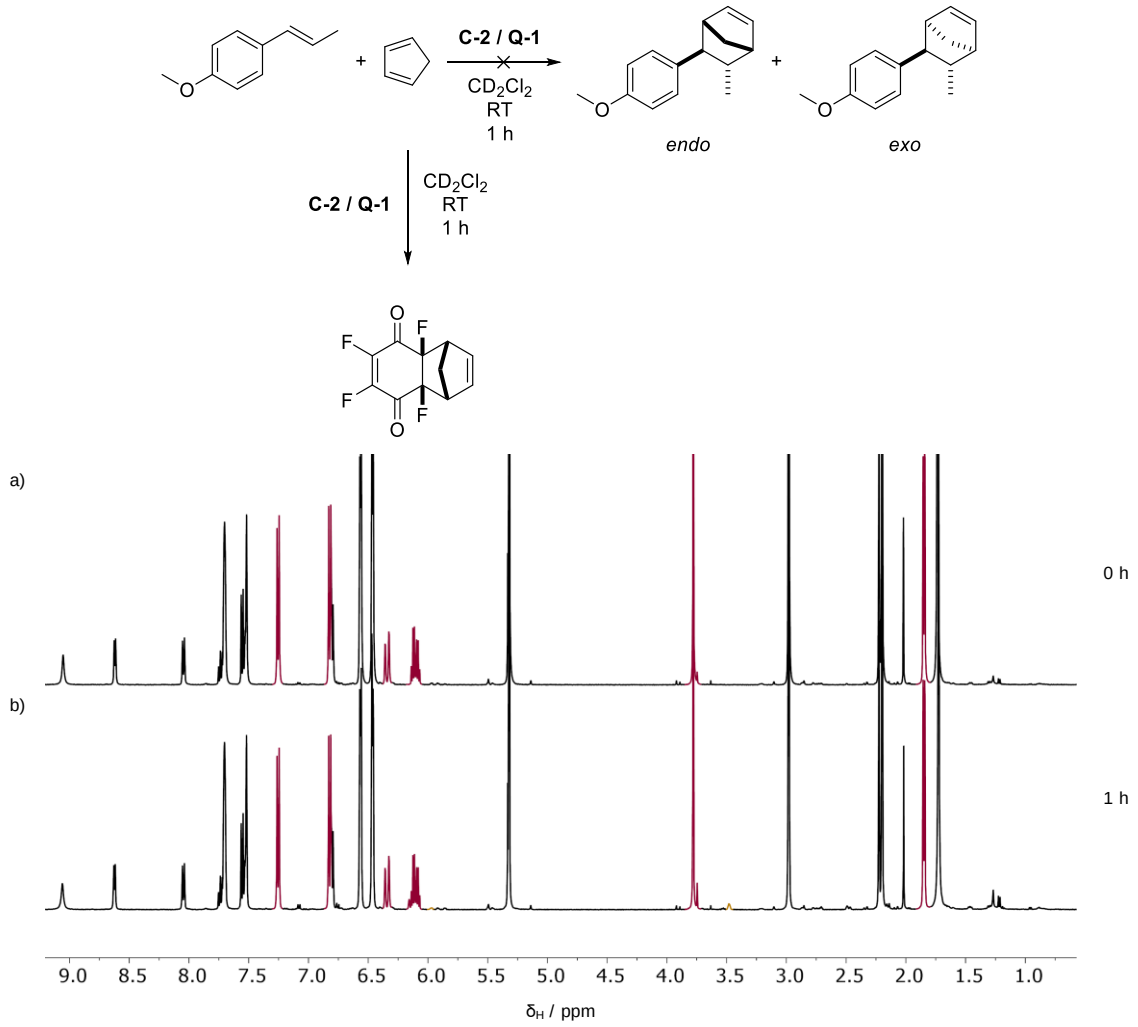

Figure S8: ^{1}H NMR spectra (500 MHz, CD_2Cl_2, 300 K) for the reaction of *trans*-anethole (10 mM) and cyclopentadiene (20 mM) in the presence of **C-2** (0.5 mM) and **Q-1** (0.5 mM). (a) *trans*-anethole, cyclopentadiene and **C-2** at T = 0 h; (b) *trans*-anethole, cyclopentadiene, **C-2** and **Q-1** at T = 1 h. *trans*-Anethole is highlighted in red, **Q-1**-cyclopentadiene cycloadduct is highlighted in yellow.

Switching from **C-1** to **C-2** enables the central cavity to be subtly changed. It was observed that when **C-2** was used rather than **C-1**, there was no formation of the target cycloadducts (Figure S8). Instead, the ^{1}H and ^{19}F NMR spectra showed the formation of new fluorine and proton containing species, which corresponds to the [4+2] cycloaddition of **Q-1** and cyclopentadiene (Figure S8, highlighted in yellow).[7]

3.4.1.3.1 *Discussion of **C-1** and **C-2** catalytic properties: Competitive Anion Binding*

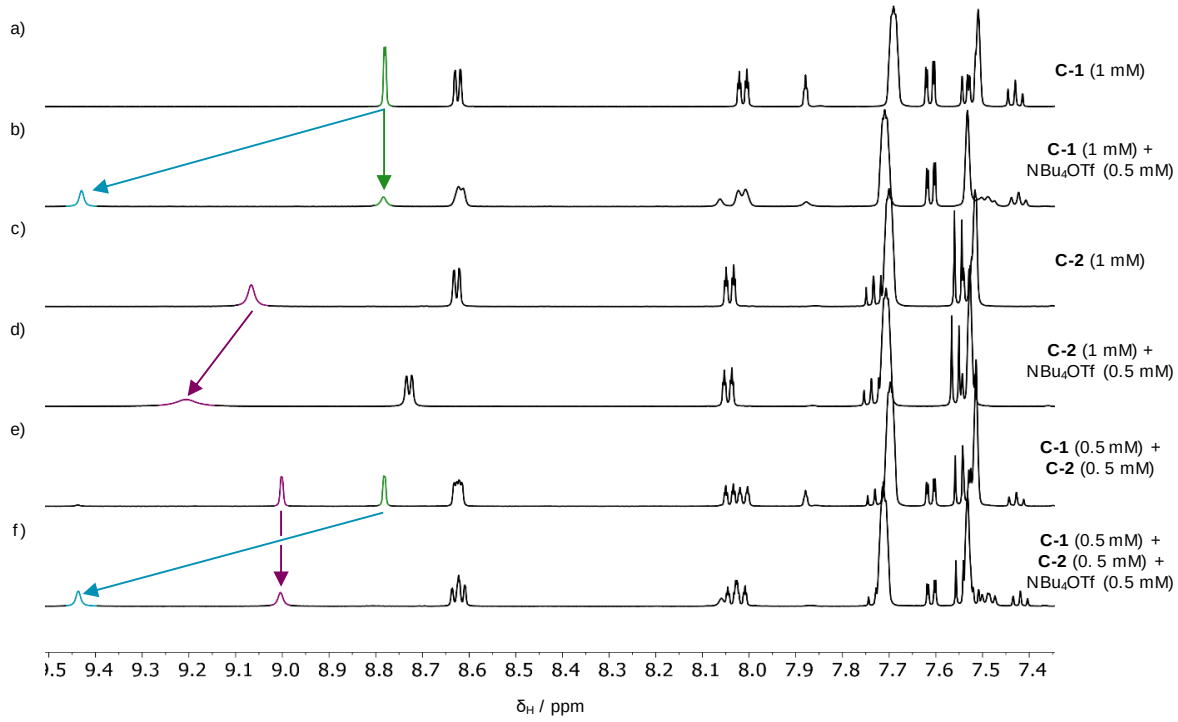

Figure S9: ^{1}H NMR spectra (500 MHz, CD_2Cl_2, 300 K) for (a) **C-1** (1 mM); (b) **C-1** (1 mM) and NBu_4OTf (0.5 mM); (c) **C-2** (1 mM); (d) **C-2** (1 mM) and NBu_4OTf (0.5 mM); (e) **C-1** (0.5 mM) and **C-2** (0.5 mM); (f) **C-1** (0.5 mM), **C-2** (0.5 mM) and NBu_4OTf (0.5 mM). Internal pyridyl protons highlighted for clarity: "empty" **C-1** signals highlighted in green and presence indicated by green arrows, OTf⊂**C-1** signals highlighted in blue and presence indicated by blue arrows and **C-2** signals highlighted in purple and presence indicated by purple arrows.

C-1 and **C-2** show a similar affinity to **Q-1** ($K_{a,\mathbf{C\text{-}1}}$ = 120 M^{-1} vs $K_{a,\mathbf{C\text{-}2}}$ = 60 M^{-1}). As catalysis is triggered by electron transfer (ET) to the neutral bound species, the activity is likely related to the stability of the semiquinone complex. As a comparison, and due to the intrinsic instability of the free semiquinone **Q-1**$^{\bullet-}$, we have assessed the relative anion binding properties **C-1** and **C-2** using the triflate anion. Determination of absolute anion binding has proved highly problematic due to the very high affinity of OTf^- for **C-1**, necessitating the use of a displacement assay. When pentacenedione⊂**C-1** was used ($K_{a,pentacenedione}$ = 10^9 M^{-1}), titration of OTf^- results in immediate precipitation of the cage complex due to exterior ion-pairing of this anion (as the out rate of pentacenedione is slow). Thus, we have pursued a competitive binding experiment using a 1:1 mixture of **C-1** and **C-2** (1:1, 0.5 mM each), to which was added 1 equivalent of OTf^- (0.5 mM). Only the ^{1}H NMR signals for **C-1** are shifted, indicating that OTf^- preferentially binds to **C-1**. This was confirmed by comparing the cages independently. We should also note that OTf^- anion is in slow exchange with **C-1** and fast exchange with **C-2**, providing further evidence of the relative affinities.

3.4.1.4 Testing for hidden Brønsted acid catalysis

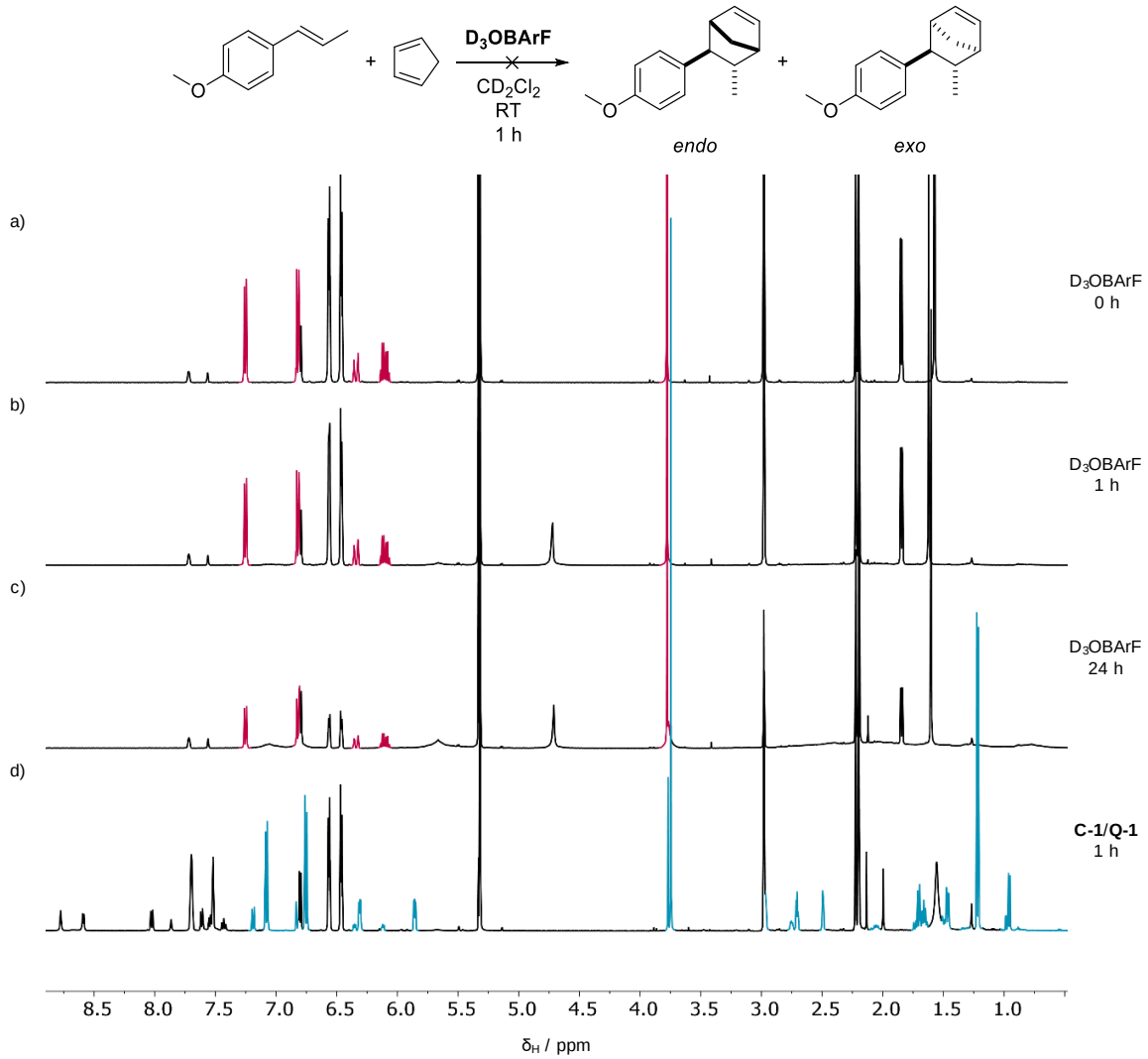

Figure S10: ^{1}H NMR spectra (500 MHz, CD_2Cl_2, 300 K) for the reaction of *trans*-anethole (10 mM) and cyclopentadiene (20 mM) in the presence of D_3OBArF (0.5 mM, generated *in situ* from NaBArF (0.5 mM) and DCl (0.5 mM)). (a) *trans*-anethole, cyclopentadiene and NaBArF at T = 0 h; (b-c) *trans*-anethole, cyclopentadiene, NaBArF and DCl at (b) T = 1 h and (c) T = 24 h. (d) The reaction of *trans*-anethole (10 mM) and cyclopentadiene (20 mM) in the presence of **C-1** (0.5 mM) and **Q-1** (0.5 mM) at T = 1 h. *trans*-Anethole is highlighted in red. cycloadducts are highlighted in blue.

If the reaction proceeds via hidden Brønsted acid catalysis, the active species would be H_3OBArF. By forming D_3OBArF *in situ*, these conditions can be emulated. After 1 h, minimal conversion of *trans*-anethole was observed and no expected product was present – in direct contrast to **C-1**/**Q-1**, where the reaction is completed in 1 h. Leaving the system for 24 h still yielded no discrete products highly indicative **C-1**/**Q-1** does not proceed via a Brønsted acid catalysis mechanism.

3.5 Preparative Scale Reaction

3.5.1 *trans*-Anethole and cyclopentadiene

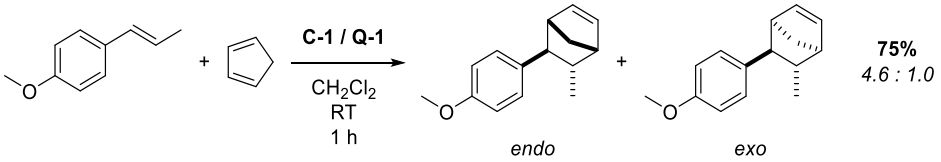

A stock solution of **Q-1** (4.0 mg, 0.022 mmol) in CH_2Cl_2 (4.44 mL) was prepared. *trans*-Anethole (14.8 mg, 0.10 mmol, 1.0 eq.) and **C-1** (23.9 mg, 0.005 mmol, 5 mol%) was dissolved in CH_2Cl_2 (9 mL). The solution was charged with **Q-1** (0.9 mg, 0.005 mmol, 5 mol%, 1 mL). The solution was stirred for 1 h at room temperature. The solvent was removed *in vacuo*. The catalyst was removed using preparative TLC (hexanes/EtOAc, 16.5:1) to give the cycloadducts as a colorless oil (16.1 mg, 0.075 mmol, 75%). **^{1}H NMR (500 MHz, $CDCl_3$) δ_H:** δ 7.23 – 7.16 (m, 2H, *exo*), 7.11 – 7.07 (m, 2H, *endo*), 6.88 – 6.81 (m, 2H, *exo*), 6.81 – 6.75 (m, 2H, *endo*), 6.35 (dd, J = 5.7, 3.1 Hz, 1H, *exo*), 6.32 (dd, J = 5.7, 3.1 Hz, 1H, *endo*), 6.12 (dd, J = 5.7, 2.9 Hz, 1H, *exo*), 5.88 (dd, J = 5.7, 2.8 Hz, 1H, *endo*), 3.80 (s, 3H, *exo*), 3.77 (s, 3H, *exo*), 2.99 – 2.95 (m, 1H, *endo*), 2.80 – 2.77 (m, 1H, *exo*), 2.77 – 2.73 (m, 1H, *exo*), 2.70 (dd, J = 4.8, 3.3 Hz, 1H, *endo*), 2.52 – 2.48 (m, 1H, *endo*), 2.12 – 2.04 (m, 1H, *exo*), 2.00 (dd, J = 5.2, 1.7 Hz, 1H, *endo*), 1.75 (ddd, J = 8.4, 1.9, 1.2 Hz, 1H, *endo*), 1.72 – 1.65 (m, 2H, *exo*), 1.58 – 1.46 (m, 2H, *endo*), 1.22 (d, J = 6.9 Hz, 3H, *endo*), 0.96 (d, J = 6.8 Hz, 3H, *exo*). **^{13}C{^{1}H} NMR (126 MHz, $CDCl_3$) δ_C:** 157.9, 157.8, 138.6, 138.2, 138.0, 137.0, 134.6, 133.8, 128.9, 128.3, 113.9, 113.4, 55.42, 55.36, 52.7, 51.9, 49.7, 49.6, 49.4, 48.0, 47.8, 47.0, 42.5, 41.5, 21.2, 19.6.

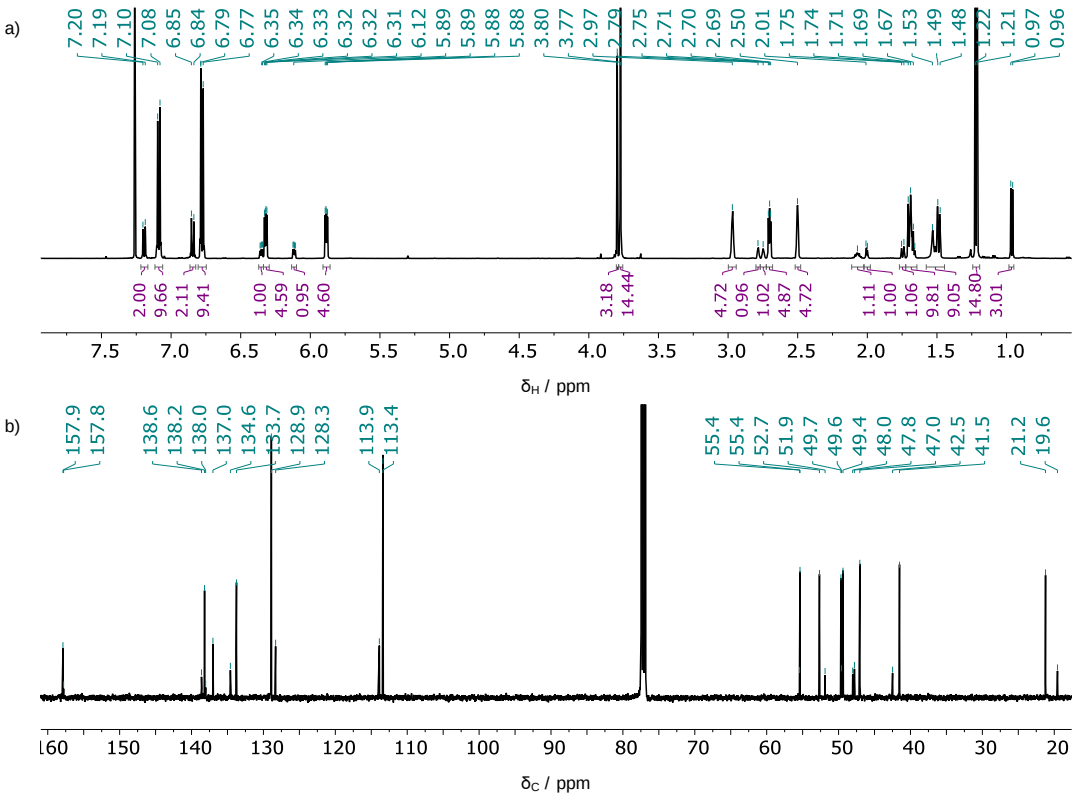

Figure S11: NMR spectra for the cycloadducts isolated from the reaction of *trans*-anethole and cyclopentadiene in the presence of **C-1** and **Q-1**. (a) ^{1}H NMR spectrum (500 MHz, $CDCl_3$, 300 K); (b) ^{13}C{^{1}H} NMR spectrum (126 MHz, CD_3Cl, 300 K).

4 Cage-Quinone Catalyzed [2+2] Homo-Cycloaddition Reactions

4.1 General Procedure

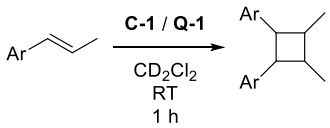

Stock solutions in CD_2Cl_2 were prepared for: 2-fluoromesitylene (internal standard, 1.20 mmol/mL), ene (2.40 mmol/mL), **Q-1** (0.12×10^{-3} mmol/mL) and cage (6.0×10^{-3} mmol/mL).

To CD_2Cl_2 (425 µL), in an NMR tube, was added internal standard (0.4 mg, 3.0×10^{-3} mmol, 0.5 eq., 25 µL), ene (6.0×10^{-3} mmol, 1.0 eq., 25 µL) and **C-1** (1.4 mg, 3.0×10^{-4} mmol, 0.05 eq., 100 µL). The reaction was initiated by addition of **Q-1** (3.0×10^{-4} mmol, 0.05 eq., 25 µL). The reaction was monitored by recording ^{1}H NMR spectra before and 1 hour after the addition of **Q-1**. Product yields were calculated by comparing integrals of the starting material and product[s] to that of the internal standard.

4.2 Product Identification

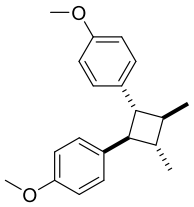

For the [2+2] cycloaddition of *trans*-anethole the product of the NMR scale reaction was identified (and thereby the yield was calculated) by comparing the spectra to previously reported ^{1}H NMR spectroscopic data. This was sourced from *Chem. Sci.*, **2012**, 3, 2807–2811.

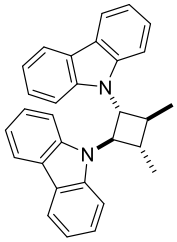

For the [2+2] cycloaddition of *trans*-β-methyl-*N*-vinylcarbazole, no previously reported ^{1}H NMR spectroscopic data was available, therefore a preparative scale reaction was completed to isolate the products (See Section 4.4.1).

4.3 ^{1}H NMR spectra of homo-[2+2] catalyzed reactions

4.3.1 *trans*-Anethole

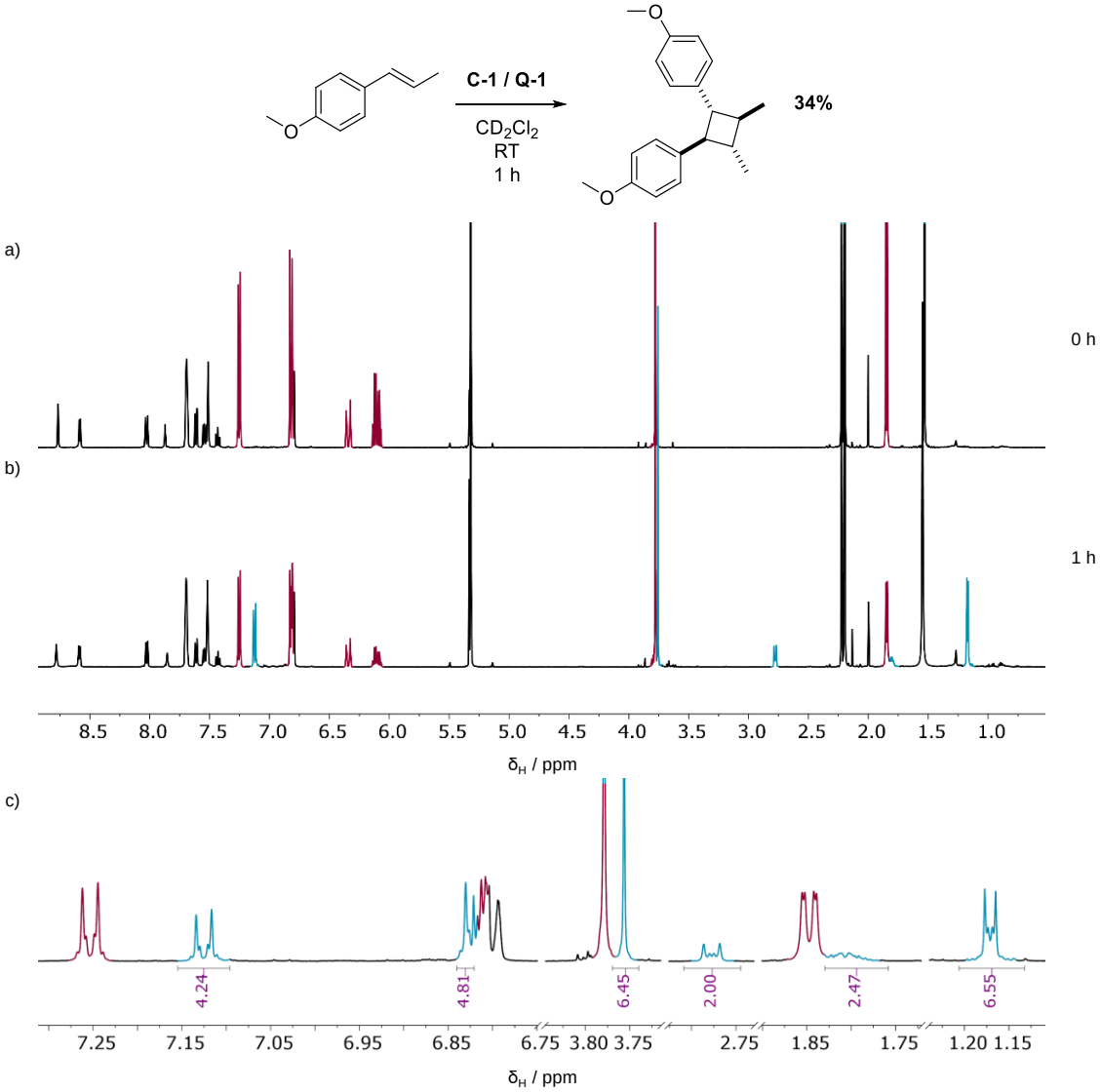

Figure S12: ^{1}H NMR spectra (500 MHz, CD_2Cl_2, 300 K) for the reaction of *trans*-anethole (10 mM) in the presence of **C-1** (0.5 mM) and **Q-1** (0.5 mM). (a) *trans*-anethole and **C-1** at T = 0 h; (b) *trans*-anethole, **C-1** and **Q-1** at T = 1 h; (c) Partial ^{1}H NMR spectrum of (b) highlighting cycloadduct peaks. *trans*-Anethole is highlighted in red, cycloadduct is highlighted in blue.

4.3.2 *trans*-β-Methyl-*N*-vinylcarbazole

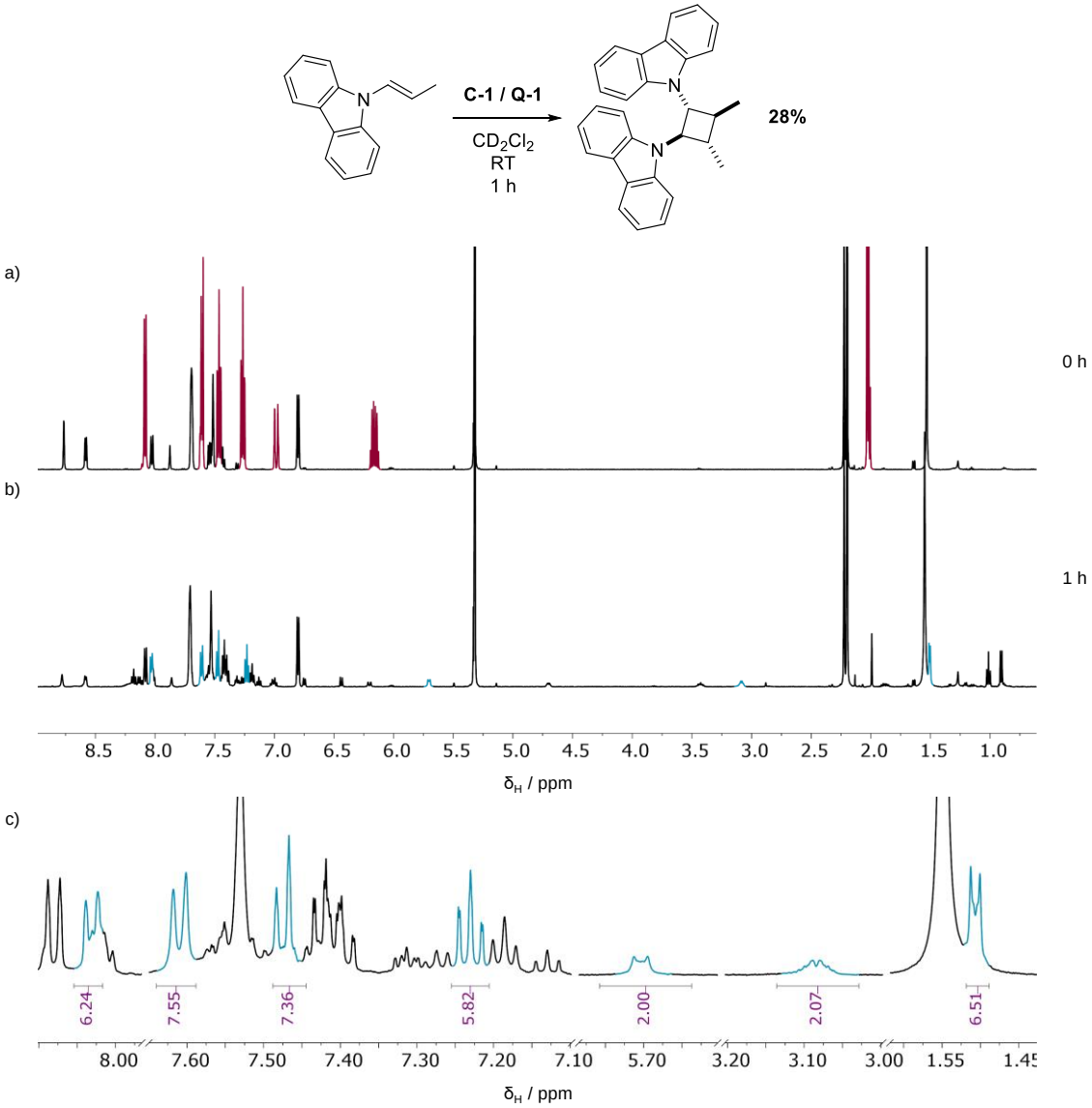

Figure S13: ^{1}H NMR spectra (500 MHz, CD_2Cl_2, 300 K) for the reaction of *trans*-β-methyl-*N*-vinylcarbazole (10 mM) in the presence of **C-1** (0.5 mM) and **Q-1** (0.5 mM). (a) *trans*-β-methyl-*N*-vinylcarbazole and **C-1** at T = 0 h; (b) *trans*-β-methyl-*N*-vinylcarbazole, **C-1** and **Q-1** at T = 1 h; (c) Partial ^{1}H NMR spectrum of (b) highlighting cycloadduct peaks. *trans*-β-methyl-*N*-vinylcarbazole is highlighted in red, cycloadduct is highlighted in blue.

4.4 Control Reaction

To ensure all components were essential for reactivity, the [2+2] cycloaddition was repeated with the substitution of **C-1** with **C-2** using *trans*-anethole as the substrate following the above procedure. As **C-2** catalyzes the background Diels-Alder reaction between **Q-1** and cyclopentadiene, this allowed the ability of **C-2** to mediate electron transfer to *trans*-anethole to be explored. No reactivity was observed (see Section 3.4.1.3 for more details).

4.4.1 ^{1}H NMR spectra of [2+2] control reaction

4.4.1.1 Cage screening (**C-1** vs **C-2**)

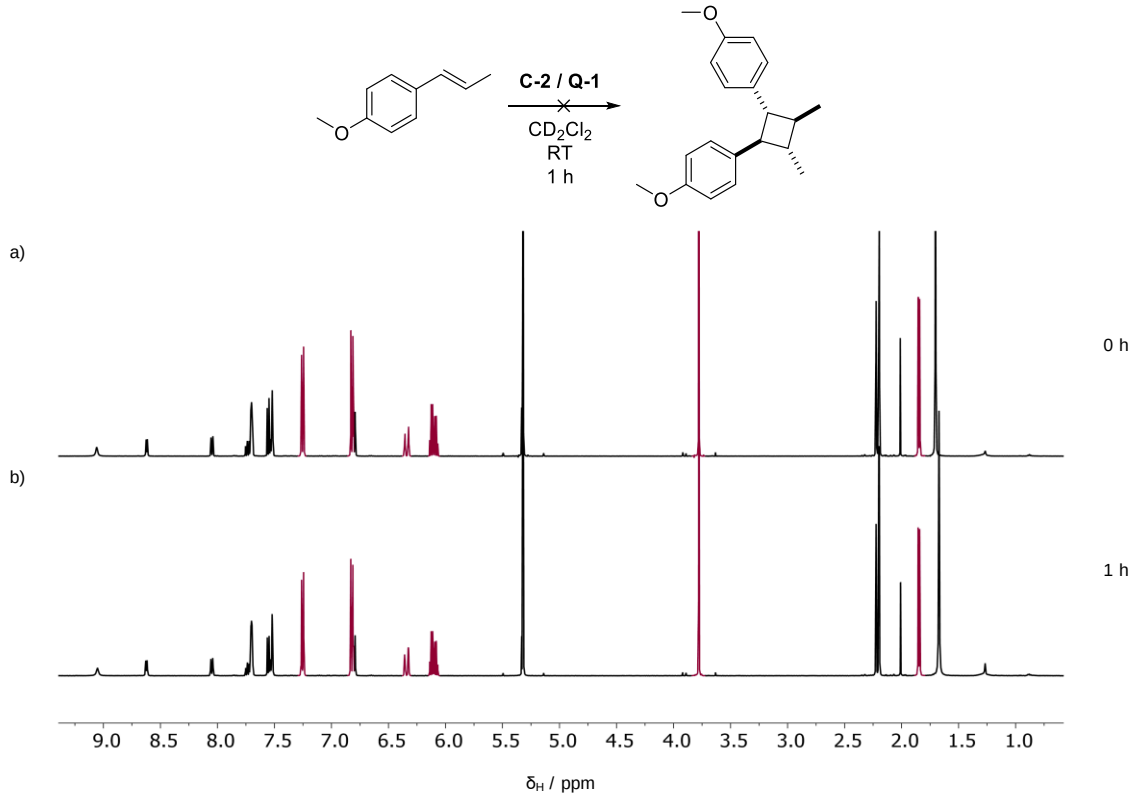

Figure S14: ^{1}H NMR spectra (500 MHz, CD_2Cl_2, 300 K) for the reaction of *trans*-anethole (10 mM) in the presence of **C-2** (0.5 mM) and **Q-1** (0.5 mM). (a) *trans*-anethole and **C-2** at T = 0 h; (b) *trans*-anethole, **C-2** and **Q-1** at T = 1 h. *trans*-Anethole is highlighted in red.

4.5 Preparative Scale Reaction

4.5.1 *trans*-β-Methyl-*N*-vinylcarbazole

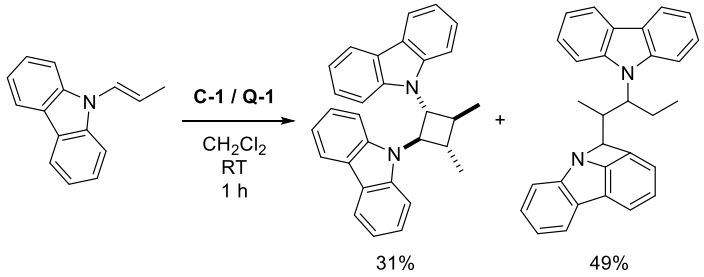

A stock solution of **Q-1** (4.0 mg, 0.022 mmol) in CH_2Cl_2 (4.44 mL) was prepared. *trans*-β-Methyl-*N*-vinylcarbazole (20.7 mg, 0.10 mmol, 1.0 eq.) and **C-1** (23.9 mg, 0.005 mmol, 5 mol%) was dissolved in CH_2Cl_2 (9 mL). The solution was charged with **Q-1** (0.9 mg, 0.005 mmol, 5 mol%, 1 mL). The solution was stirred for 1 h at room temperature. The solvent was removed *in vacuo*. The catalyst was removed using preparative TLC (hexanes/EtOAc, 9:1) to give a mixture of products as a colorless solid (16.6 mg, 0.040 mmol, 80%). **^{1}H NMR (500 MHz, $CDCl_3$) δ_H:** 8.03 (ddd, *J* = 7.7, 1.3, 0.7 Hz, 4H), 7.58 (dt, *J* = 8.4, 0.8 Hz, 4H), 7.39 (ddd, *J* = 8.4, 7.2, 1.3 Hz, 4H), 7.19 (ddd, *J* = 7.9, 7.2, 0.9 Hz, 4H), 5.74–5.71 (m, 2H), 3.12–3.03 (m, 2H), 1.52–1.49 (m, 6H); **^{13}C{^{1}H} NMR (126 MHz, $CDCl_3$) δ_C:** 140.5, 125.9, 123.7, 120.6, 119.4, 109.6, 59.0, 37.4, 19.5; **HRMS (EI):** $C_{30}H_{26}N_2$ [M]$^{\cdot+}$ found 414.20781, requires 414.20905.

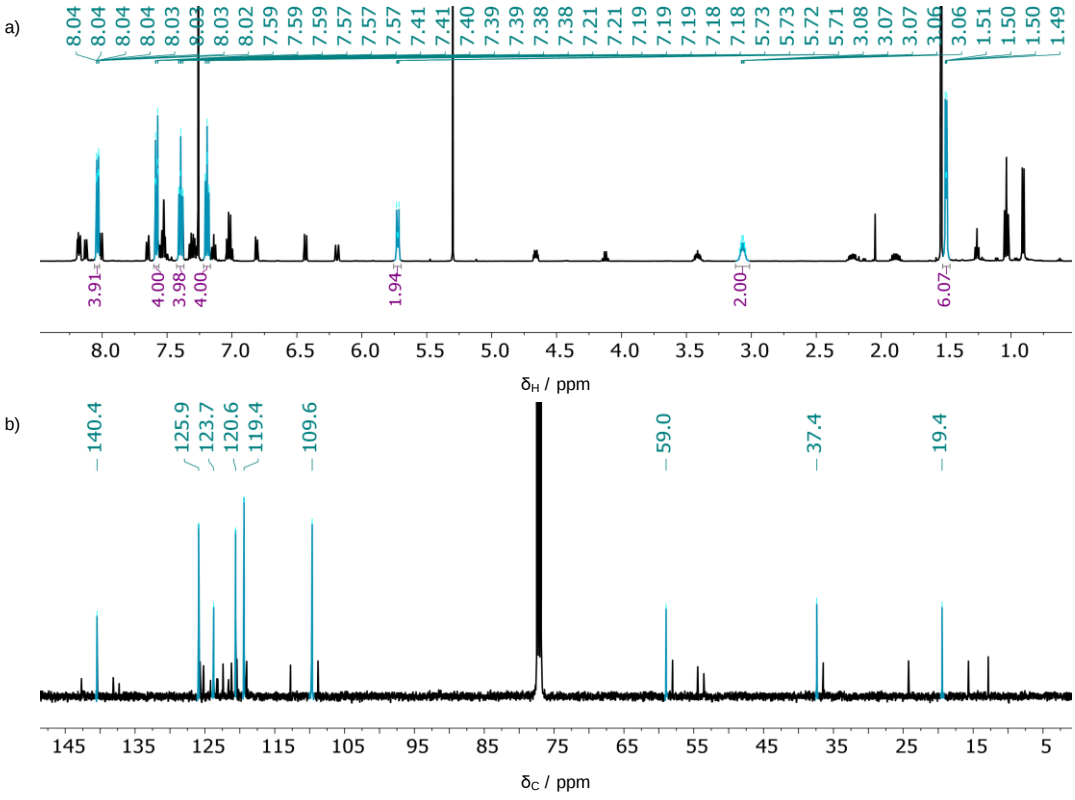

Figure S15: NMR spectra for the species isolated from the reaction of *trans*-β-methyl-*N*-vinylcarbazole in the presence of **C-1** and **Q-1**. [2+2] cycloadduct highlighted in blue. (a) ^{1}H NMR spectrum (500 MHz, $CDCl_3$, 300 K); (b) ^{13}C{^{1}H} NMR spectrum (126 MHz, CD_3Cl, 300 K).

5 Cage-Quinone Catalyzed [2+2] Hetero-Cycloaddition Reactions

5.1 β-Methylstyrene Reactions

5.1.1 General Procedure

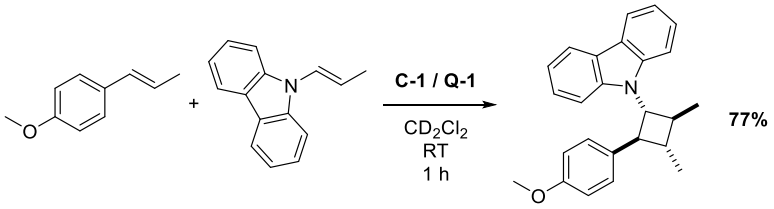

Stock solutions in CD_2Cl_2 were prepared for: 2-fluoromesitylene (internal standard, 1.20 mmol/mL), *trans*-β-methyl-*N*-vinylcarbazole (2.40 mmol/mL), *trans*-anethole (2.40 mmol/mL), **Q-1** (0.12×10^{-3} mmol/mL) and **C-1** (6.0×10^{-3} mmol/mL).

To CD_2Cl_2 (250 µL), in an NMR tube, was added internal standard (0.4 mg, 3.0×10^{-3} mmol, 0.5 eq., 25 µL), *trans*-β-methyl-*N*-vinylcarbazole (6.0×10^{-3} mmol, 1.0 eq., 25 µL), *trans*-anethole (3.0×10^{-2} mmol, 5.0 eq., 175 µL) and **C-1** (1.4 mg, 3.0×10^{-4} mmol, 0.05 eq., 100 µL). The reaction was initiated by addition of **Q-1** (3.0×10^{-4} mmol, 0.05 eq., 25 µL). The reaction was monitored by recording ^{1}H NMR spectra before and 1 hour after the addition of **Q-1**. Product yields were calculated by comparing integrals of the starting material and product[s] to that of the internal standard.

5.2 Product Identification

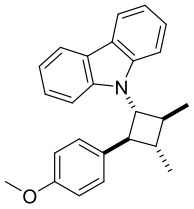

The product of the reaction between *trans*-anethole and *trans*-β-methyl-*N*-vinylcarbazole was identified (and thereby the yield was calculated) by comparing the spectra to previously reported ^{1}H NMR spectroscopic data. The source for this data is *Adv. Synth. Catal.*, **2001**, 343, 481–489.

5.2.1 ^{1}H NMR spectra of hetero-[2+2] catalyzed reaction

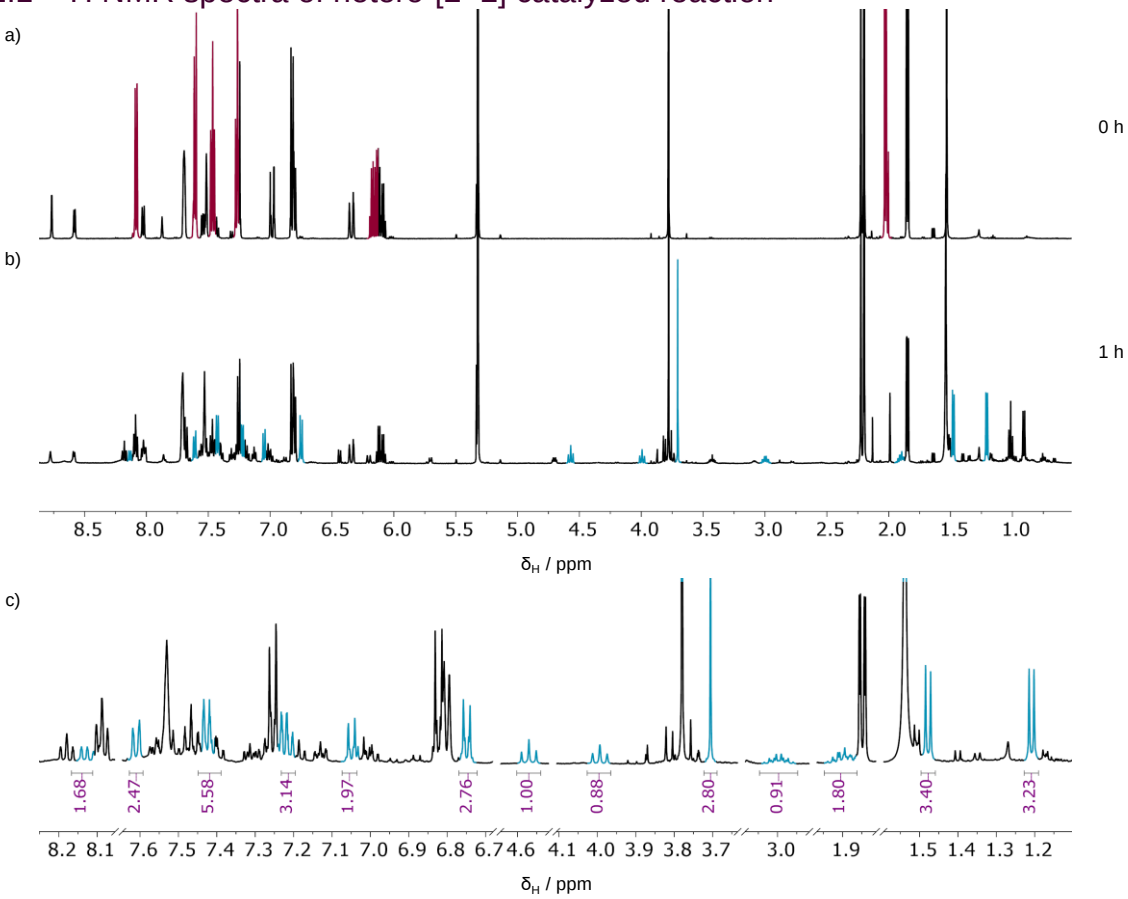

Figure S16: ^{1}H NMR spectra (500 MHz, CD_2Cl_2, 300 K) for the reaction of *trans*-β-methyl-*N*-vinylcarbazole (10 mM) and *trans*-anethole (50 mM) in the presence of **C-1** (0.5 mM) and **Q-1** (0.5 mM). (a) *trans*-anethole, *trans*-β-methyl-*N*-vinylcarbazole and **C-1** at T = 0 h; (b) *trans*-anethole, *trans*-β-methyl-*N*-vinylcarbazole, **C-1** and **Q-1** at T = 1 h; (c) Partial ^{1}H NMR spectrum of (b) highlighting cycloadduct peaks. *trans*-β-Methyl-*N*-vinylcarbazole is highlighted in red, cycloadduct is highlighted in blue.

5.3 *trans*-Anethole and Styrenes

5.3.1 General Procedure

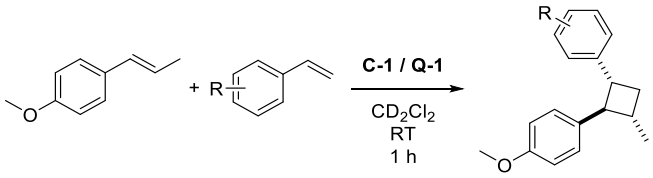

Stock solutions in CD_2Cl_2 were prepared for: 2-fluoromesitylene (internal standard, 1.20 mmol/mL), *trans*-anethole (2.40 mmol/mL), styrene derivative (24.0 mmol/mL), **Q-1** (0.12×10^{-3} mmol/mL) and **C-1** (6.0×10^{-3} mmol/mL).

To CD_2Cl_2 (400 µL), in an NMR tube, was added internal standard (0.4 mg, 3.0×10^{-3} mmol, 0.5 eq., 25 µL), *trans*-anethole (6.0×10^{-3} mmol, 1.0 eq., 25 µL), styrene derivative (6.0×10^{-2} mmol, 10.0 eq., 25 µL) and **C-1** (1.4 mg, 3.0×10^{-4} mmol, 0.05 eq., 100 µL). The reaction was initiated by addition of **Q-1** (3.0×10^{-4} mmol, 0.05 eq., 25 µL). The reaction was monitored by recording ^{1}H NMR spectra before and 1 hour after the addition of **Q-1**. Product yields were calculated by comparing integrals of the starting material and product[s] to that of the internal standard.

5.4 Product Identification

The products of each NMR scale reaction were identified (and thereby yields calculated) by comparing the spectra to previously reported ^{1}H NMR spectroscopic data. The sources for this data are listed below:

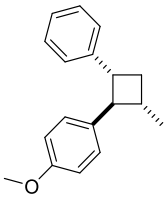

Chem. Sci., **2012**, 3, 2807–2811

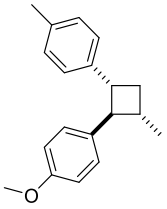

Chem. Sci., **2012**, 3, 2807–2811

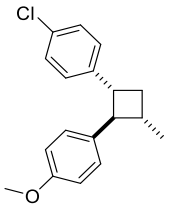

Chem. Sci., **2012**, 3, 2807–2811

5.4.1 ^{1}H NMR spectra of hetero-[2+2] catalyzed reactions

5.4.1.1 *trans*-Anethole and styrene

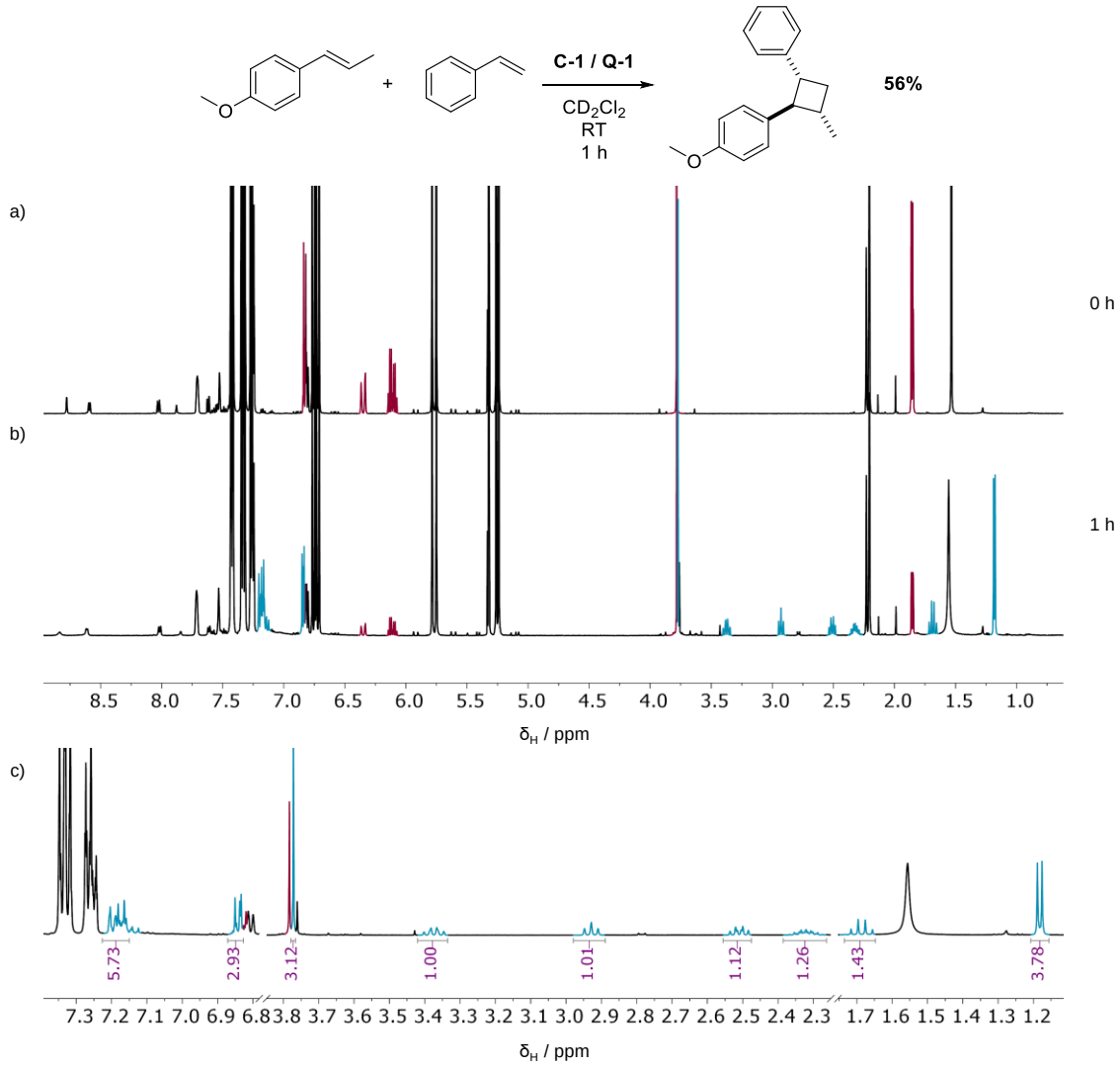

Figure S17: ^{1}H NMR spectra (500 MHz, CD_2Cl_2, 300 K) for the reaction of *trans*-anethole (10 mM) and styrene (100 mM) in the presence of **C-1** (0.5 mM) and **Q-1** (0.5 mM). (a) *trans*-anethole, styrene and **C-1** at T = 0 h; (b) *trans*-anethole, styrene, **C-1** and **Q-1** at T = 1 h; (c) Partial ^{1}H NMR spectrum of (b) highlighting cycloadduct peaks. *trans*-Anethole is highlighted in red, cycloadduct is highlighted in blue.

5.4.1.2 *trans*-Anethole and *p*-methylstyrene

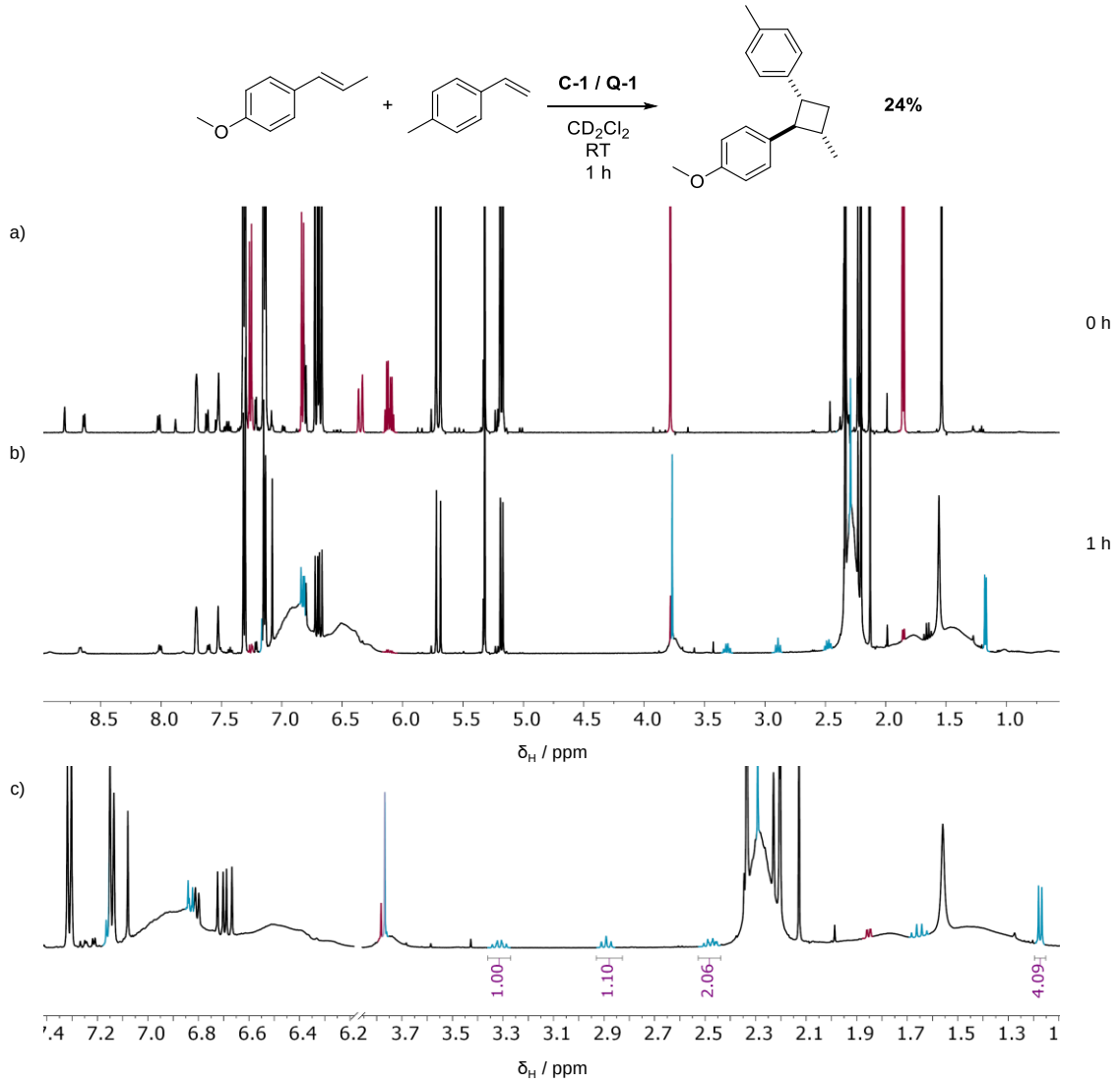

Figure S18: ^{1}H NMR spectra (500 MHz, CD_2Cl_2, 300 K) for the reaction of *trans*-anethole (10 mM) and *p*-methylstyrene (100 mM) in the presence of **C-1** (0.5 mM) and **Q-1** (0.5 mM). (a) *trans*-anethole, *p*-methylstyrene and **C-1** at T = 0 h; (b) *trans*-anethole, *p*-methylstyrene, **C-1** and **Q-1** at T = 1 h; (c) Partial ^{1}H NMR spectrum of (b) highlighting cycloadduct peaks. *trans*-Anethole is highlighted in red, cycloadduct is highlighted in blue.

5.4.1.3 *trans*-Anethole and *p*-chlorostyrene

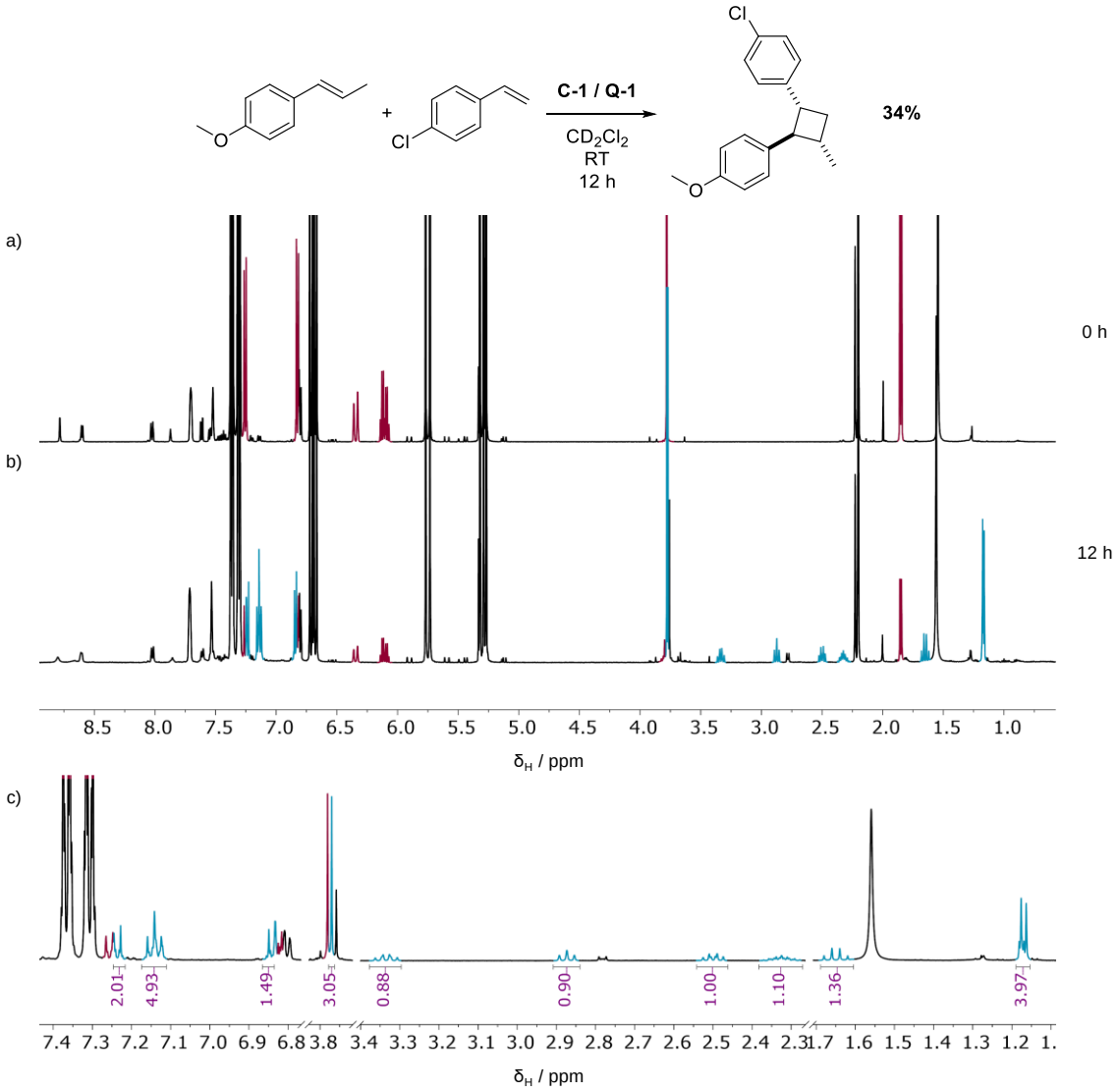

Figure S19: ^{1}H NMR spectra (500 MHz, CD_2Cl_2, 300 K) for the reaction of *trans*-anethole (10 mM) and *p*-chlorostyrene (100 mM) in the presence of **C-1** (0.5 mM) and **Q-1** (0.5 mM). (a) *trans*-anethole, *p*-chlorostyrene and **C-1** at T = 0 h; (b) *trans*-anethole, *p*-chlorostyrene, **C-1** and **Q-1** at T = 1 h; (c) Partial ^{1}H NMR spectrum of (b) highlighting cycloadduct peaks. *trans*-Anethole is highlighted in red, cycloadduct is highlighted in blue.

6 Reaction Optimisation for Cage-Quinone Catalyzed [4+2] Cycloaddition of *trans*-anethole and cyclopentadiene

The reaction between *trans*-anethole and isoprene was used to probe optimal cage/quinone/substrate ratios. Initially **C-1** and **Q-1** concentrations were kept constant (1 mM) and the concentrations of *trans*-anethole and isoprene were increased to give an overall effect of reduced catalyst loading (Table S1, entries 1–3). This decreased catalyst loading/increased *trans*-anethole and isoprene concentrations was accompanied by lower yields of [4+2] cycloadduct yet increased preference for the [2+2] homodimer and incomplete consumption of the starting material. Keeping the **C-1** and *trans*-anethole concentrations constant (1 mM and 100 mM respectively) and increasing the **Q-1** concentration 10-fold (entries 3 vs 4) improved the conversion to the [4+2] product, whilst not impacting the yield for the [2+2] homodimer. This is attributed to the higher loading of **Q-1** shifting the equilibrium towards more **Q-1⊂C-1**. The *trans*-anethole/isoprene concentrations were also kept constant and the **C-1** and **Q-1** concentrations were dropped equally, maintaining a 1:1 ratio (Table S1, entries 5 and 6). Notably, 5 mol% total catalyst loading gave a slightly improved yield compared to 10 mol% (Table S1, entries 1 vs 5). However, dropping to 1 mol% led to incomplete consumption of the *trans*-anethole and again more [2+2] cycloadduct. Decreasing the ratio of **C-1** to **Q-1** was also investigated at fixed substrate concentrations (entries 7 and 8). At 10 mol% **Q-1**, the reaction appears quite insensitive to **C-1** loading; this can be decreased to 1 mol% with minimal reduction in product yield.

Table S1: C-1 and **Q-1** reaction optimisation for the [4 + 2] cycloaddition of *trans*-anethole (1 eq.) and isoprene (2 eq.)

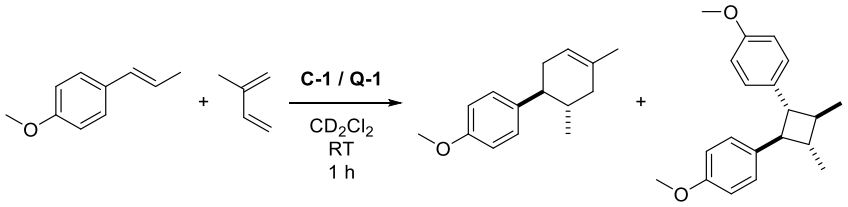

Entry	**[C-1]** / mM (Loading / mol%)	**[Q-1]** / mM (Loading / mol%)	[*trans*-Anethole] / mM	[4+2] Yield / %[a]	[2+2] Yield / %[a]	*trans*-Anethole / %[a]
1	1.0 (10)	1.0 (10)	10	89	3	1
2	1.0 (2)	1.0 (2)	50	67	11	3
3	1.0 (1)	1.0 (1)	100	53	12	10
4	1.0 (1)	10.0 (10)	100	77	11	2
5	0.5 (5)	0.5 (5)	10	92	5	3
6	0.1 (1)	0.1 (1)	10	62	12	26
7	0.5 (5)	1.0 (10)	10	84	9	7
8	0.1 (1)	1.0 (10)	10	78	11	3

[a] Yield calculated using ^{1}H NMR spectroscopy at 1 h.

7 Quinone Scope for Cage-Quinone Catalyzed [4+2] Cycloaddition of *trans*-anethole and cyclopentadiene

7.1 General Procedure

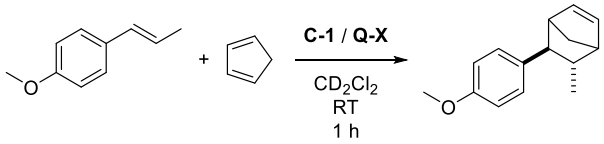

Stock solutions in CD_2Cl_2 were prepared for: 2-fluoromesitylene (internal standard, 1.20 mmol/mL), dienophile (2.40 mmol/mL), diene (4.80 mmol/mL), *p*-quinone (0.12×10^{-3} mmol/mL) and **C-1** (6.0×10^{-3} mmol/mL).

To CD_2Cl_2 (400 µL), in an NMR tube, was added internal standard (0.4 mg, 3.0×10^{-3} mmol, 0.5 eq., 25 µL), dienophile (6.0×10^{-3} mmol, 1.0 eq., 25 µL), diene (1.2×10^{-2} mmol, 2.0 eq., 25 µL) and *p*-quinone (3.0×10^{-4} mmol, 0.05 eq., 25 µL). The reaction was initiated by addition of **C-1** (1.4 mg, 3.0×10^{-4} mmol, 0.05 eq., 100 µL). The reaction was monitored by recording ^{1}H NMR spectra before and 1 hour after the addition of **C-1**. Product yields were calculated by comparing integrals of the starting material and product[s] to that of the internal standard.

Table S2: Quinone scope for the reaction between *trans*-anethole and cyclopentadiene using **C-1** (5 mol%) and varying **Q-X** (5 mol%)

Entry	Quinone	Yield / %[a]	*Endo* : *Exo*	Entry	Quinone	Yield / %[a]	*Endo* : *Exo*
1	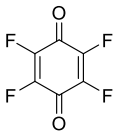 **Q-1**	99	4.8 : 1.0	*6*	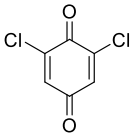 **Q-6**	5 (16)	4.7 : 1.0 (4.5 : 1.0)
2	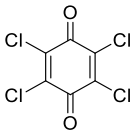 **Q-2**	96	4.8 : 1.0	*7*	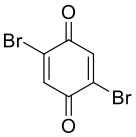 **Q-7**	4 (16)	4.3 : 1.0 (4.5 : 1.0)
3	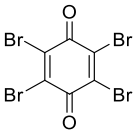 **Q-3**	99	4.6 : 1.0	*8*	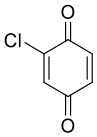 **Q-8**	0	n/a
4	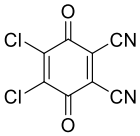 **Q-4**	94	3.6 : 1.0	*9*	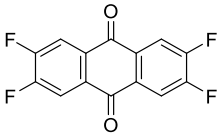 **Q-9**	0	n/a
5	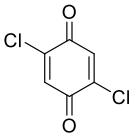 **Q-5**	5 (22)	4.6 : 1.0 (4.8 : 1.0)	*10*	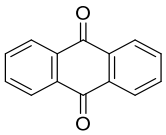 **Q-10**	0	n/a

[a] Yield calculated using ^{1}H NMR spectroscopy at 1 h. Values in parentheses calculated at 24 h.

7.2 ^{1}H NMR spectra of [4+2] catalyzed reactions

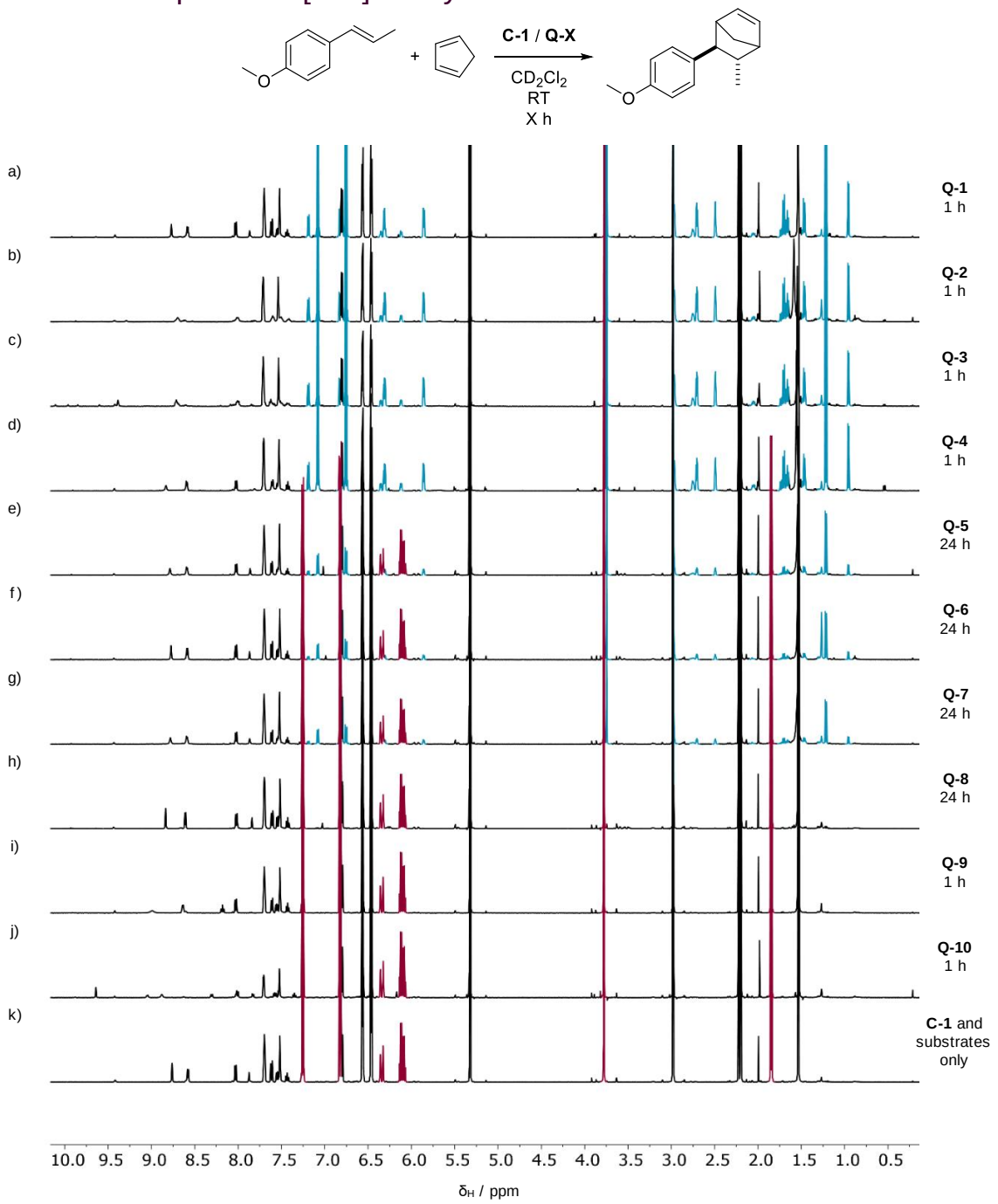

Figure S20: ^{1}H NMR spectra (500 MHz, CD_2Cl_2, 300 K) for the reaction of *trans*-anethole (10 mM) and cyclopentadiene (20 mM) in the presence of **C-1** (0.5 mM) and **Q-X** (0.5 mM). Each sample contains *trans*-anethole, cyclopentadiene, **C-1** and (a) **Q-1** at T = 1 h; (b) **Q-2** at T = 1 h; (c) **Q-3** at T = 1 h; (d) **Q-4** at T = 1 h; (e) **Q-5** at T = 24 h; (f) **Q-6** at T = 24 h; (g) **Q-7** at T = 24 h; (h) **Q-8** at T = 24 h; (i) **Q-9** at T = 1 h; (j) **Q-10** at T = 1 h; (k) **C-1** and substrates only. *trans*-Anethole is highlighted in red, cycloadducts are highlighted in blue.

7.3 Control Reactions

To ensure each *p*-quinone was not active in the absence of **C-1**, all of the reactions were repeated with **C-1** omitted using *trans*-anethole and cyclopentadiene as substrates. These followed the above procedure and included replacing the **C-1** stock solution volume with CD_2Cl_2. In all cases, no reactivity was observed.

8 **C-1**/**Q-4** Catalyzed [4+2] Cycloaddition of Cyclohexadiene

8.1 General Procedure

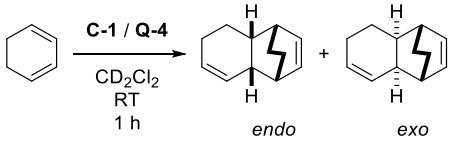

Stock solutions in CD_2Cl_2 were prepared for: 2-fluoromesitylene (internal standard, 1.20 mmol/mL), cyclohexadiene (2.40 mmol/mL), **Q-4** (0.12×10^{-3} mmol/mL) and **C-1** (6.0×10^{-3} mmol/mL).

To CD_2Cl_2 (425 µL), in an NMR tube, was added internal standard (0.4 mg, 3.0×10^{-3} mmol, 0.5 eq., 25 µL), cyclohexadiene (6.0×10^{-3} mmol, 1.0 eq., 25 µL) and **C-1** (1.4 mg, 3.0×10^{-4} mmol, 0.05 eq., 100 µL). The reaction was initiated by addition of **Q-4** (3.0×10^{-4} mmol, 0.05 eq., 25 µL). The reaction was monitored by recording ^{1}H NMR spectra before and 1 hour after the addition of **Q-4**. Product yields were calculated by comparing integrals of the starting material and product[s] to that of the internal standard.

Control reactions were run following the above procedure but included the following changes:

- Omitting **C-1**.
- Omitting **C-1** and **Q-4**.
- Using **Q-1** in lieu of **Q-4**.

Where species were omitted, stock solution volumes were replaced with CD_2Cl_2.

Table S3: Effect of altering **Q-X** (0.5 mM) and increasing **C-1** loading for the [4+2] cycloaddition of cyclohexadiene (20 mM).

Entry	Quinone	Cage	Yield cyclohexadiene dimer / %[a]	*Endo* : *Exo*	Cyclohexadiene / %[a]	Yield **Q-X**-cyclohexadiene adduct / %[a][b]
1	**Q-4**	**C-1**	32	4.7 : 1.0	61	2
2	**Q-4**	-	0	-	96	3
3	**Q-1**	**C-1**	0	-	98	0
4	**Q-1**	-	0	-	98	0.4
5	-	**C-1**	0	-	100	-
6	-	-	0	-	100	-

[a] Yield calculated using ^{1}H NMR spectroscopy at 1 h. [b] Calculated with respect to cyclohexadiene

8.2 Product Identification

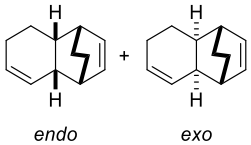

The products of each NMR scale reaction were identified (and thereby yields calculated) by comparing to previously reported ^{1}H NMR spectroscopic data. The source for this data is *J. Am. Chem. Soc.*, **1987**, 109, 1157–1160.

8.2.1 **Q-1**-cyclohexadiene cycloadduct

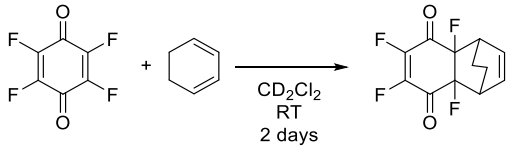

p-Fluoranil (1.1 mg, 6 × 10^{-3} mmol, 1 eq.) and cyclohexadiene (1.0 mg, 1.2 × 10^{-2} mmol, 2 eq.) were added to CD_2Cl_2 (600 µL). The reaction was left for 2 days. The product was characterised without isolation or further purification. **^{1}H NMR (500 MHz, CD_2Cl_2) δ_H:** δ 6.23 (ddt, J = 4.6, 2.8, 1.3 Hz, 2H), 3.41 – 3.31 (m, 2H), 2.20 – 2.15 (m, 2H), 1.41 – 1.34 (m, 2H).

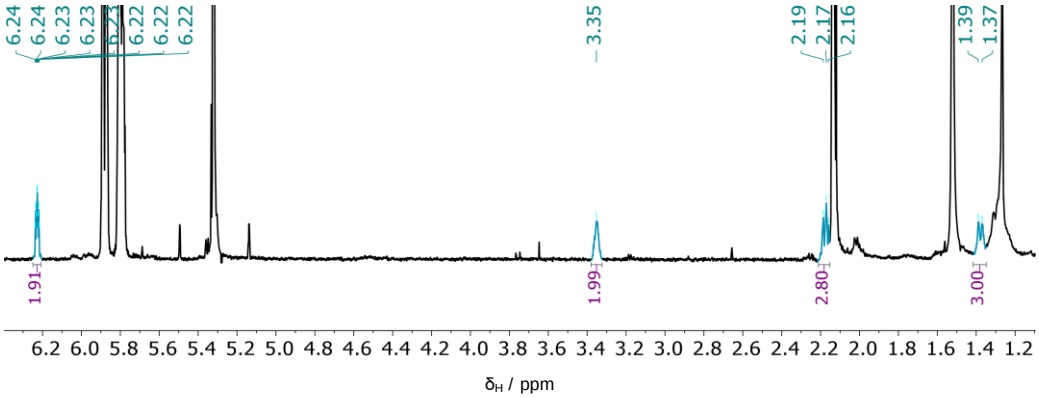

Figure S21: ^{1}H NMR spectrum (500 MHz, CD_2Cl_2, 300 K) of the [4+2] cycloadduct of **Q-**1 and cyclohexadiene.

8.2.2 **Q-4**-cyclohexadiene cycloadduct

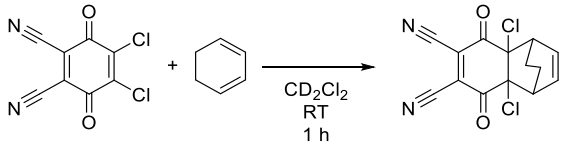

2,3-Dichloro-4,5-dicyano-1,4-benzoquinone (1.4 mg, 6 × 10^{-3} mmol, 1 eq.) and cyclohexadiene (1.0 mg, 1.2 × 10^{-2} mmol, 2 eq.) were added to CD_2Cl_2 (600 µL). The reaction was left for 1 h. The product was characterised without isolation or further purification. **^{1}H NMR (500 MHz, CD_2Cl_2) δ_H:** 6.35 (dd, *J* = 4.6, 3.1 Hz, 2H), 3.50 (ddp, *J* = 4.5, 3.0, 1.5 Hz, 2H), 2.44 – 2.38 (m, 2H), 1.58 – 1.53 (m, 2H).

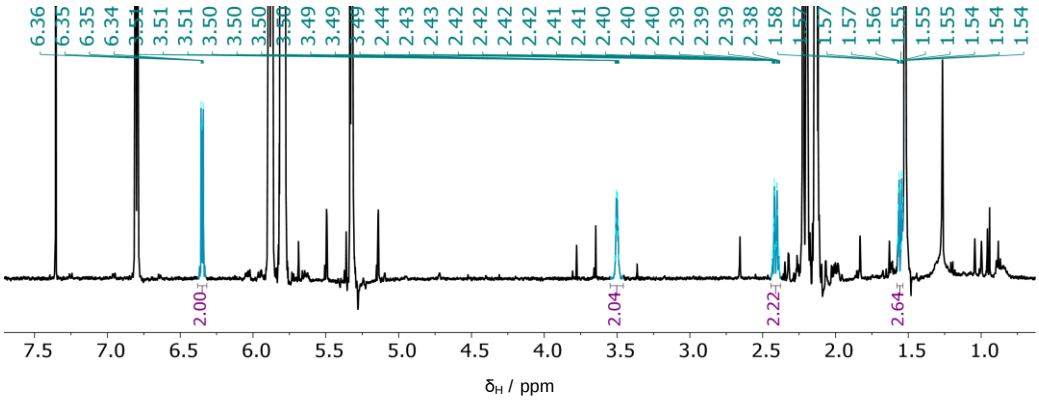

Figure S22: ^{1}H NMR spectrum (500 MHz, CD_2Cl_2, 300 K) of the [4+2] cycloadduct of **Q-4** and cyclohexadiene.

8.3 ^{1}H NMR spectra of [4+2] cyclohexadiene reactions

8.3.1 Catalysis Reaction

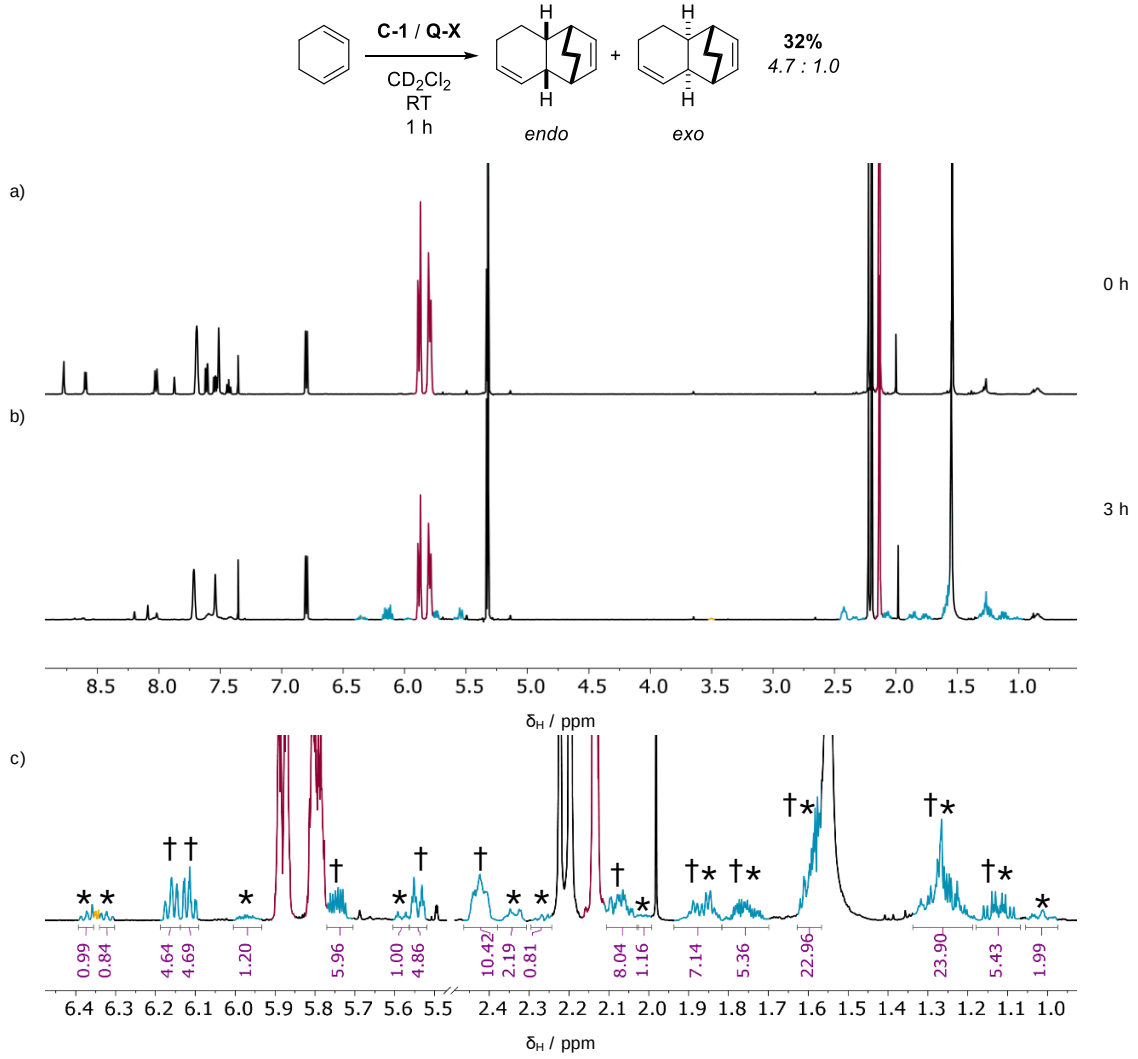

Figure S23: ^{1}H NMR spectra (500 MHz, CD_2Cl_2, 300 K) for the reaction of cyclohexadiene (20 mM) in the presence of **C-1** (0.5 mM) and **Q-4** (0.5 mM). (a) cyclohexadiene and **C-1** at T = 0 h; (b) cyclohexadiene, **C-1** and **Q-4** at T = 1 h; (c) Partial ^{1}H NMR spectrum of (b) highlighting cycloadduct peaks. Cyclohexadiene is highlighted in red, dicyclohexadiene is highlighted in blue (*endo* product is denoted by †, *exo* product is denoted by *), **Q-4**-cyclohexadiene cycloadduct is highlighted in yellow.

8.3.2 Control Reactions

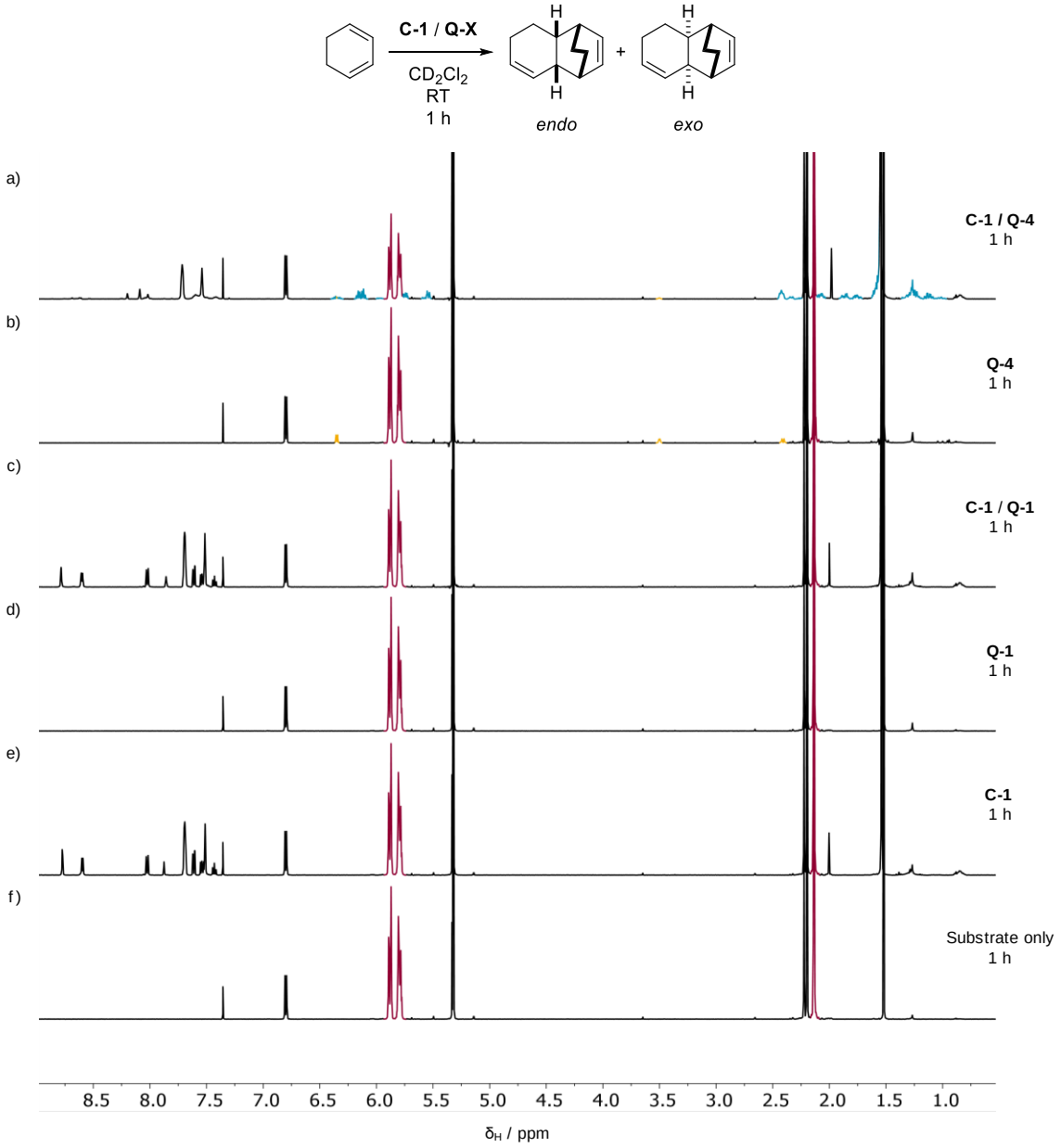

Figure S24: ^{1}H NMR spectra (500 MHz, CD_2Cl_2, 300 K) for the reaction of cyclohexadiene (20 mM) in the presence of (a) **C-1** (0.5 mM) and **Q-4** (0.5 mM) at T = 1 h; (b) **Q-4** (0.5 mM) at T = 1 h; (c) **C-1** (0.5 mM) and **Q-1** (0.5 mM) at T = 1 h; (d) **Q-1** (0.5 mM) at T = 1 h; (e) **C-1** (0.5 mM) at T = 1 h; (f) no other substrates at T = 1 h. Cyclohexadiene is highlighted in red, dicylohexadiene cycloadduct is highlighted in blue., **Q-4**-cyclohexadiene cycloadduct highlighted in yellow.

9 Cage-Quinone Catalyzed Cycloaddition of *tert*-butyl benzoquinone and dimethylanthracene

9.1 General Procedure

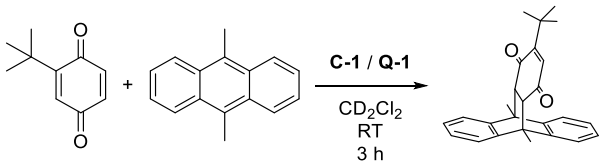

Stock solutions in CD_2Cl_2 were prepared for: 2-fluoromesitylene (internal standard, 1.20 mmol/mL), 9,10-dimethylanthracene (2.40 mmol/mL), *tert*-butyl benzoquinone (4.80 mmol/mL), **Q-1** (0.12×10^{-3} mmol/mL) and **C-1** (6.0×10^{-3} mmol/mL).

To CD_2Cl_2 (400 µL), in an NMR tube, was added internal standard (0.4 mg, 3.0×10^{-3} mmol, 0.5 eq., 25 µL), 9,10-dimethylanthracene (6.0×10^{-3} mmol, 1.0 eq., 25 µL) and **C-1** (1.4 mg, 3.0×10^{-4} mmol, 0.05 eq., 100 µL). The reaction was initiated by addition of *tert*-butyl benzoquinone (1.2×10^{-2} mmol, 2.0 eq., 25 µL) and **Q-1** (3.0×10^{-4} mmol, 0.05 eq., 25 µL). The reaction was monitored by recording ^{1}H NMR spectra before and 3 hours after the addition of **Q-1**. Product yields were calculated by comparing integrals of the starting material and product[s] to that of the internal standard.

9.2 Product Identification

The products of each NMR scale reaction were identified (and thereby yields calculated) by comparing to previously reported ^{1}H NMR spectroscopic data. The sources for this data are listed below:

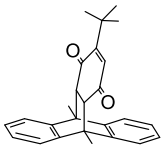

J. Am. Chem. Soc. 2018, 140, 8, 2863–2868

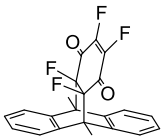

^{1}H NMR (500 MHz, $CDCl_3$) δ_H: 7.53 (dd, *J* = 5.7, 3.3 Hz, 2H), 7.39 (dd, *J* = 5.7, 3.2 Hz, 2H), 7.35 (brs, 4H), 2.05 (s, 6H);

^{13}C{^{1}H} NMR (126 MHz, $CDCl_3$) δ_C: 139.0, 138.9, 129.2, 128.0, 124.3, 123.8, 49.6, 12.3;

^{19}F NMR (376 MHz, $CDCl_3$) δ_F: -132.80 – -132.87 (m), -169.96 – -170.04 (m);

HRMS (EI): $C_{22}H_{14}O_2F_4$ [M] $^{\cdot+}$ found 386.09301, requires 386.09244.

9.2.1 **Q-1**-dimethylanthracene cycloadduct synthesis

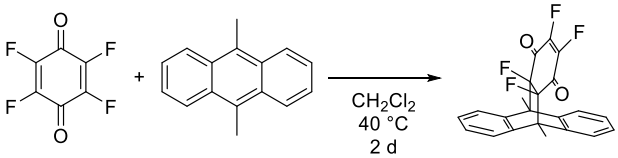

p-Fluoranil (46 mg, 0.255 mmol, 1.0 equiv.) and 9,10-dimethylanthracene (53 mg, 0.255 mmol, 1.0 equiv.) were dissolved in dichloromethane (5 mL) and refluxed for 2 days. The solvent was removed *in vacuo* and the crude product was recrystallized from acetonitrile to give yellow crystals (66 mg, 0.171 mmol, 67%). **^{1}H NMR (500 MHz, $CDCl_3$) δ_H:** 7.53 (dd, *J* = 5.7, 3.3 Hz, 2H), 7.39 (dd, *J* = 5.7, 3.2 Hz, 2H), 7.35 (brs, 4H), 2.05 (s, 6H); **^{13}C{^{1}H} NMR (126 MHz, $CDCl_3$) δ_C:** 139.0 (t), 138.9, 129.2, 128.0, 124.3, 123.8, 49.6 (d), 12.3; **^{19}F NMR (376 MHz, $CDCl_3$) δ_F:** -132.8 – -132.9 (m), -167.0 – -170.0 (m); **HRMS (EI):** $C_{22}H_{14}O_2F_4$ [M] $^{\cdot+}$ found 386.09301, requires 386.09244.

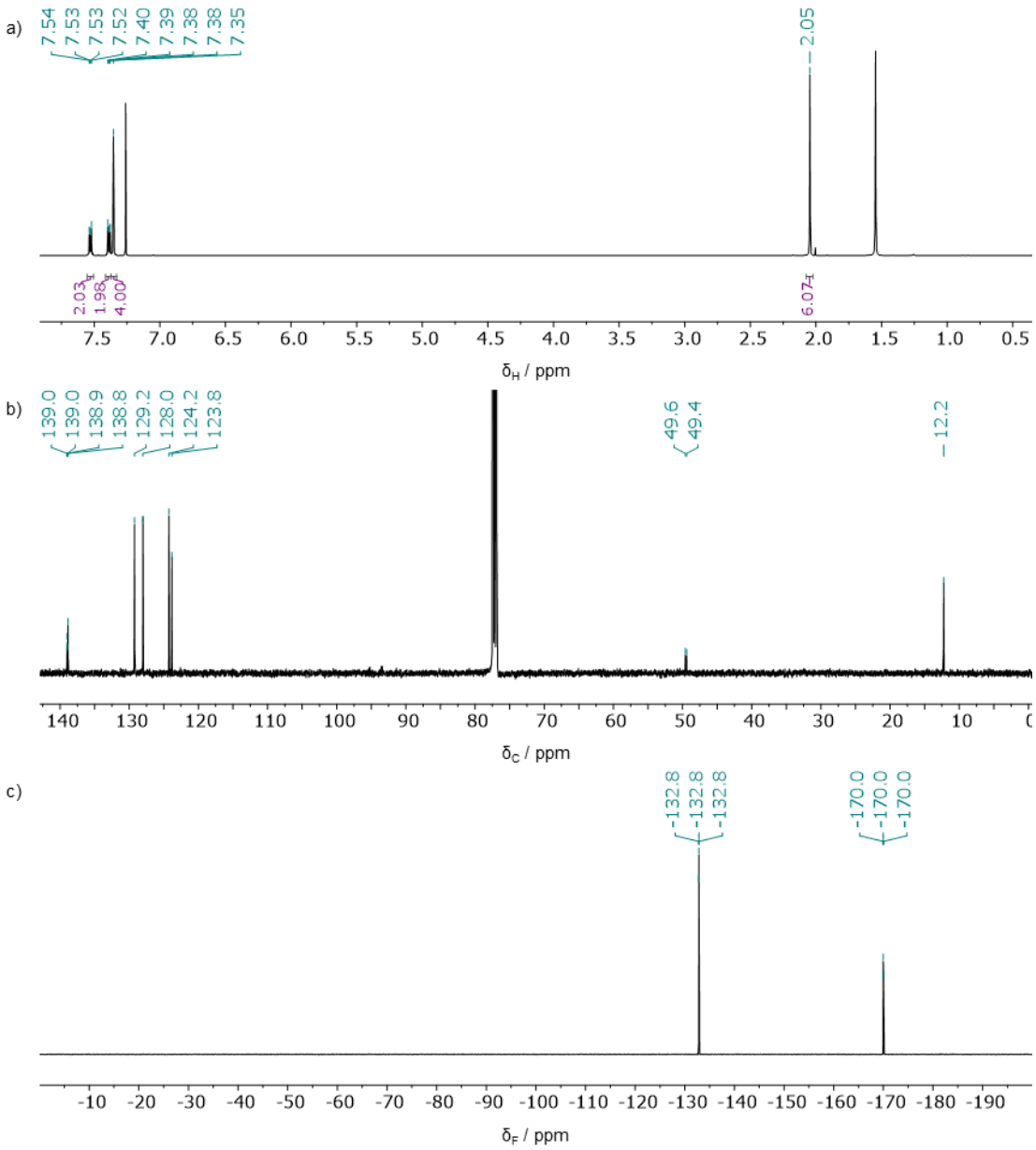

Figure S25: NMR spectra for the [4+2] cycloadduct of **Q-1** and 9,10-dimethylanthracene. (a) ^{1}H NMR spectrum (500 MHz, $CDCl_3$, 300 K); (b) $^{13}C\{^{1}H\}$ NMR spectrum (126 MHz, CD_3Cl, 300 K); (a) ^{19}F NMR spectrum (376 MHz, CD_3Cl, 300 K).

9.3 ^{1}H NMR spectra of [4+2] catalyzed reactions

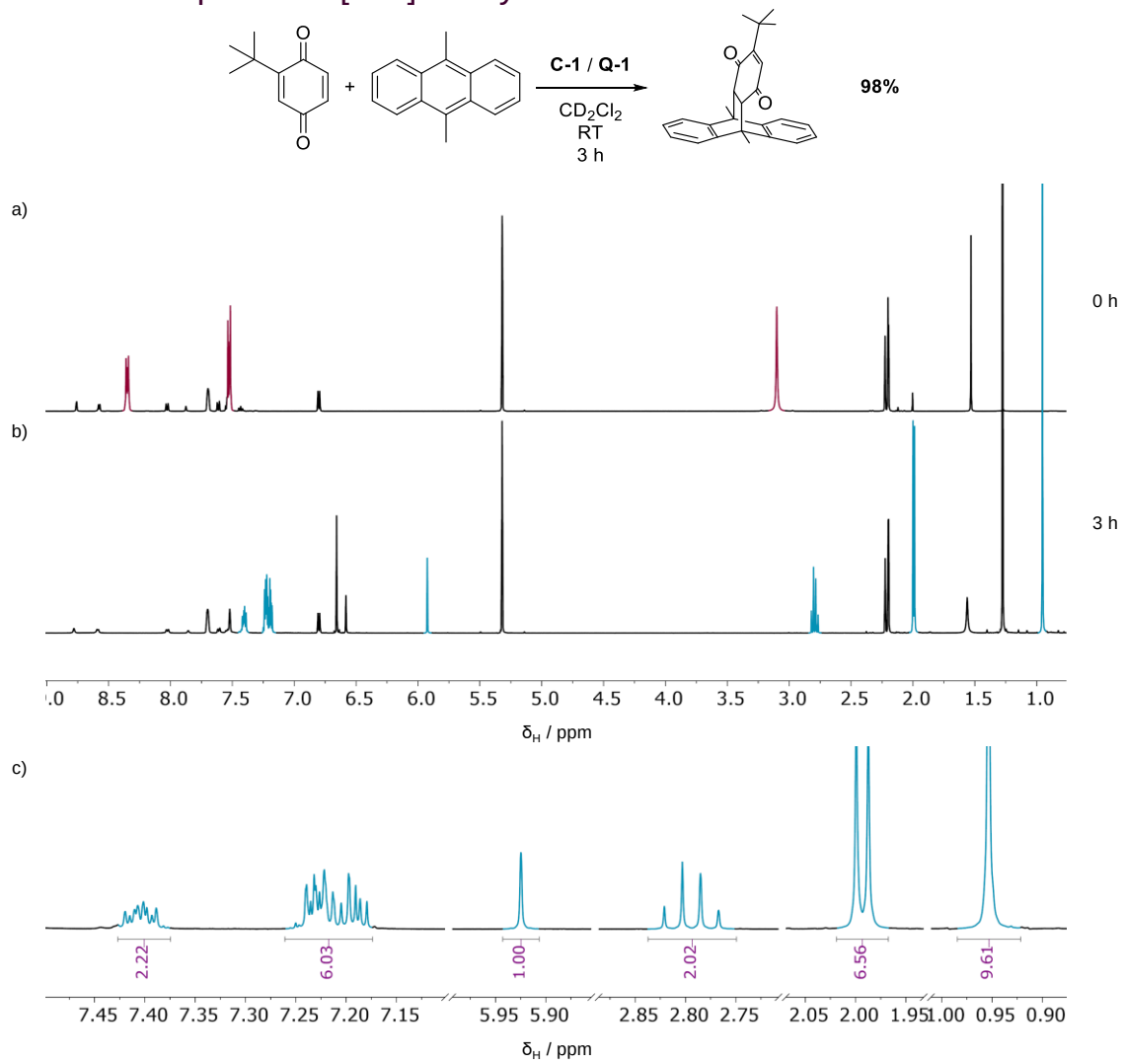

Figure S26: ^{1}H NMR spectra (500 MHz, CD_2Cl_2, 300 K) for the reaction of 9,10-dimethylanthracene (10 mM) and *tert*-butyl benzoquinone (20 mM) in the presence of **C-1** (0.5 mM) and **Q-1** (0.5 mM). (a) 9,10-dimethylanthracene and **C-1** at T = 0 h; (b) 9,10-dimethylanthracene, *tert*-butyl benzoquinone, **C-1** and **Q-1** at T = 1 h; (c) Partial ^{1}H NMR spectrum of (b) highlighting cycloadduct peaks. 9,10-Dimethylanthracene is highlighted in red, cycloadduct is highlighted in blue.

9.4 Control Reactions

Control reactions were run following the above procedure but included the following changes:

- Omitting **C-1**.
- Omitting **C-1** and **Q-1**.

Where species were omitted, stock solution volumes were replaced with CD_2Cl_2.

9.4.1 ^{1}H NMR spectra of [4+2] control reactions

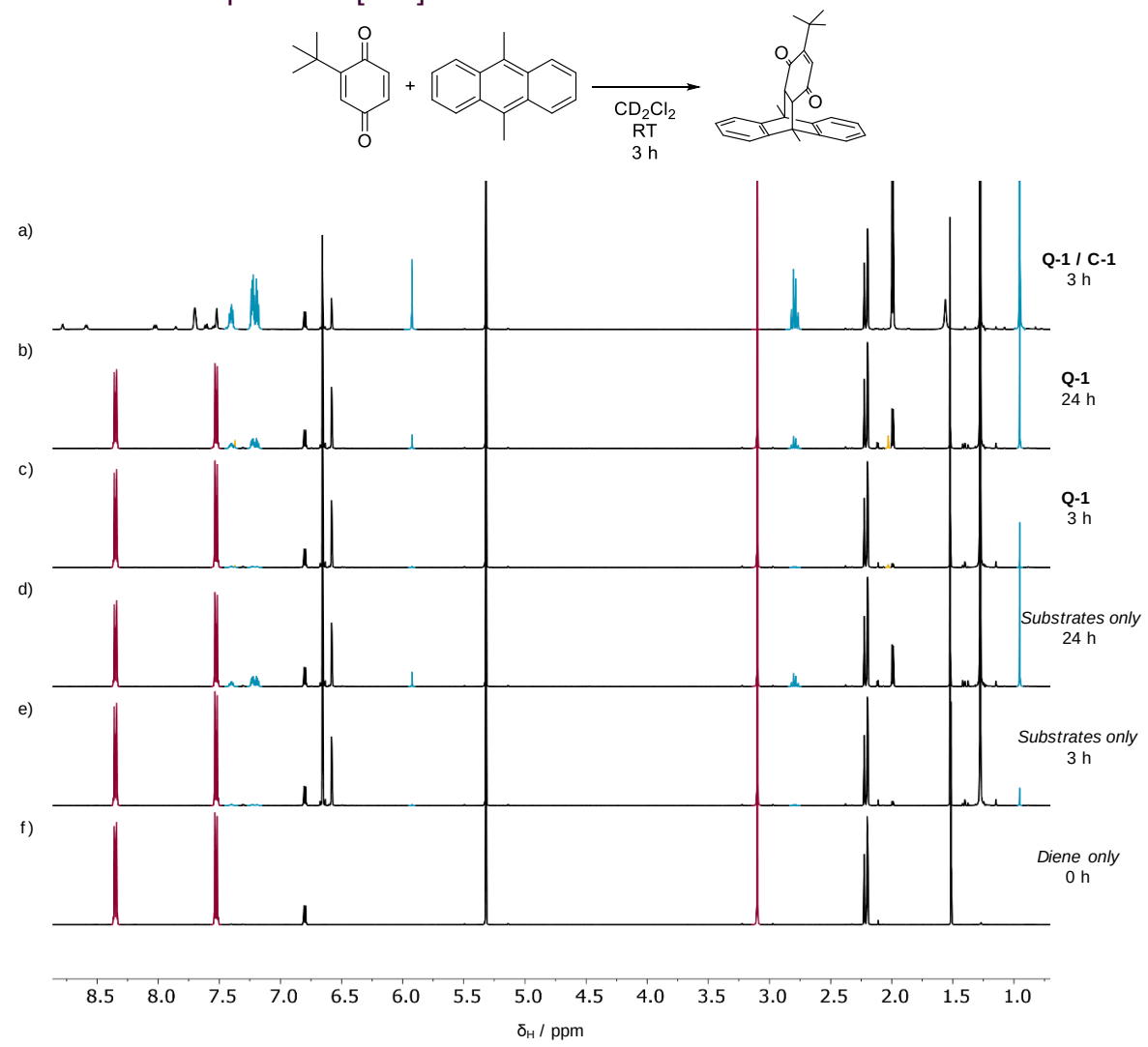

Figure S27: ^{1}H NMR spectra (500 MHz, CD_2Cl_2, 300 K) for the reaction of 9,10-dimethylanthracene (10 mM) and *tert*-butyl benzoquinone (20 mM). (a) 9,10-dimethylanthrancene, *tert*-butyl benzoquinone, **Q-1** and **C-1** at T = 3 h; (b-c) 9,10-dimethylanthracene, *tert*-butyl benzoquinone and **Q-1** at (b) T = 24 h; (c) T = 3 h; (d-e) 9,10-dimethylanthracene and *tert*-butyl benzoquinone at (d) T = 24 h; (e) T = 3 h; (f) 9,10-dimethylanthracene at T = 0 h. 9,10-Dimethylanthracene is highlighted in red, *tert*-butyl benzoquinone-dimethylanthracene cycloadduct is highlighted in blue, **Q-1**-dimethylanthracene cycloadduct is highlighted in yellow.

10 Determination of Binding Constants

10.1 Fast Exchange Titration Procedure

For each titration, a solution of **C-1** (0.5 mM) with a guest compound was titrated into a solution of **C-1** (0.5 mM), maintaining a constant concentration (0.5 mM) of **C-1** throughout. For each observable peak shift of **C-X** in the ^{1}H NMR spectrum, the peak position was plotted against the concentration of guest. A global non-linear curve fitting function was then applied to the combined plots using the 1:1 binding model given by:[8]

$$y = y_0 + \Delta y \left(\frac{\left(1 + K_a(P + x)\right) - \sqrt{\left(1 + K_a(P + x)\right)^2 - 4K_a^2 Px}}{2K_a P} \right)$$

$$y = y_0 + \Delta y * z$$

$$y_0 = peak\ position\ with\ no\ guest$$

$$\Delta y = peak\ position\ with\ 100\%\ bound$$

$$x = concentration\ of\ guest$$

$$z = \frac{-b \pm \sqrt{b^2 - 4ac}}{2a}$$

$$where\ a = K_a * P, b = 1 + K_a(P + x)\ and\ c = K_a$$

$$P = concentration\ of\ host$$

Origin Function: y=y0+DY*((1+Ka*(P+x))-sqrt(((1+Ka*(P+x))^2)-4*Ka*Ka*P*x))/(2*Ka*P)

10.2 **Q-1** and **C-1** titration

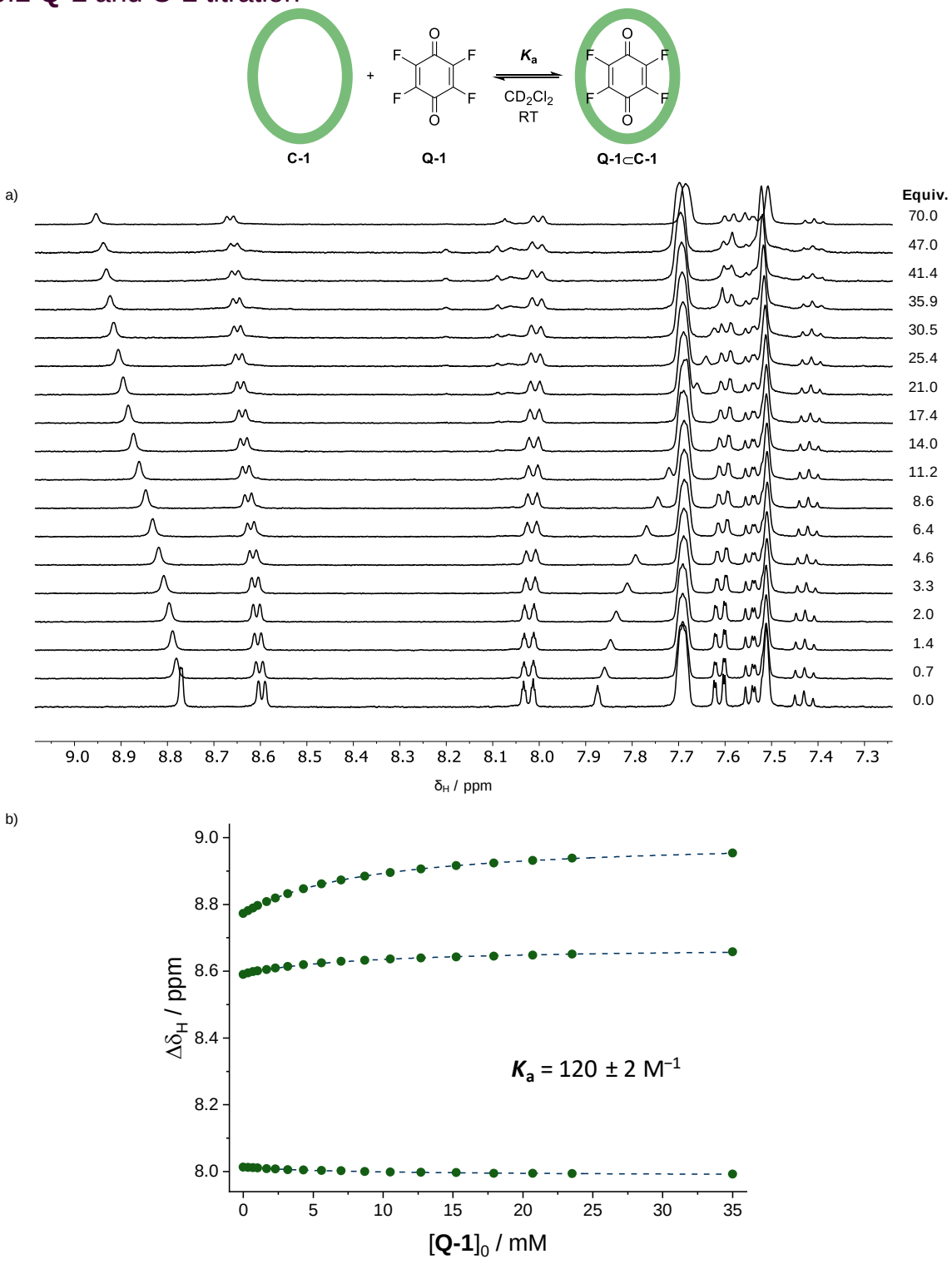

Figure S28: (a) Partial ^{1}H NMR (400 MHz, CD_2Cl_2, 300 K) titration data for titration of **Q-1** into **C-1**; (b) Fitted data for change in peak position with increasing **Q-1** concentration.

10.3 **Q-1** and **C-2** titration

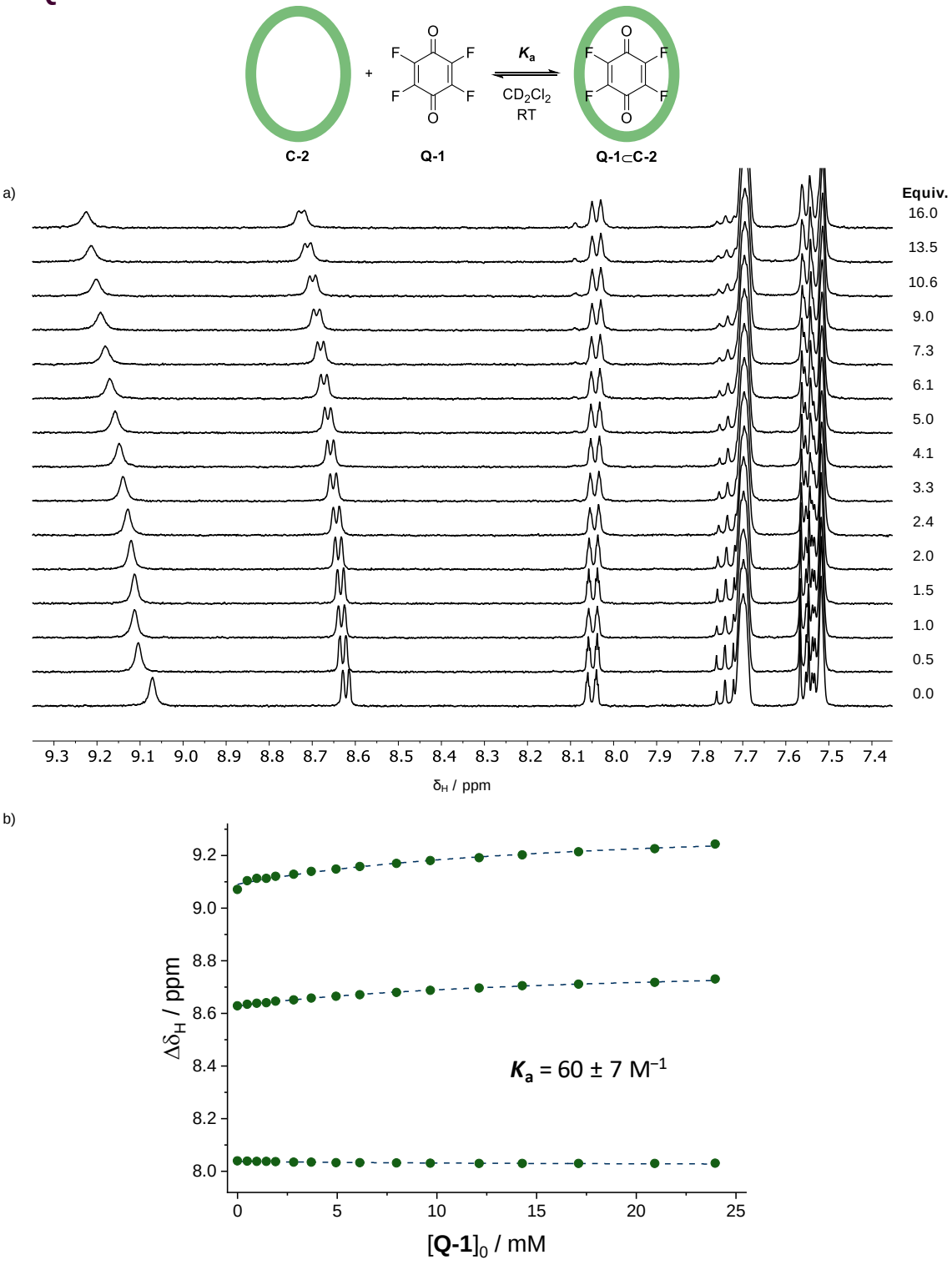

Figure S29: (a) Partial ^{1}H NMR (400 MHz, CD_2Cl_2, 300 K) titration data for titration of **Q-1** into **C-2**; (b) Fitted data for change in peak position with increasing **Q-2** concentration.

10.4 **Q-6** and **C-1** titration

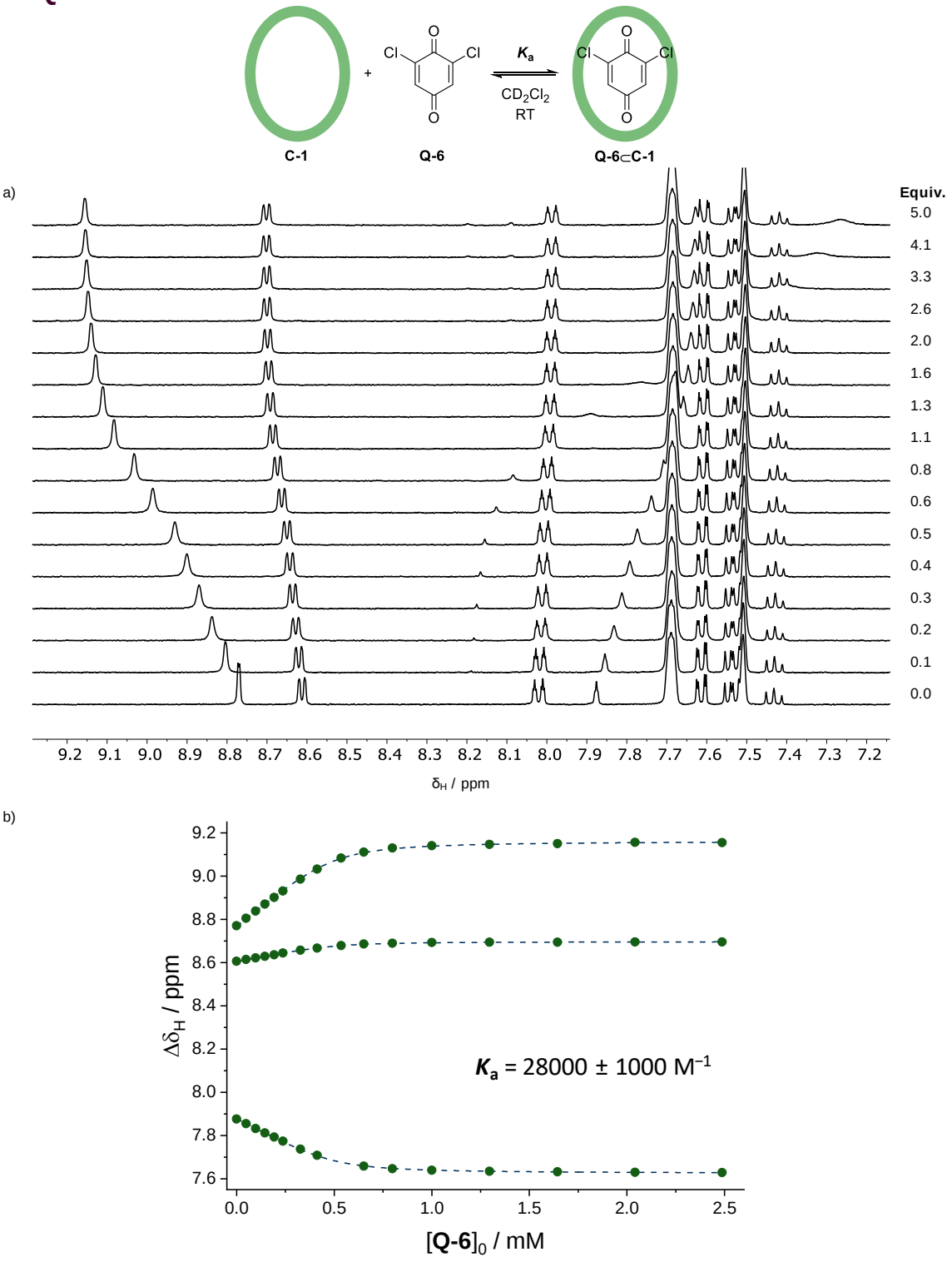

Figure S30: (a) Partial ^{1}H NMR (400 MHz, CD_2Cl_2, 300 K) titration data for titration of **Q-6** into **C-1**; (b) Fitted data for change in peak position with increasing **Q-6** concentration.

10.5 **Q-8** and **C-1** titration

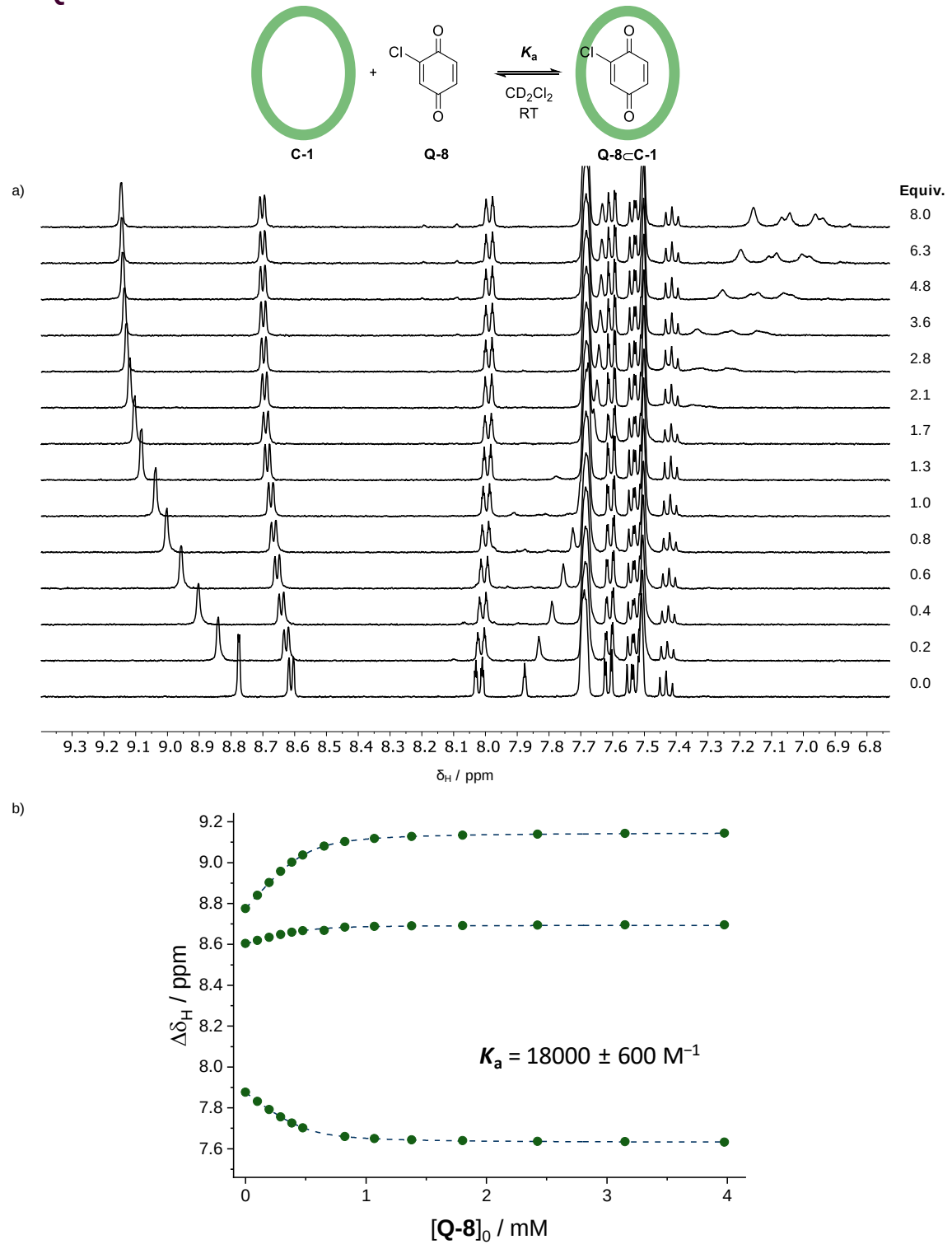

Figure S31: (a) Partial ^{1}H NMR (400 MHz, CD_2Cl_2, 300 K) titration data for titration of **Q-8** into **C-1**; (b) Fitted data for change in peak position with increasing **Q-8** concentration.

11 Electrochemical Studies

11.1 General Procedure

The electrochemical studies were performed in a three-electrode configuration using a single chamber cell and a CH Instruments CHI600D potentiostat. A glassy carbon button electrode, with a working area of 0.071 cm^2, was used as the working electrode, a platinum wire was used as the counter electrode, and a $Ag/AgNO_3$ electrode was used as a pseudo reference electrode. Potentials were then converted to the ferrocenium/ferrocene couple by spiking samples with ferrocene. The glassy carbon working electrode was polished using polishing powder and then washed with deionized water and acetone prior to use.

Cyclic voltammograms were collected at room temperature (25 °C) at a scan rate of 100 mVs^{-1} in 0.1 M NBu_4BArF electrolyte in CH_2Cl_2. The concentration of all analyte compounds was 2 mM in a total electrolyte volume of 2 mL, unless otherwise stated. All the measurements were conducted without stirring and with iR compensation enabled. All electrolyte solutions were kept under N_2 atmosphere throughout the measurements.

The CVs of the individual compounds are below.

11.2 Cyclic Voltammograms

11.2.1 **Q-1**

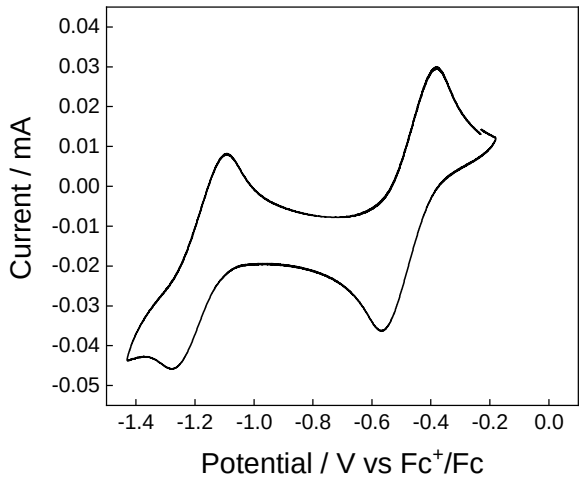

Figure S32: Cyclic voltammogram of **Q-1** (2 mM) in CH_2Cl_2 with NBu_4BArF (0.1 M) electrolyte vs Fc^+/Fc.

11.2.2 **Q-2**

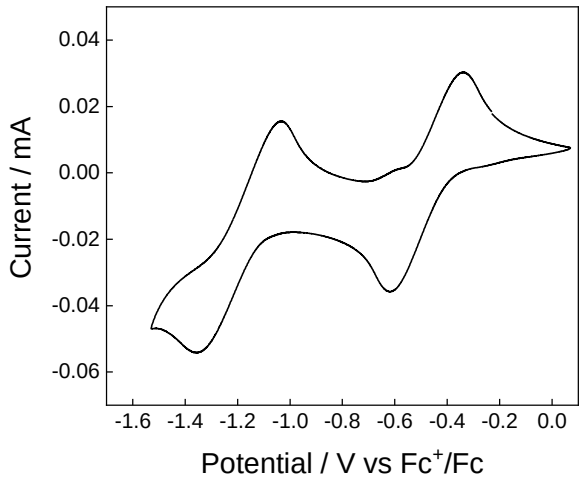

Figure S33: Cyclic voltammogram of **Q-2** (2 mM) in CH_2Cl_2 with NBu_4BArF (0.1 M) electrolyte vs Fc^+/Fc.

11.2.3 **Q-6**

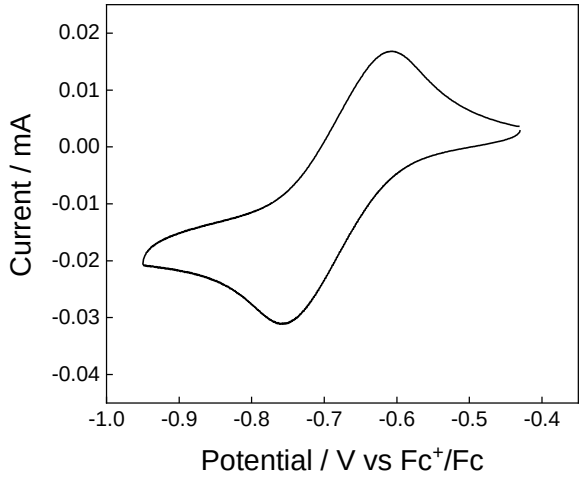

Figure S34: Cyclic volatammogram of the isolated first redox wave of **Q-6** (2 mM) in CH_2Cl_2 with NBu_4BArF (0.1 M) electrolyte vs Fc^+/Fc.

11.2.4 **Q-8**

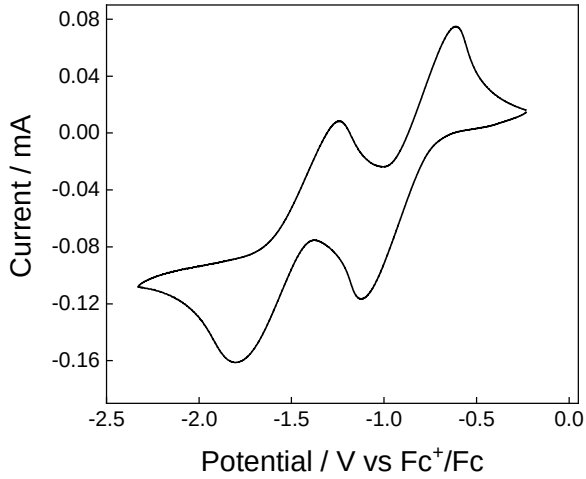

Figure S35: Cyclic voltammogram of **Q-8** (4 mM) in CH_2Cl_2 with NBu_4BArF (0.1 M) electrolyte vs Fc^+/Fc.

11.2.5 **Q-10**

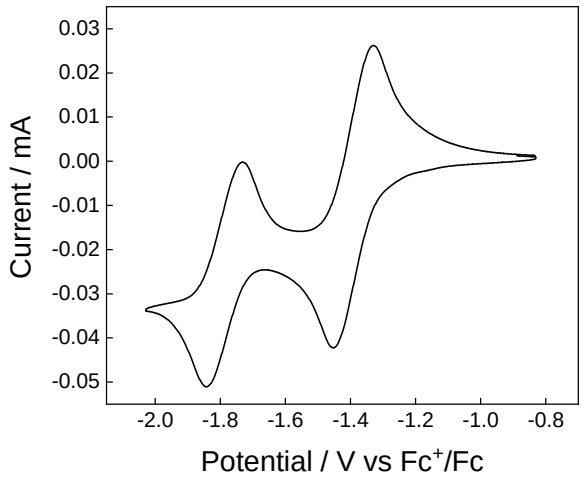

Figure S36: Cyclic voltammogram of **Q-10** (2 mM) in CH_2Cl_2 with NBu_4BArF (0.1 M) electrolyte vs Fc^+/Fc.

11.2.6 Bromoferrocene

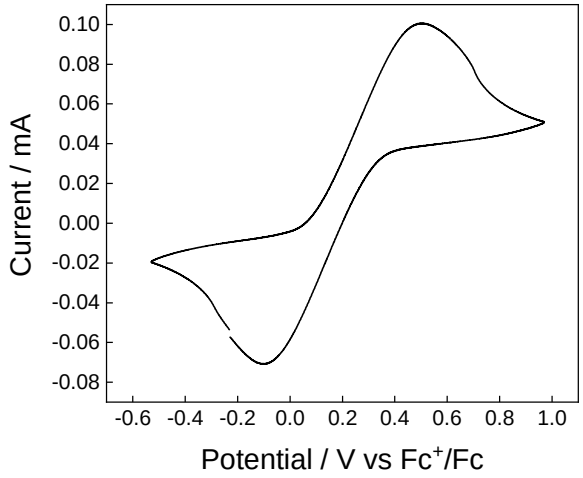

Figure S37: Cyclic voltammogram of bromoferrocene (4 mM) in CH_2Cl_2 with NBu_4BArF (0.1 M) electrolyte vs Fc^+/Fc.

11.2.7 1,1'-Dibromoferrocene

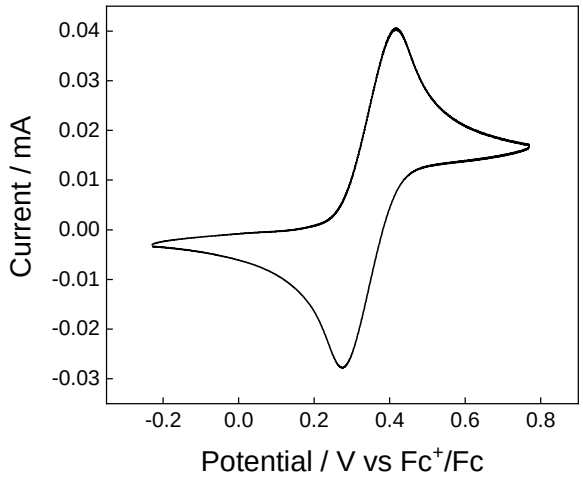

Figure S38: Cyclic voltammogram of 1,1'-dibromoferrocene (2 mM) in CH_2Cl_2 with NBu_4BArF (0.1 M) electrolyte vs Fc^+/Fc.

11.2.8 9,10-Dimethylanthracene

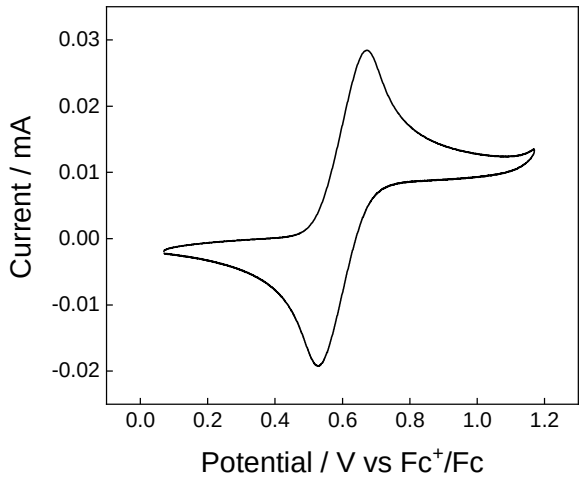

Figure S39: Cyclic voltammogram of 9,10-dimethylanthracene (2 mM) in CH_2Cl_2 with NBu_4BArF (0.1 M) electrolyte vs Fc^+/Fc.

11.2.9 Tris(*p*-bromophenyl)amine

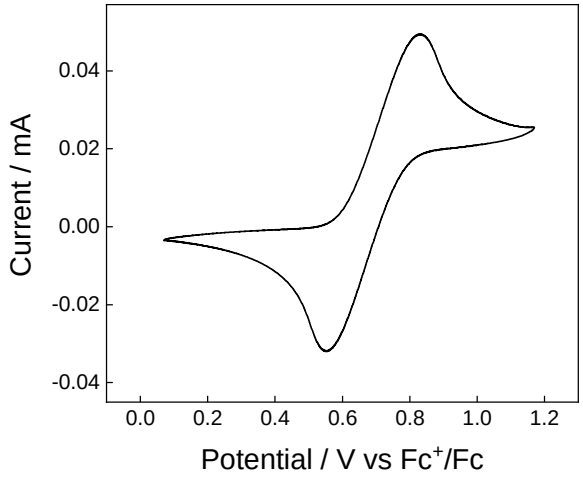

Figure S40: Cyclic voltammogram of tris(*p*-bromophenyl)amine (2 mM) in CH_2Cl_2 with NBu_4BArF (0.1 M) electrolyte vs Fc^+/Fc.

11.2.10 *trans*-Anethole

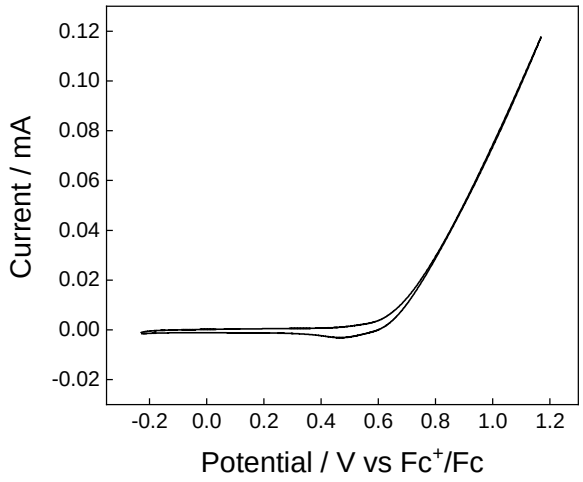

Figure S41: Cyclic voltammogram of *trans*-anethole (4 mM) in CH_2Cl_2 with NBu_4BArF (0.1 M) electrolyte vs Fc^+/Fc.

11.2.11 *trans*-β-Methyl-*N*-vinylcarbazole

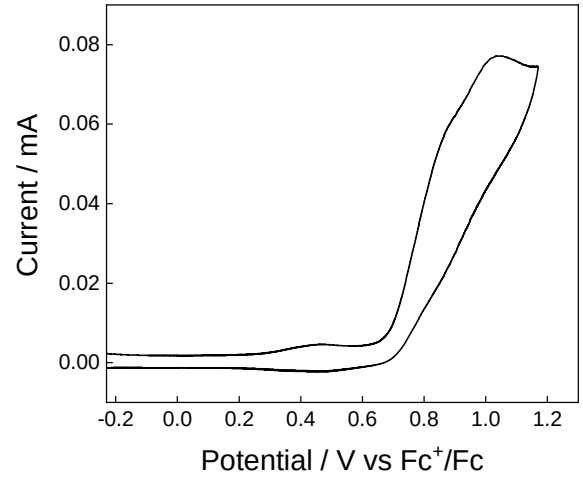

Figure S42: Cyclic voltammogram of *trans*-β-methyl-*N*-vinylcarbazole (2 mM) in CH_2Cl_2 with NBu_4BArF (0.1 M) electrolyte vs Fc^+/Fc.

11.2.12 1,3-Cyclohexadiene

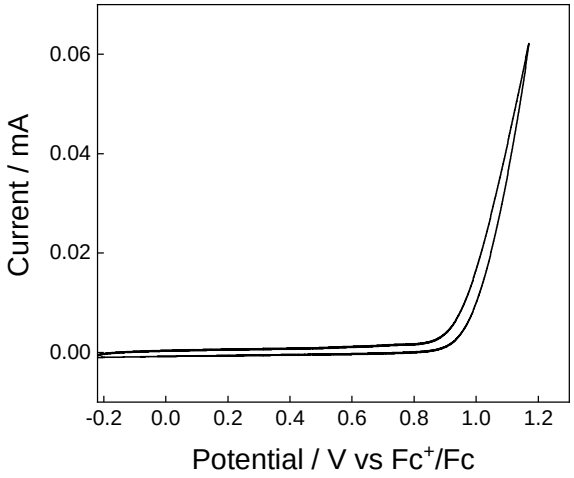

Figure S43: Cyclic voltammogram of cyclohexadiene (2 mM) in CH_2Cl_2 with NBu_4BArF (0.1 M) electrolyte vs Fc^+/Fc.

11.3 $E_{1/2}$ values

Table S4: $E_{1/2}$ values from CV studies of compounds (2 mM) in CH_2Cl_2 using NBu_4BArF (0.1 M) electrolyte vs Fc^+/Fc.

Quinone	$E_{1/2}$ / V[a]
Q-1	−0.47
Q-2	−0.47
Q-6	−0.67
Q-8	−0.83
Q-10	−1.39
BrFc	+0.19
Br_2Fc	+0.34
DMA	+0.59
N(*p*-BrPh)$_3$	+0.68

[a] $E_{1/2}$ values are given for the wave corresponding to the one electron reduction of the quinone to the semiquinone radical anion.

12 UV/Vis Electron Transfer Experiments

12.1 Qualitative Comparison of Cage Electron Transfer Properties

12.1.1 General Procedure

For each reaction, **C-X** (0.5 mM) was added to a solution of **Q-1** (0.5 mM) and donor (0.5 mM) in CH_2Cl_2, taking a spectrum before and after addition of **C-X**.

12.1.2 UV/Vis spectra

12.1.2.1 Tris(*p*-bromophenyl)amine

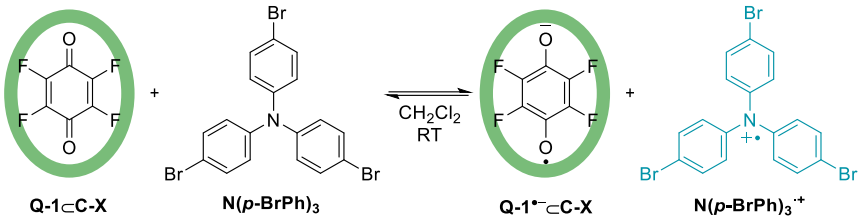

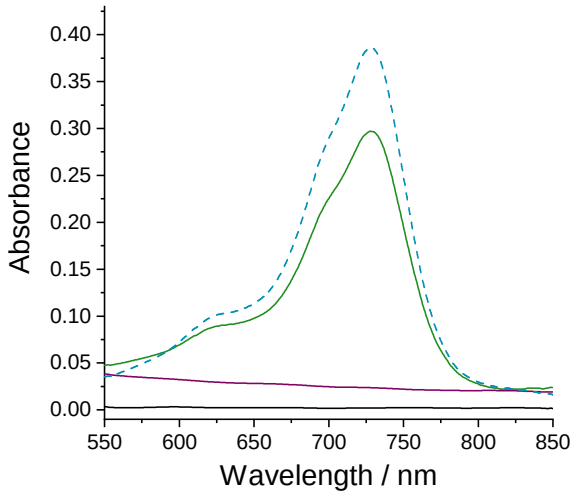

Figure S44: UV-vis spectra (CH_2Cl_2, 298 K) of (i) black line = **Q-1** (0.5 mM) and tris(*p*-bromophenyl)amine (0.5 mM); (ii) green line = **Q-1** (0.5 mM), tris(*p*-bromophenyl)amine (0.5 mM) and **C-1** (0.5 mM); (iii) purple line = **Q-1** (0.5 mM), tris(*p*-bromophenyl)amine (0.5 mM) and **C-2** (0.5 mM), (d) blue dashed line = tris(*p*-bromophenyl)aminium hexachloroantimonate (0.4 mM).

12.1.2.2 9,10-Dimethylanthracene

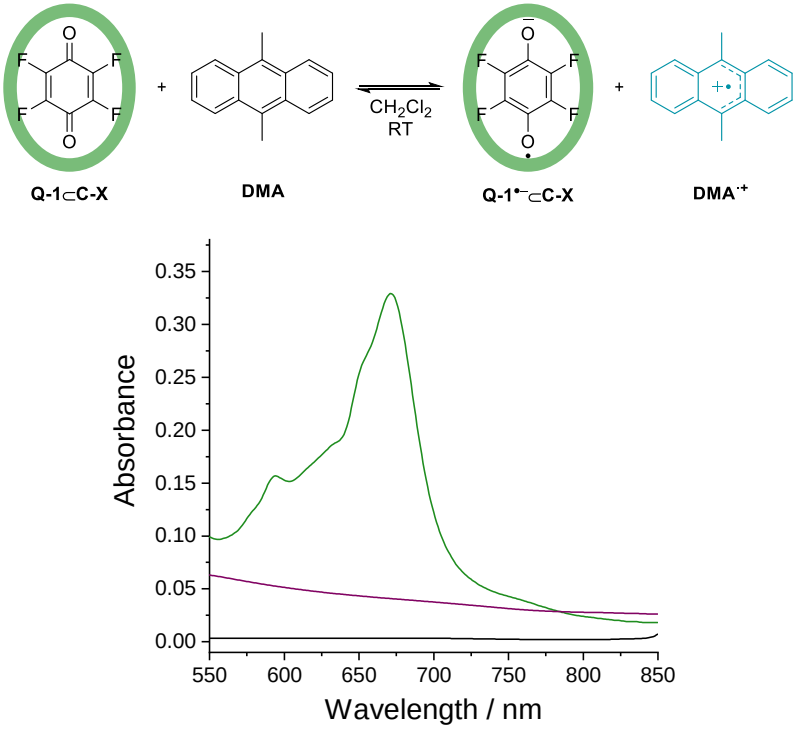

Figure S45: UV-vis spectra (CH_2Cl_2, 298 K) of (i) black line = **Q-1** (0.5 mM) and 9,10-dimethylanthracene (0.5 mM); (ii) green line = **Q-1** (0.5 mM), 9,10-dimethylanthracene (0.5 mM) and **C-1** (0.5 mM); (iii) purple line = **Q-1** (0.5 mM), 9,10-dimethylanthracene (0.5 mM) and **C-2** (0.5 mM). λ_{max} at 670 nm is in accordance to previously reported values.[9]

12.1.2.3 Ferrocene

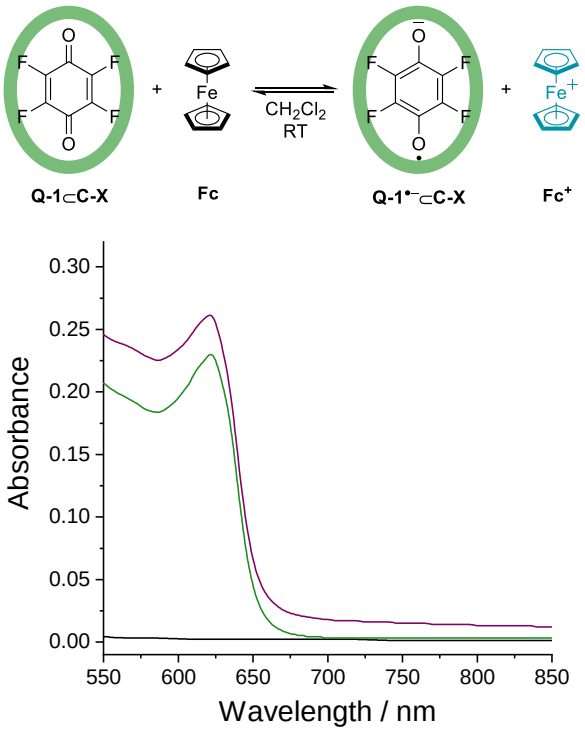

Figure S46: UV-vis spectra (CH_2Cl_2, 298 K) of (i) black line = **Q-1** (0.5 mM) and ferrocene (0.5 mM); (ii) green line = **Q-1** (0.5 mM), ferrocene (0.5 mM) and **C-1** (0.5 mM); (iii) purple line = **Q-1** (0.5 mM), ferrocene (0.5 mM) and **C-2** (0.5 mM). λ_{max} at 620 nm is in accordance to previously reported values.[10]

12.1.2.4 Bromoferrocene

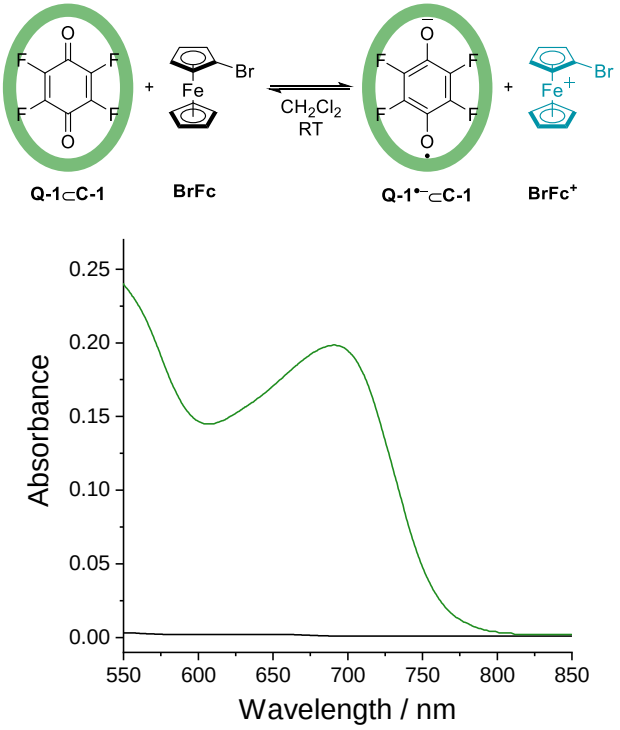

Figure S47: UV-vis spectra (CH_2Cl_2, 298 K) of (i) black line = **Q-1** (0.5 mM) and bromoferrocene (0.5 mM); (ii) green line = **Q-1** (0.5 mM), bromoferrocene (0.5 mM) and **C-1** (0.5 mM). λ_{max} at 687 nm is in accordance to previously reported values.[10]

12.1.2.5 1,1'-Dibromoferrocene

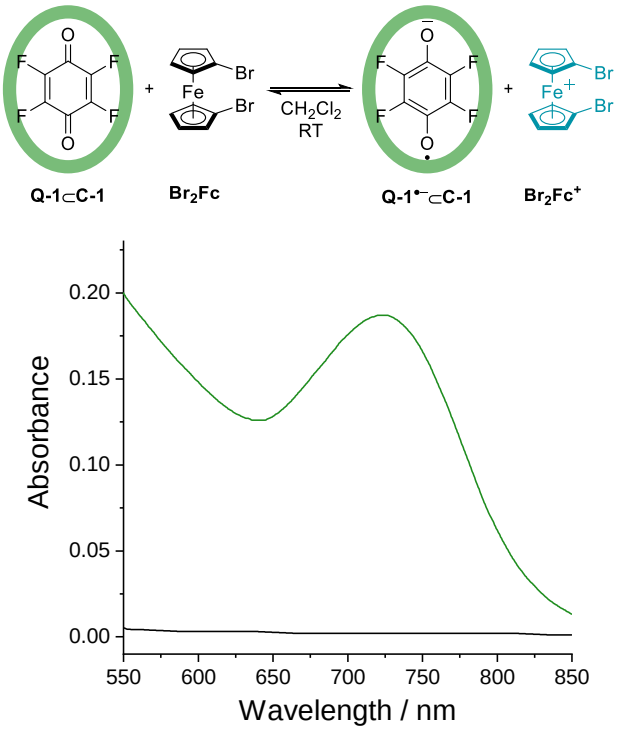

Figure S48: UV-vis spectra (CH_2Cl_2, 298 K) of (i) black line = **Q-1** (0.5 mM) and 1,1'-dibromoferrocene (0.5 mM); (ii) green line = **Q-1** (0.5 mM), 1,1'-dibromoferrocene (0.5 mM) and **C-1** (0.5 mM). λ_{max} at 720 nm is in accordance to previously reported values.[10]

12.2 UV/Vis Electron Transfer Titration Experiments

12.2.1 General Procedure

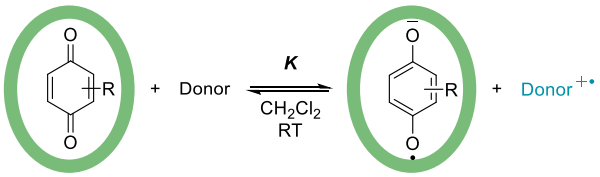

For each titration, a solution of **C-X** (0.5 mM), **Q-X** (0.5 mM) with the electron donor was titrated into a solution of **C-X** (0.5 mM) and **Q-X** (0.5 mM), maintaining a constant concentration (0.5 mM) of **C-1** and **Q-X** throughout.

12.2.2 Qualitative UV/Vis Spectra for **C-1**/**Q-1**

Titrations were completed with **C-1**, **Q-1** and different electron donors to quantify the position of equilibrium between the 'neutral' and ionised species. Whilst the oxidised donor could be observed by UV/vis spectroscopy, the organic radicals are not stable over time (see Section 12.2.2.3). This prevented these species being used to obtain quantitative data for **C-1**/**Q-1**. Although the ferrocenium species are stable over time, formation of the oxidised species was near quantitative and thus *K* was too large to measure reliably.

12.2.2.1 **C-1**, **Q-1** and tris(*p*-bromophenyl)amine

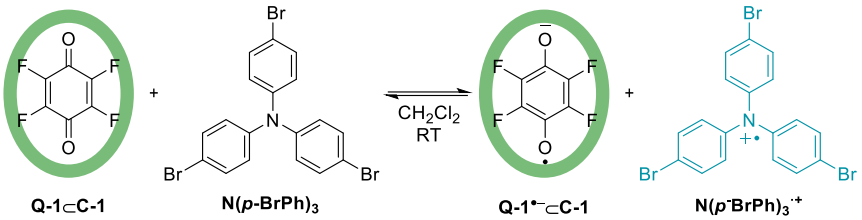

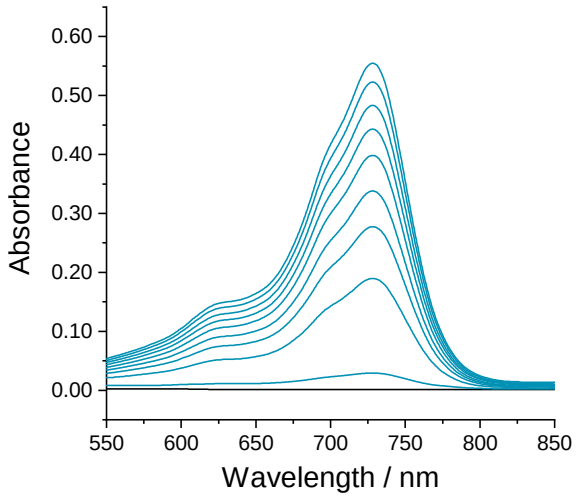

Figure S49: UV-vis spectra (CH_2Cl_2, 298 K) of (i) black line = **Q-1** (0.5 mM) and **C-1** (0.5 mM); (ii) blue lines = **Q-1** (0.5 mM), **C-1** (0.5 mM) and increasing tris(*p*-bromophenyl)amine.

12.2.2.2 **C-1**, **Q-1** and 9,10-dimethylanthracene

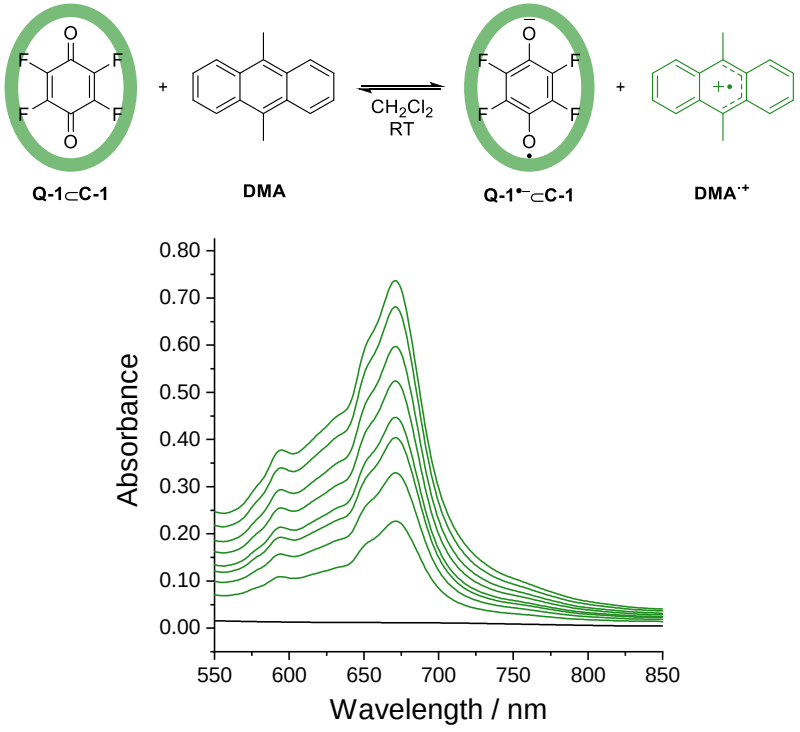

Figure S50: UV-vis spectra (CH_2Cl_2, 298 K) of (i) black line = **Q-1** (0.5 mM) and **C-1** (0.5 mM); (ii) green lines = **Q-1** (0.5 mM), **C-1** (0.5 mM) and increasing 9,10-dimethylanthracene.

12.2.2.3 Stability of oxidised species over time

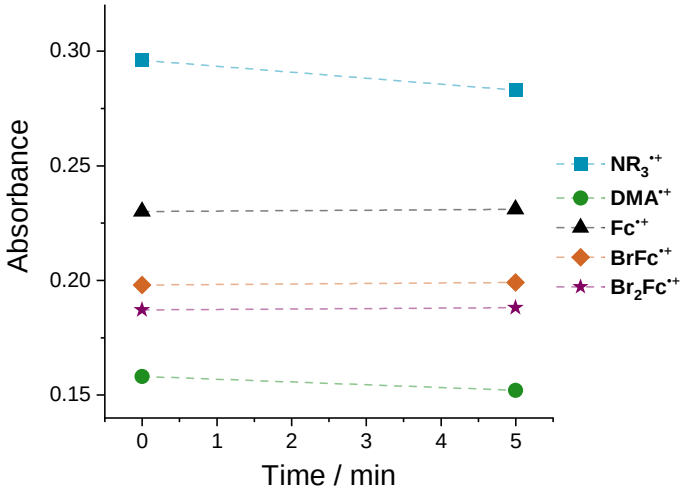

Figure S51: Absorbance from UV-vis spectra (CH_2Cl_2, 298 K) at λ_{max} at T = 0 and 5 min for **C-1** (0.5 mM), **Q-1** (0.5 mM) and (i) tris(*p*-bromophenyl)amine (0.5 mM) at 729 nm (blue squares); (ii) 9,10-dimethylanthracene (0.5 mM) at 672 nm (green circles); (iii) ferrocene (0.5 mM) at 622 nm (black triangles); (iv) bromoferrocene (0.5 mM) at 690 nm (orange diamonds); (v) 1,1'-dibromoferrocene (0.5 mM) at 720 nm (purple stars).

12.2.3 UV/Vis Spectra for Quantifying *K*

12.2.3.1 **C-1**, **Q-8** and bromoferrocene

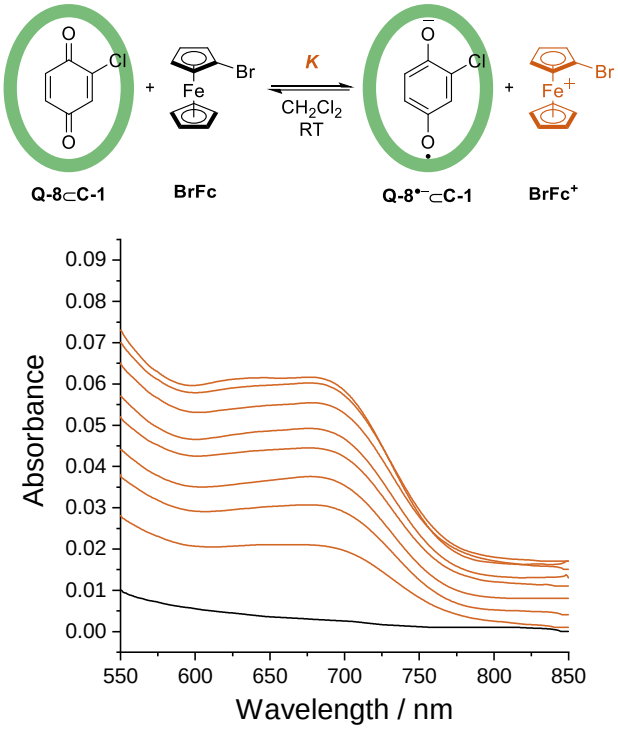

Figure S52: UV-vis spectra (CH_2Cl_2, 298 K) of (i) black line = **Q-8** (0.5 mM) and **C-1** (0.5 mM); (ii) orange lines = **Q-8** (0.5 mM), **C-1** (0.5 mM) and increasing bromoferrocene.

12.2.3.2 **C-1**, **Q-6** and 1,1'-dibromoferrocene

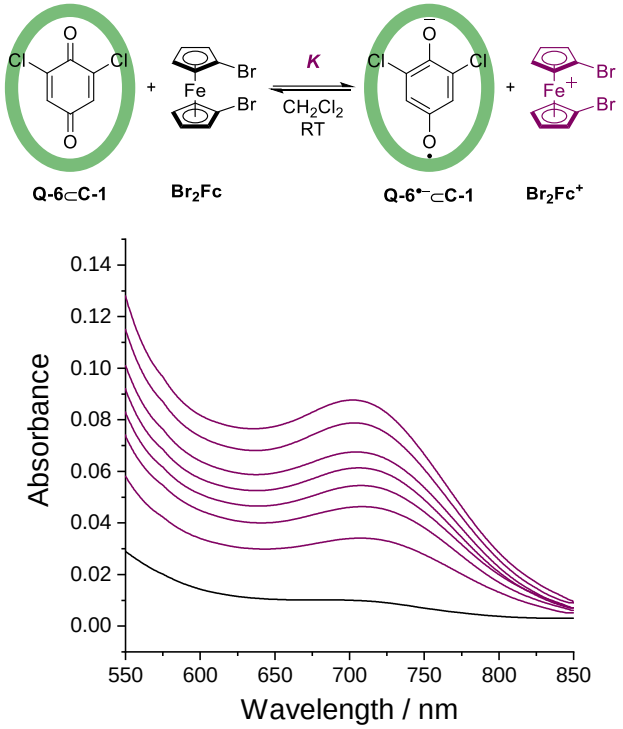

Figure S53: UV-vis spectra (CH_2Cl_2, 298 K) of (i) black line = **Q-6** (0.5 mM) and **C-1** (0.5 mM); (ii) purple lines = **Q-6** (0.5 mM), **C-1** (0.5 mM) and increasing 1,1'-dibromoferrocene.

12.2.4 Fitting for *K*

12.2.4.1 Procedure for Fitting for *K*

The absorption at λ_{max} was converted into [Donor^{+}] using the Beer-Lambert Law and plotted against [Donor]$_0$. A non-linear curve fitting function was then applied using the following equation to measure *K*:

$$y = \frac{-\sqrt{K}\sqrt{C^2K - 2C(K-2)x + Kx^2} + CK + Kx}{2(K-1)} \text{ as long as } K \neq 1 \qquad \text{Eq. 1}$$

Where:

$$y = [\mathrm{D}^{\cdot+}]$$

$$x = [\mathrm{D}]_0$$

Origin function: y=(-(K)^(1/2)*(C^2*K-2*C*(K-2)*x+K*x^2)^(1/2)+C*K+K*x)/(2*(K-1))

This was derived using:

$$K = \frac{[\mathrm{D}^{\cdot+}][\mathrm{Q}^{\cdot-}\subset\mathrm{C}]}{[\mathrm{D}][\mathrm{Q}\subset\mathrm{C}]}$$

Where:

$$[\mathrm{D}^{\cdot+}] = [\mathrm{Q}^{\cdot-}\subset\mathrm{C}]$$

$$[\mathrm{D}] = [\mathrm{D}]_0 - [\mathrm{D}^{\cdot+}]$$

$$[\mathrm{Q}\subset\mathrm{C}] = [\mathrm{C}]_0 - [\mathrm{Q}^{\cdot-}\subset\mathrm{C}] = [\mathrm{C}]_0 - [\mathrm{D}^{\cdot+}]$$

Substituting $[\mathrm{D}^{\cdot+}] = y$ and $[\mathrm{D}]_0 = x$ gives:

$$K = \frac{y^2}{(x-y)(C-y)}$$

$$K(x-y)(C-y) = y^2$$

$$K(x-y)(C-y) - y^2 = 0$$

Which solves for y to give Eq. 1.

12.2.4.2 Fittings for *K*

The ε values for the ferrocenium BArF derivatives in CH_2Cl_2 have been previously reported.[10]

*12.2.4.2.1 **C-1**, **Q-8** and bromoferrocene*

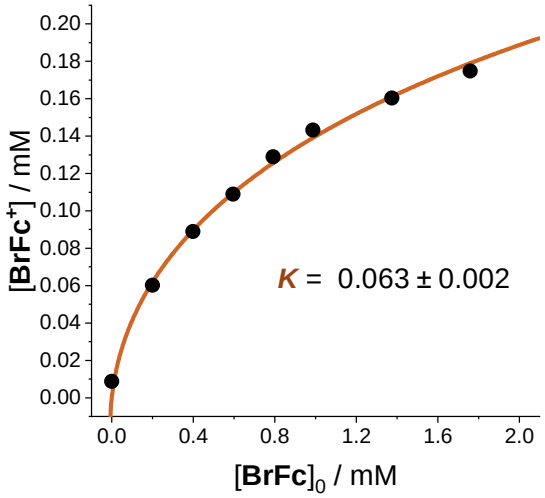

Figure S54: [**BrFc**$^{+}$] calculated at λ = 687 nm using ε = 349 M^{-1}cm^{-1}.[10] Curve (orange line) fitted using non-linear fitting to give *K* = 0.063 for **Q-8**/**C-1** and bromoferrocene.

*12.2.4.2.2 **C-1**, **Q-6** and 1,1'-dibromoferrocene*

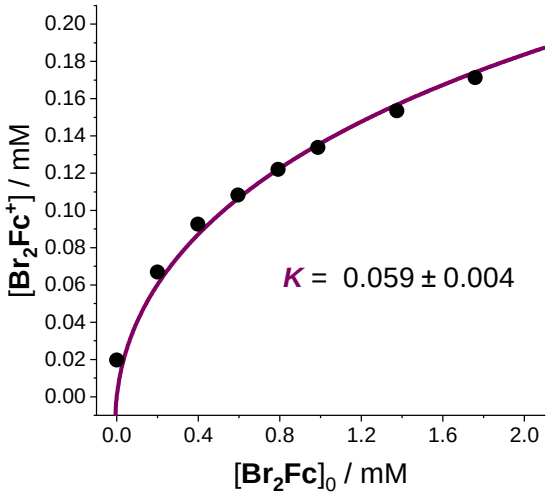

Figure S55: [Br_2Fc^+] calculated at λ = 720 nm using ε = 508 $M^{-1}cm^{-1}$.[10] Curve (purple line) fitted using non-linear fitting to give *K* = 0.059 for **Q-6**/**C-1** and 1,1'-dibromoferrocene.

12.2.5 Calculating E_K, $E_{Q\text{-}X\subset C\text{-}1}$ and $\Delta E_{enc.}$

Using the Nernst equation gives E_K for the system, where T = 298 K:

$$\Delta G = -RTlnK = -nFE_K$$

$$E_K = \frac{RTlnK}{nF} \qquad \text{Eq. 2}$$

E_K is used to calculate absolute $E_{1/2}$ for **Q-X⊂C-1** from the experimentally obtained $E_{1/2}$ values (from cyclic voltammetry, see Section 11.3):

$$E_{\mathbf{Q-X\subset C-1}} = E_{\mathrm{Donor}} + E_K \qquad \text{Eq. 3}$$

Which can subsequently be used to calculate $\Delta E_{enc.}$:

$$\Delta E_{enc.} = E_{\mathbf{Q-X\subset C-1}} - E_{\mathbf{Q-X}} \qquad \text{Eq. 4}$$

Table S5: Conversion from experimentally measured *K* to calculate the absolute redox potential of **Q-X⊂C-1** and also $\Delta E_{enc.}$.

Quinone	Electron Donor	*K*	E_K / V[a]	$E_{1/2}$ Electron Donor / V[b]	$E_{Q\text{-}X\subset C\text{-}1}$ / V[c]	$E_{1/2}$ Quinone / V[b]	ΔE_{enc} / V[d]
Q-8	**BrFc**	0.0063	−0.07	+0.19	+0.12	−0.83	+0.95
Q-6	**Br_2Fc**	0.0059	−0.07	+0.34	+0.27	−0.67	+0.94

[a] Calculated from Eq. 2. [b] Measured using cyclic voltammetry. [c] Calculated from Eq. 3. [d] Calculated from Eq. 4.

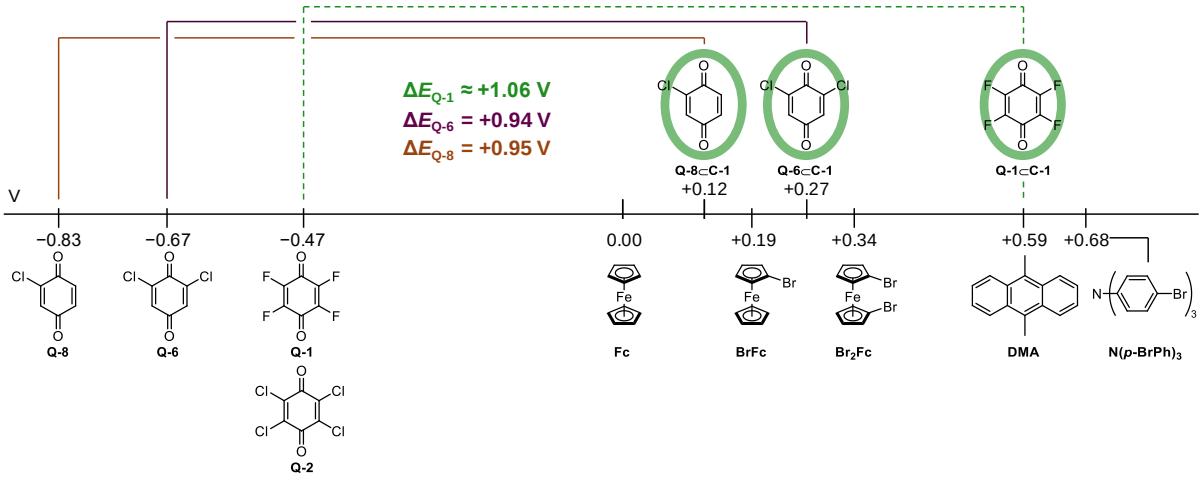

Figure S56: Comparison of electrochemically measured $E_{1/2}$ values vs Fc^+/Fc of free quinones and electron donors (below the line) and absolute $E_{1/2}$ values for **Q-X⊂C-1** calculated through UV/vis spectroscopy and the Nernst equation (above the line).

13 Computational Studies

13.1 Computational Methods

Geometry optimizations were performed in ORCA v. 4.1.1.11 at the PBE0-D3BJ/def2-SVP (which includes the ECP28MWB effective core potential).[11–16] The resolution of identity (RI) technique for Coulomb type terms (J) and the chain of spheres (COS) algorithm for exchange, RIJCOSX, was used to accelerate the calculations (default fitting basis).[17] Spin density was calculated at the same level of theory and plotted at an isovalue of 0.003 in Chimera.

13.2 Spin Density Plots

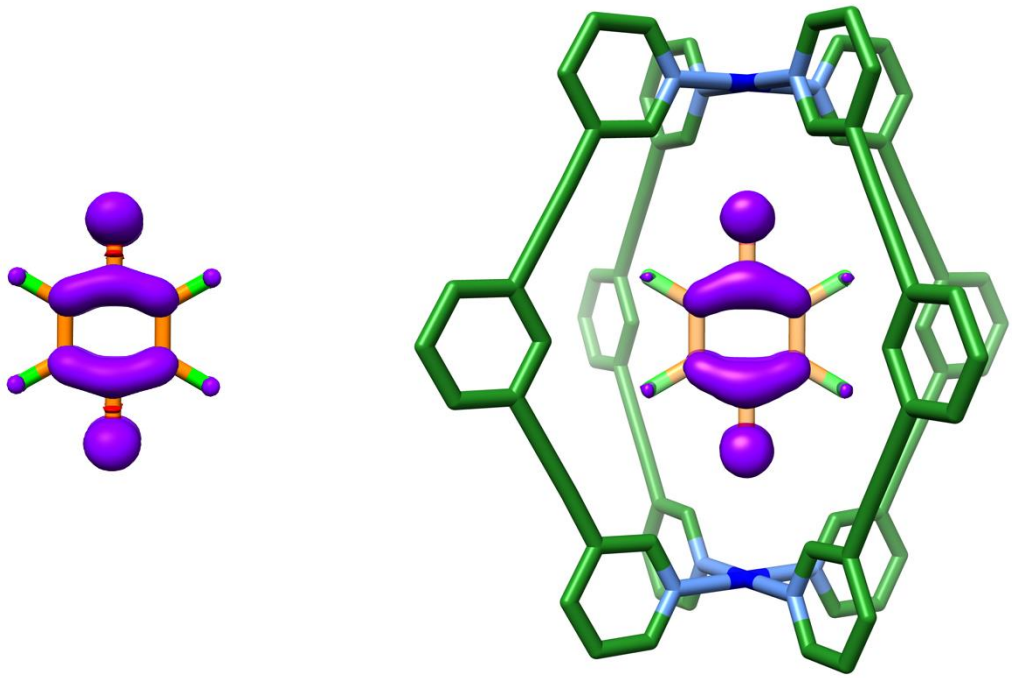

Figure S57: Spin density of isolated **Q-1** (left) and **Q-1⊂C-1** (right) calculated at PBE0-D3BJ/def2-SVP and plotted at an isovalue of 0.003 in Chimera.

14 References

(1) August, D. P.; Nichol, G. S.; Lusby, P. J. Maximizing Coordination Capsule-Guest Polar Interactions in Apolar Solvents Reveals Significant Binding. *Angew. Chem. Int. Ed.* **2016**, *55*, 15022–15026.

(2) Martí-Centelles, V.; Lawrence, A. L.; Lusby, P. J. High Activity and Efficient Turnover by a Simple, Self-Assembled “Artificial Diels–Alderase.” *J. Am. Chem. Soc.* **2018**, *140*, 2862–2868.

(3) Roh, Y.; Gao, D.; Bauld, N. L. The Cation Radical Chain Cycloaddition Polymerization OfN,3-Bis(Trans-1-Propenyl)Carbazole: The Critical Importance of Intramolecular Hole Transfer in Cation Radical Cycloaddition Polymerization. *Adv. Synth. Catal.* **2001**, *343*, 481–489.

(4) López-Alvarado, P.; Avendaño, C.; Carlos Menéndez, J. Efficient, Multigram-Scale Synthesis of Three 2,5-Dihalobenzoquinones. *Synth. Commun.* **2002**, *32*, 3233–3239.

(5) Hayashi, H.; Aratani, N.; Yamada, H. Semiconducting Self-Assembled Nanofibers Prepared from Photostable Octafluorinated Bisanthene Derivatives. *Chem. - Eur. J.* **2017**, *23*, 7000–7008.

(6) Li, Y.; Josowicz, M.; Tolbert, L. M. Diferrocenyl Molecular Wires. The Role of Heteroatom Linkers. *J. Am. Chem. Soc.* **2010**, *132*, 10374–10382.

(7) Wilson, R. M. Cyclopentadiene Bisadduct of Tetrafluoro-p-Benzoquinone: Its Stereochemistry, Reactivity toward Nucleophiles, and Photochemistry. *J. Org. Chem.* **1983**, *48*, 707–711.

(8) Hristova, Y. R.; Smulders, M. M. J.; Clegg, J. K.; Breiner, B.; Nitschke, J. R. Selective Anion Binding by a “Chameleon” Capsule with a Dynamically Reconfigurable Exterior. *Chem. Sci.* **2011**, *2*, 638–641.

(9) Rathore, R.; Kochi, J. K.; Canavesi, A.; Miller, L. L.; Sebastiani, G. V.; Francis, G. W.; Szúnyog, J.; Långström, B. Acid Catalysis vs. Electron-Transfer Catalysis via Organic Cations or Cation-Radicals as the Reactive Intermediate. Are These Distinctive Mechanisms? *Acta Chem. Scand.* **1998**, *52*, 114–130.

(10) Turek, A. K.; Hardee, D. J.; Ullman, A. M.; Nocera, D. G.; Jacobsen, E. N. Activation of Electron-Deficient Quinones through Hydrogen-Bond-Donor-Coupled Electron Transfer. *Angew. Chem. Int. Ed.* **2016**, *55*, 539–544.

(11) Neese, F. Software Update: The ORCA Program System, Version 4.0. *Wiley Interdiscip. Rev.: Comput. Mol. Sci.* **2018**, *8*, e1327.

(12) Adamo, C.; Barone, V. Toward Reliable Density Functional Methods without Adjustable Parameters: The PBE0 Model. *J. Chem. Phys.* **1999**, *110*, 6158–6170.

(13) Grimme, S.; Ehrlich, S.; Goerigk, L. Effect of the Damping Function in Dispersion Corrected Density Functional Theory. *J. Comput. Chem.* **2011**, *32*, 1456–1465.

(14) Grimme, S.; Antony, J.; Ehrlich, S.; Krieg, H. A Consistent and Accurate Ab Initio Parametrization of Density Functional Dispersion Correction (DFT-D) for the 94 Elements H-Pu. *J. Chem. Phys.* **2010**, *132*, 154104–154119.

(15) Weigend, F.; Ahlrichs, R. Balanced Basis Sets of Split Valence, Triple Zeta Valence and Quadruple Zeta Valence Quality for H to Rn: Design and Assessment of Accuracy. *Phys. Chem. Chem. Phys.* **2005**, *7*, 3297–3305.

(16) Andrae, D.; Häußermann, U.; Dolg, M.; Stoll, H.; Preuß, H. Energy-Adjusted Ab Initio Pseudopotentials for the Second and Third Row Transition Elements. *Theor. Chim. Acta* **1990**, *77*, 123–141.

(17) Weigend, F. Accurate Coulomb-Fitting Basis Sets for H to Rn. *Phys. Chem. Chem. Phys.* **2006**, *8*, 1057–1065.